Influence of different concrete mixtures (a.o. HSC and LWC) and specimen) and specimen size on the softening of concrete under uniaxial compression

Faculteit Bouwkunde
Vakgroep
Konstruktie

Technische Universiteit Eindhoven

Influence of different concrete mixtures (a.o. HSC and LWC) and specimen size on the softening of concrete under uniaxial compression

TUE/BKO/94.07.

Dr. D. Stys 1)
Prof.dr.ir. H.S. Rutten
Ir. H.J. Fijneman
April 1994

1) Technical University Wroclaw, Poland

Contents

1. Introduction

The comprehensive studies of concrete under multiaxial states of stresses have been performed since the beginning of the eighties at the T.U. Eindhoven. Numerous experimental and numerical results have been presented by Van Mier [1984], and Vonk [1992] in their dissertations. In spite of the impression that a great deal of problems concerning the behaviour of concrete under uniaxial compression seem to be explained relatively well, quantitatively and qualitatively, there are still some topics, which should be posed as a goal for future researches. Among them, there is the influence of compressive strength of concrete on post-peak behaviour of concrete, what has been put forward by Vonk [1992]. This is especially important in the case of more brittle types of concrete, like high strength concrete (HSC) and light-weight concrete (LWC), since the type of concrete has a significant influence on failure process. Another important aspect of concrete post-peak behaviour is the influence of specimen's size on 'strain softening' phenomenon. Aforementioned investigations confirmed, that may be a size effect in softening of concrete loaded in compression. It was found interesting also, to investigate the significance of the variation in compressive strength and structural parameters (gravel size) for post-peak behaviour of specimens with different height-to-width ratio.

2. Analysis of the experiment

There are some crucial points in every experiment determining the charakteristics of the composite material, especially such as concrete. A specimen of certain geometry and size, with a given material structure is loaded under combination of mechanical loadings and specific boundary conditions. Depending on the interaction among these four factors, changes may occur within the material structure, resulting in an observable macroscopic response of the specimen. The basic idea for testing of concrete is schematically shown in Fig. 2.1.

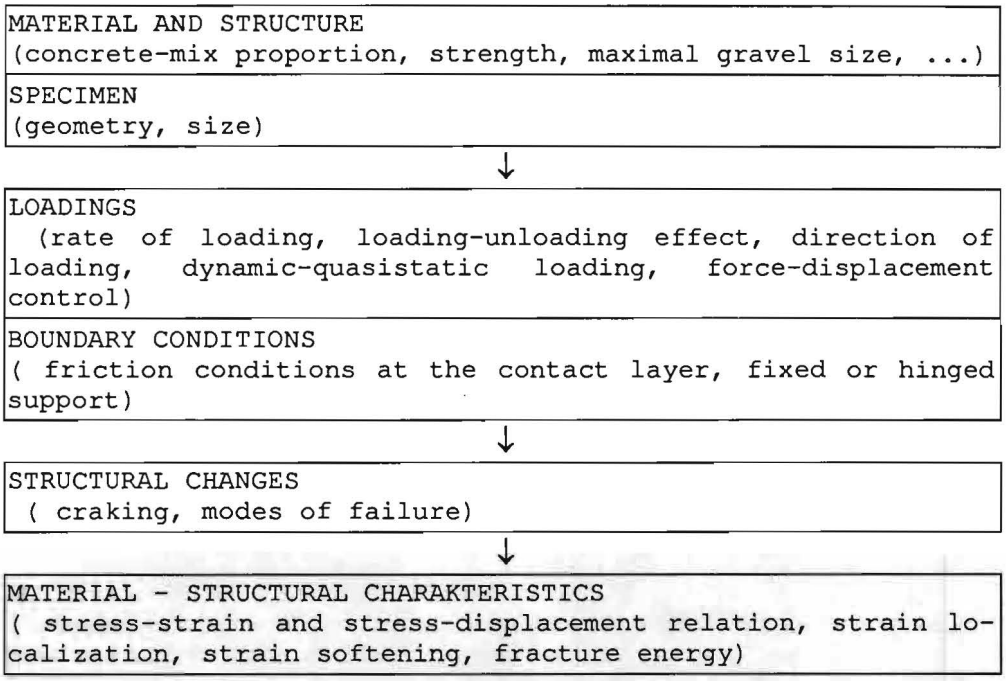

Fig.2.1. Basic problems in experimental testing of concrete.

The conclusions provided by Hordijk et al. [1989], Van Mier [1984], Vonk [1992] furnish the critical path for compression testing in a following stages:

- size effect in terms of specimen geometry, compressive strength, composition of concrete,
- displacement-control loading, direction of loading: parallel or vertical to the direction of casting,
- friction condition between loading platens and specimen,
- mode of failure and fracture energy,
- strain softening effects,
- strain localization versus structural behaviour.

It is important to make a distinction between the two aspects of size effect, which are not expressed clearly sometimes, when dealing with the experimental data. It pertains particularly to the process of strain localization.
First, the phenomena in the material 'per se' have to be dealt with, what means that volumetric fissurization, bulk behaviour and strain localization proceed in the direct context of the inherent internal structure of concrete. They are present in the material independently from our measurement method. Another aspect of scale effect is a human induced factor.

Regarding the techniques and methods of observation, the phenomenological description of specimen deterioration is a matter of the level and the scale of observations, so the same physical phenomena may be interpreted in different ways. It is visualized in the uniaxial tensile test for concrete. For a certain level of loading the fracture process and deformation depend on: specimen geometry, structural parameters (concrete-mix proportions, gravel size etc.), boundary conditions, loading rate and these are direct factors the scale effect depends on.
A question, how it is observed is a subjective one and is 'measurement-dependent'. It is shown in. Fig.2.2.

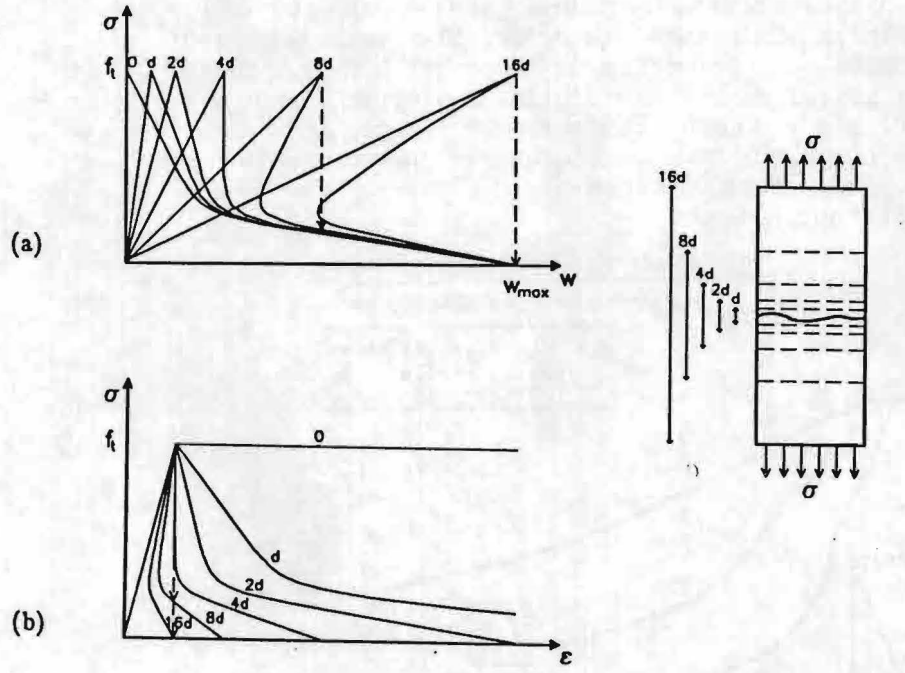

Fig.2.2. Stress-deformation relation (a), and stress-strain relation (b), according to different ranges of measurements.

Obviously, both aspects of scale effects are interrelated.
If we assume that measuring length equals specimen size, then increasing the measuring lenght means that the elastic deformations of the continuum in the vicinity of a crack become more important throughout the whole spectrum of loading.
The slope of post-peak curve changes and becomes steeper due to the increase of volumetric unloading (bulk behaviour). To avoid snap-back behaviour short specimens should be tested or the test controlling parameter should be increased monotonically.

2.1. Size effect in uniaxial compression

The term 'size effects' describes the situation when behaviour of the material manifesting - for instance - through compressive strength or post-peak softening, becomes dependent on the size of the specimen.
Though, it was already accepted that 'size effect' strongly influences the tensile properties of concrete (Carpinteri

[1989], Van Mier [1987], Bažant et al. [1990]), it is a matter of past few years to come to the conclusion, that it may be present in compressive softening also (Fanella and Krajcinovic [1988], Vonk [1992], Van Mier [1987], Hurlbut [1985]). Some numerical procedures have been developed for constitutive modelling of concrete under compression. Bažant and Ožbolt [1991c] developed a model of microplane type based on nonlocal continuum mechanics. Also 'nonlocal damage model' proved to be applicable for the description of 'size effect' in concrete (Bažant and Yumping [1991b]).
The two comprehensive experimental programs-Van Mier [1984] and Vonk [1992] obtained ambiguous results as far as post-peak softening curves are under consideration.
Van Mier [1984] investigated prisms with varying height (h=50, 100, 200 mm) and constant cross-sectional area(A=100x100 mm^2), loaded between platens with steel brushes. The material used was ordinary concrete with compressive strength about fc=49 N/ mm^2 and maximum gravel size d_{max} = 16 mm. The upper brush was effectively pinned, while the bottom one was clamped. The loading direction was perpendicular to the direction of casting.
Fig. 2.3. presents the axial stress-strain curves for three specimens with different heigth.

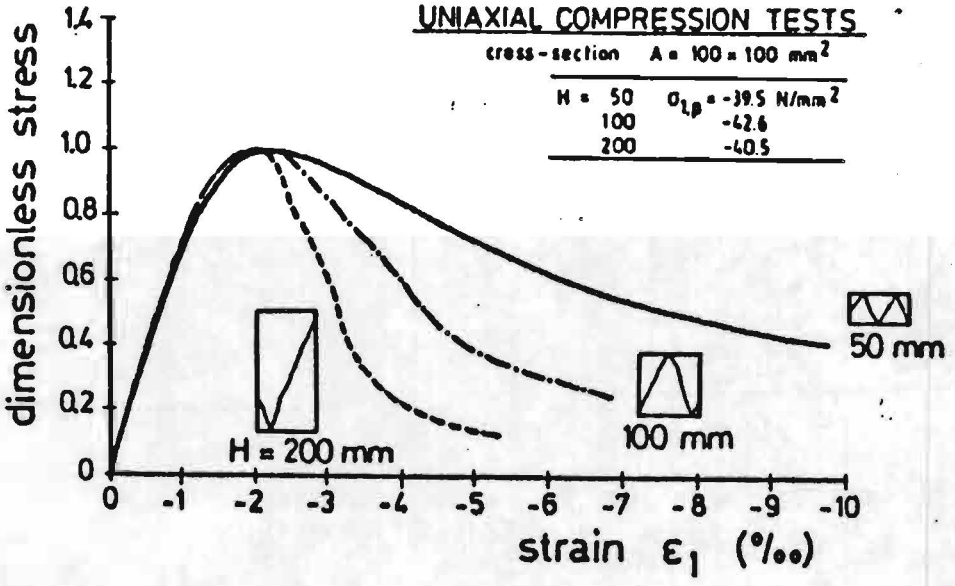

Fig.2.3. Influence of the specimen height on the uniaxial stress-strain curve in compression (Van Mier [1984]).

The stress axis has been made dimensionless with respect to the peak stress measured in each experiment. The differences are distinct. In the pre-peak region the stress-strain curves follow the same path, in the descending branch however, the slope of the softening part decreases when the height of the specimen decreases. No significant difference in strength response was measured for the specimens with different height. If we transform the post-peak curves from Fig. 2.3. into load-displacement curves, the differences in the post-peak behaviour can hardly be noticed. This is shown in Fig.2.4.

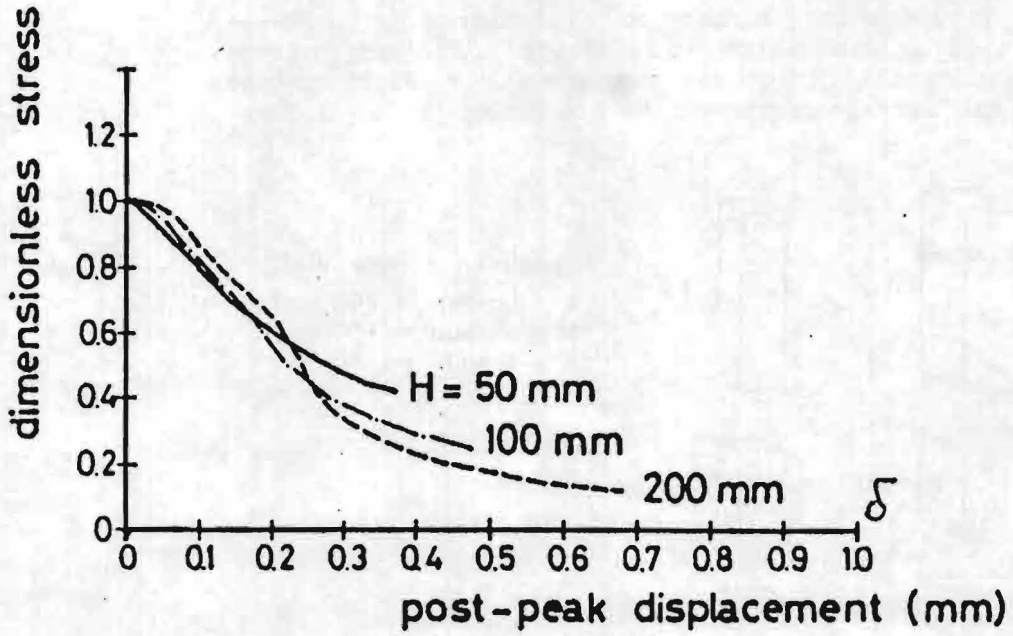

Fig.2.4. Post-peak stress-displacement diagrams for the curves from Fig.2.3.

The post-peak displacement δ in Fig.2.4. is calculated following the relation:

$$\delta = \delta_t - \delta_p \qquad (2.1.)$$

what means, that the total deformation of specimen (δ_t) has been reduced by the deformation at the peak (δ_p).
When a localized deformation is smeared over different specimen heights (50, 100, 200 mm) the decrease of the softening slope in terms of stress-strain dependence is visualized. At the same time, the post-peak displacement of each type of specimen are almost the same. One may expect that it is the same phenomenon of localized fracture like for uniaxial tension, however the localization and orientation of macroscopic fracture planes is different in each case. In uniaxial tension a localized macroscopic fracture plane developes perpendicular to the tensile direction,while in uniaxial compression a shear type fracture plane developes. In uniaxial compression a shear type fracture plane often takes the form of a zig-zag band when the specimen height is decreased. For high specimens a few large pieces are formed, whereas for the smaller ones many small size fragments results after fracture. In the limit, a horizontal softening branch is reached (stress-strain relation) and the specimen would be separated into infinite number of pieces.
Some important conclusions have been drawn from the above findings:

- post-peak softening curves in terms of stress-displacement relation seem to be independent of the material bulk behaviour,
- in spite of different failure modes, the amount of energy required for fracturing a specimen (failure energy is defined as the area under the softening part of stress

displacement diagram) occurs to be independent of the specimen heigth.

Vonk [1992] performed a series of experiments on concrete prisms with similar dimensions (h = 50, 100, 200 mm) introducing additional parameter-cross-section: WxL = 50x50 mm^2 and 100x100 mm^2. The different geometries are shown in Fig.2.5.

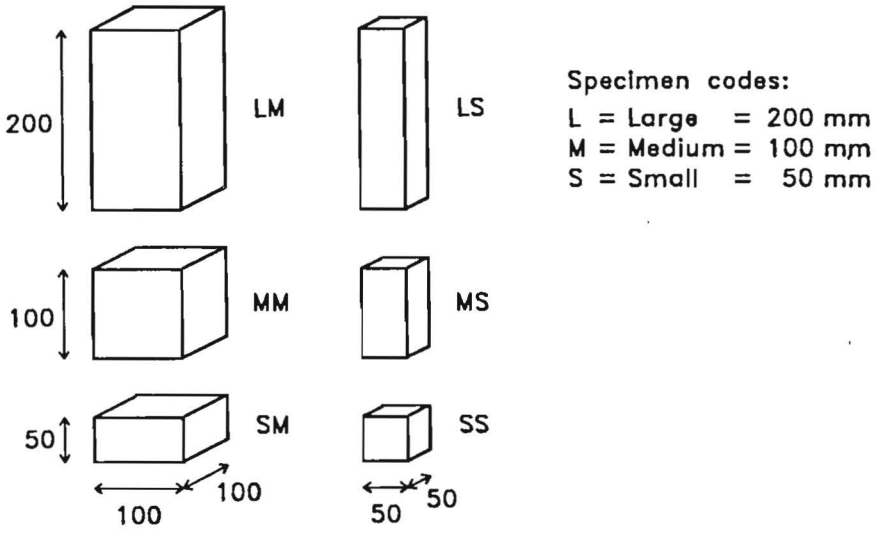

Fig.2.5. Different specimen geometries (Vonk [1992]).

All tests were carried out with teflon platens (see chapter 4). A constant strain rate: 1 x 10^{-5} s^{-1} was applied in all the tests. The nominal stress-strain curves for the different specimens are presented in Fig.2.6.

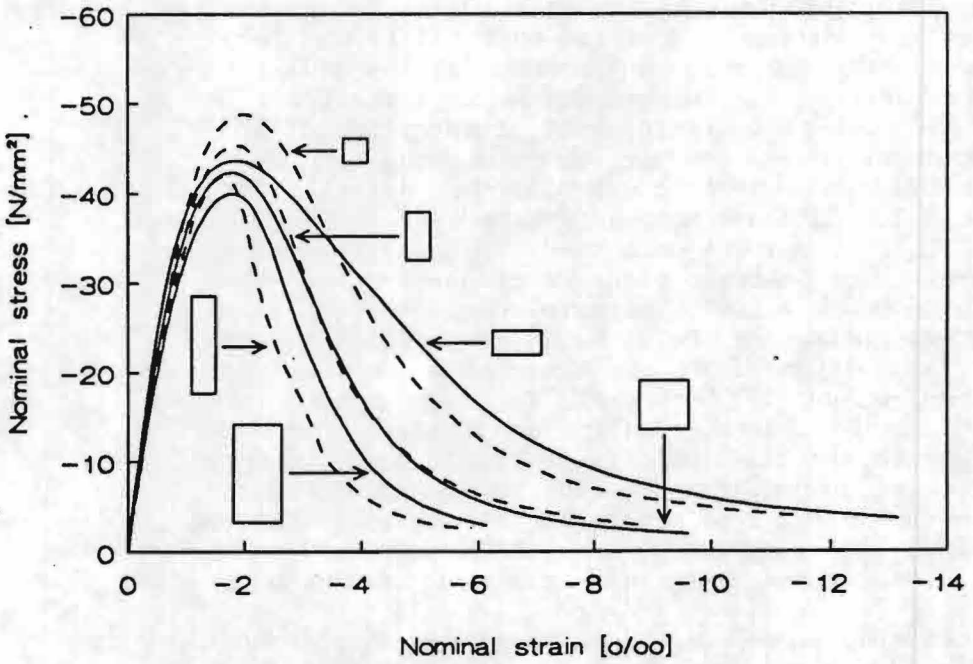

Fig.2.6. Nominal stress-strain curves for the different specimens (Vonk [1992]).

The individual results are shown in Fig.2.7.

a.

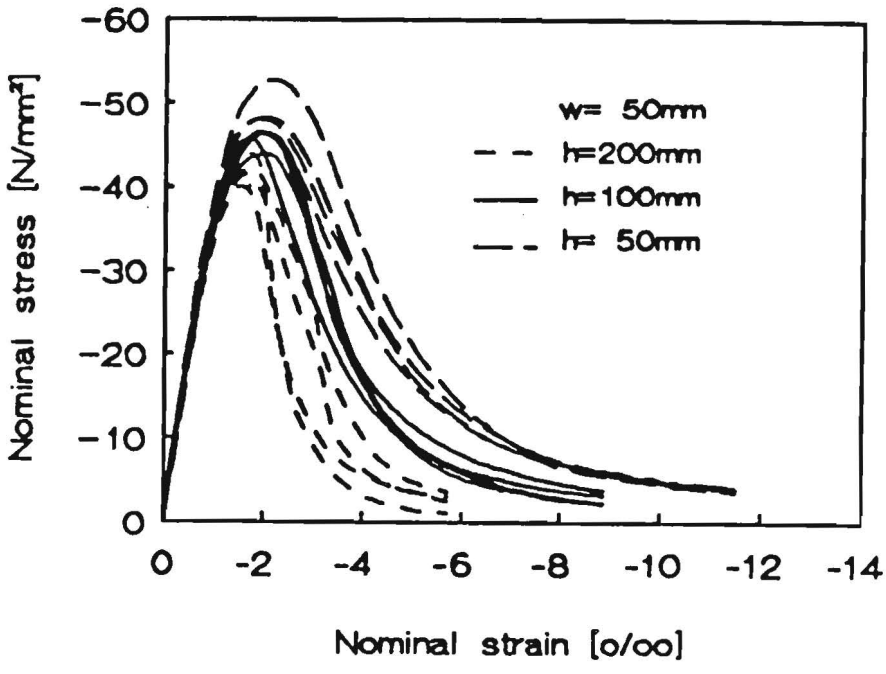

b.

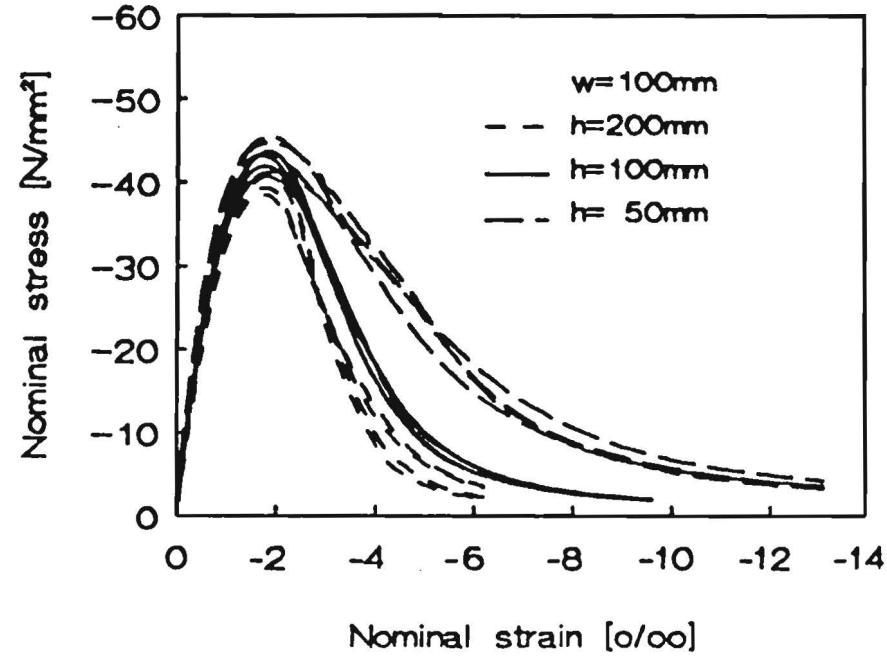

Fig.2.7. Separate test results for slender (a), and more massive specimens (b)

It is plausible, that the width of the specimen evokes some minor differences in the stress-strain relation. It was also found, that the influence of the specimen geometry on the stress-strain relation extends into the pre-peak region.
As a consequence, there was measured an increase in peak-stress as the height or the width of the specimens was decreased.

The same tendency is reflected by the energy considerations. The fracture energies have been calculated by integrating the stress-strain curves to a softening stress of - 2,9 N/mm^2 . It is depicted in Fig.2.8.

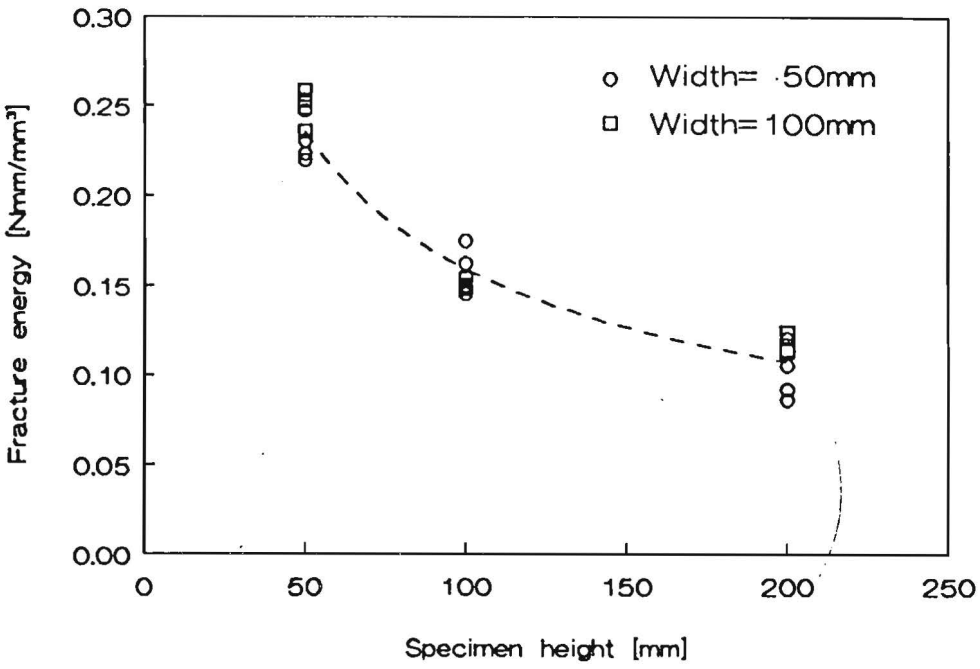

Fog.2.8. Fracture energies per unit of volume (Vonk [1992[).

A clear difference between the crack patterns for specimens with a height-width ratio h/w ≤ 1,0 and h/w ≥ 2 was reported. For lower specimens (h/w ≤ 1,0) the cracks were distributed over the whole specimen, while for higher specimens (h/w ≥ 2) the fragments free of macrocracks were found. The crack patterns were also recorded by ultraviolet photography (Vonk [1992]). Localization of cracking and deformations in the direction of compressive loading was not very pronounced.
For the specimens with the height of 50 mm it could be observed, that the number of inclined shear cracs crossed by a vertical line decreased but was often still greater than one. This could have been due to certain localization of fracture. For higher specimens the crack pattern became more complex and the number of observed inclined cracks was often greater than 1 or 2. Another finding pertains to the values of peak-stress for particular tests as presented in Fig.2.9.

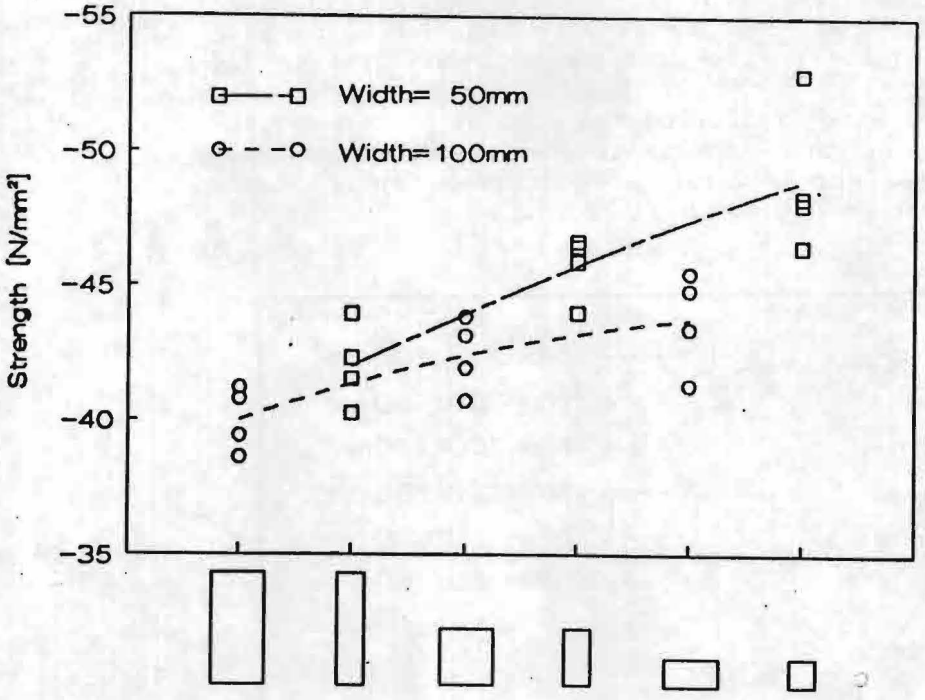

Fig.2.9. Peak-stresses for different specimens (Vonk [1992]).

The scatter in test results was significant but the increase of peak-stress with the decrease of the height (or width) of the specimens was considered statistically important. Frictional boundary restraint and the drying condition for concrete were reported as possible reasons.
Experiments performed by Vonk showed, that a similar size effect in softening was found in the test with teflon platens as had been found before by Van Mier. The comparison of the post-peak curves for geometrically identical specimens is presented in Fig. 2.10.

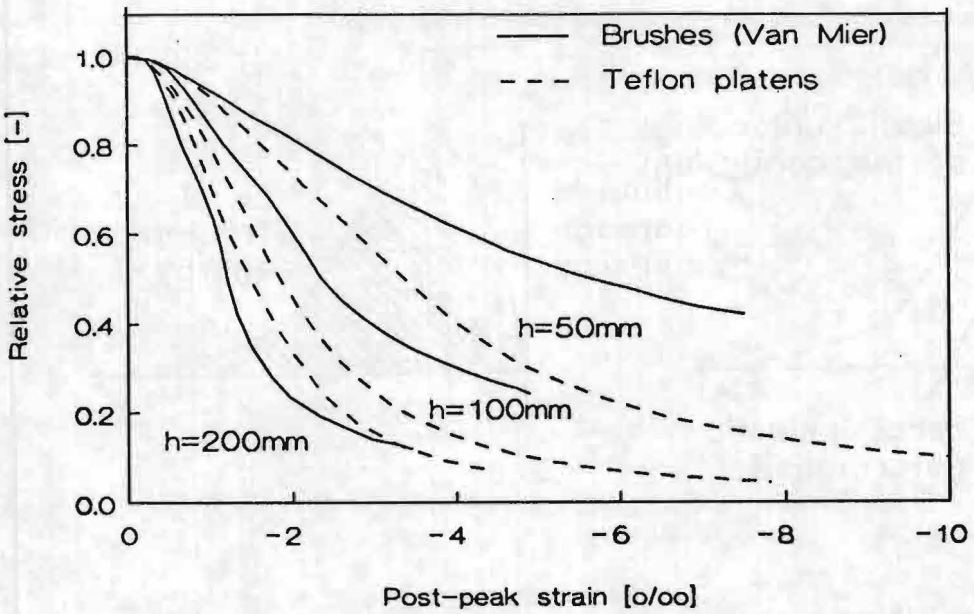

Fig.2.10 Comparison of softening curves found by Van Mier [1984] and Vonk [1992].

The stresses are made again dimensionless with reference to the peak-stress. The tests with the steel brushes (Van Mier) show a more ductile post-peak behaviour than the tests with the teflon platens (Vonk), the differences being greater for lower specimens.
A comparison can be made following the similar procedure like in Fig.2.4., assuming that localization of deformation takes place. The post-peak stress-displacement curves for the tests with the teflon platens are shown in Fig.2.11.

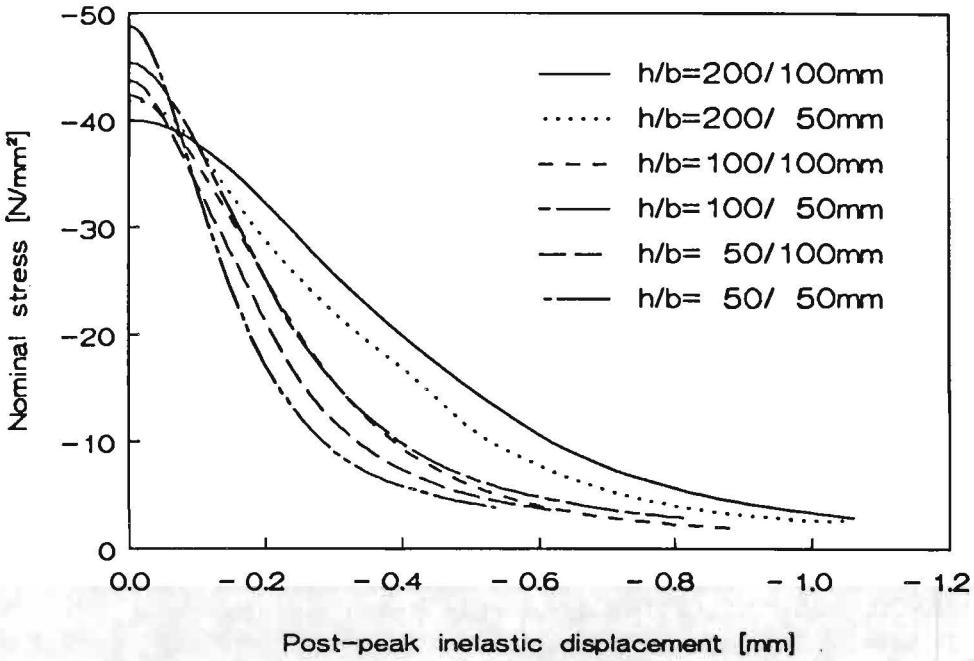

Fig.2.11. Post peak displacement curves found by Vonk [1992].

In order to take into account elastic unloading of the continuum due to softening, they were determined by substracting the inelastic pre-peak deformations as shown in Fig.2.12.

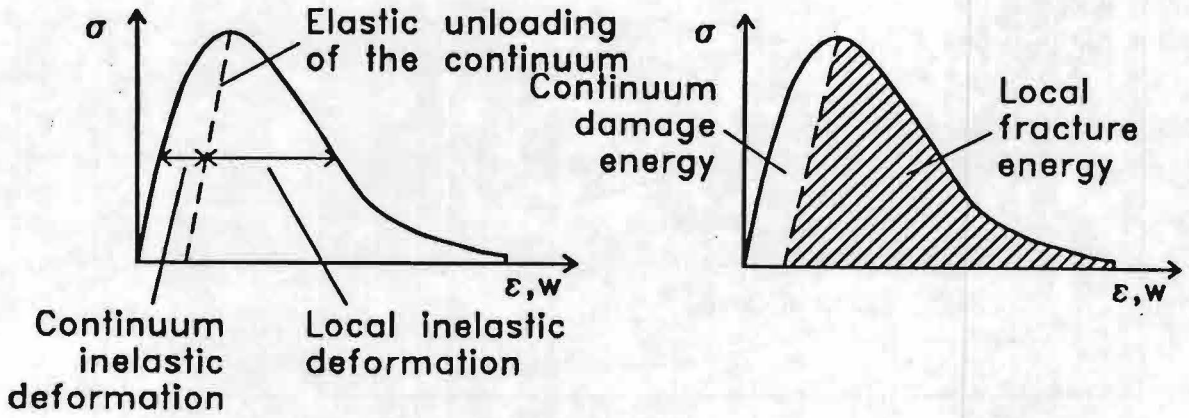

Fig.2.12. Procedure for the determination of continuum and local components of deformations and energies.

It comes out from Fig.2.11. that the post-peak curves are not equal and differ from those of Van Mier. It is probably due to the differences in boundary restraints caused by the steel brushes and teflon platens, the later being less severe.
The post-peak stress for a presumed deformation increases as the height of the specimen increases. In this case the post-peak resistance should not be considered as a result of a local process only, but also a diffuse volumetric proces should be taken into account.
In terms of the energy considerations, if a local fracture energy per unit of area is compared for the different specimens, the same tendency is clearly observed. These fracture energies are essentialy different from those in Fig.2.8.
They have been calculated by integrating the post-peak curves from Fig.2.7. down to the softening stress - 2,9 N/mm^{-2}, according to procedure outlined in Fig.2.12 and distributed over specimen cross-section (not the volume like Fig.2.8).
A possible redistribution of local and volumetric energy components is also presented in Fig.2.13.

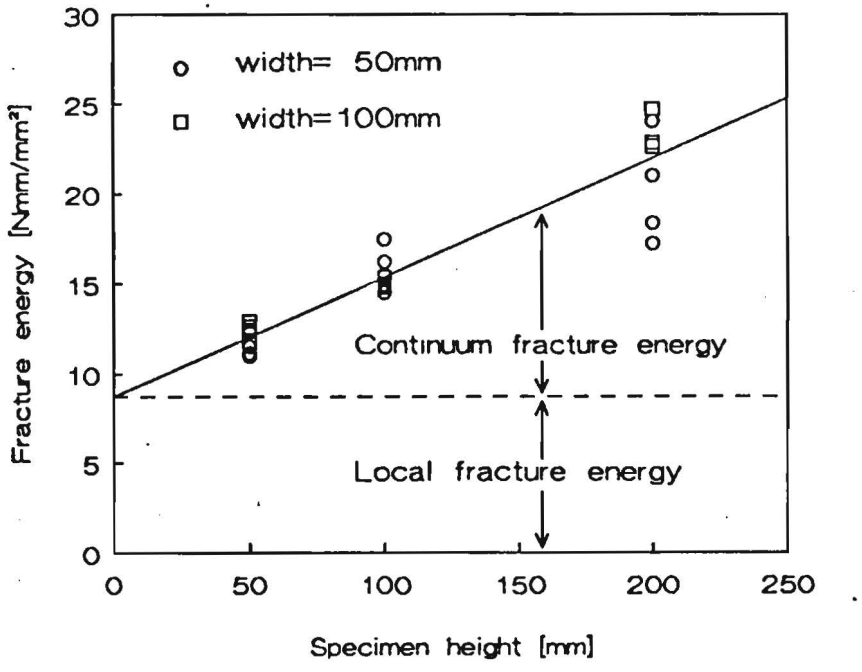

Fig.2.13 Post-peak fracture energies subdivided into local and continuum components (Vonk [1992]).

As a final conclusion, it seems that there are some serious contradictions pertaining to the local and nonlocal approach and size effects, as far as the post-peak softening curves for concrete under compression are considered. However, the localization of cracking and deformation is present in compressive softening, it is not so strongly pronounced like in tensile softening tests. Compressive softening of concrete is more a combination of a local process and a diffuse proces. Energy considerations show the influence of the volume of a specimen on the fracture energy also.

2.2. Strain localization and strain softening effect

Deformation-controlled uniaxial compression tests for concrete display a gradual decrease of load carrying capacity with increasing axial strain after maximum stress is reached.

A complete stress-strain curve for concrete in compression and tension has an ascending branch, a peak, and a descending branch. In the ascending branch the deformations can be expressed 'via' strains, what means that they are equally distributed and characterize every part of material in the same way. In the post-peak region an increase of deformations is accompanied by a decrease of stress, what is called 'a softening behaviour'.

After peak-stress is reached the deformations are usually localized in certain zones, while in the same time, material outside these zones is unloaded. It is a common practise for tensile tests to describe 'strain localization' in terms of 'cohesive crack model with bulk dissipation'. The descending branch is described in terms of stress-displacement curve (Fig.2.14).

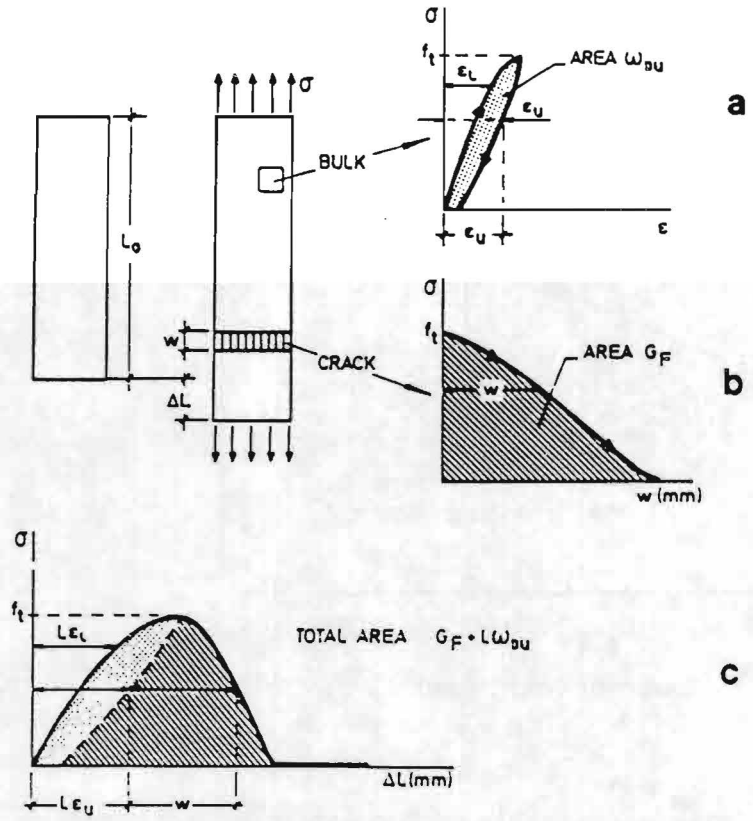

Fig.2.14. Influence of 'strain localization' on 'softening' of concrete:a) stress-strain relation for bulk behaviour, b) stress-localized displacement (crack width-w) relation, c) resultant stress-displacement curve (Elice and Planes [1989]).

External tractions being exerted on a highly nonuniform material entail nonuniform distribution of internal stesses and deformations. In the context of intrinsic microstructure - stochastic distribution of the tough and weak gravels,

different mechanical properties of concrete components and interphase connections - progressive failure occurs. Initially, it is a slow crack growth process leading finally to macrocracks initiation, which are unstable. In a deformation-controlled test, macrocracks growth leads to softening and localization of deformation - all further deformations concentrate in macrocracks. In tensile, or compressive tests in unrestrained concrete specimens localization is unavoidable and the determination of the entire stress-strain curve, the necessary characteristic of the classical continuum mechanics model becomes impossible.
From the continuum mechanics point of view the existence of the descending branch is excluded. It was Bažant remark (Bažant [1976]), that a structure must loose stability as soon as the peak-stress level is exceeded. Thus the material models based on continuum mechanics assumptions, like 'nonlinear-elastic',or 'elastoplastic' models cover only certain aspects of concrete behaviour (de Borst and Muhlhaus [1991]).
A potentially powerfull tool for the analysis of structures composed of strain softening materials are numerical methods. Numerical procedures, which incorporate the constitutive models phrased in terms of stress-strain laws and not a force displacement relation suffer from mesh-unobjectiveness (de Borst and Muhlhaus [1991]).
To compensate the deficiencies of the conventional continuum models several different approaches may be mentioned:
a. non-local or gradient continuum theories,
b. micro-polar continua,
c. stochastic models,
d. continuum damage mechanics models,
e. micromechanical modelling.
Some of them are the augmentations of classical theory, postulating 'localization criteria' or ' localization limiters'.
It also happens, that some of them are unified into one numerical procedure.

Non-local theories

In recent applications of non-local models (Bažant [1991], Bažant and Yumping Xi [1991b,c], Pijaudier-Cabot and Bažant [1988]), continuum damage mechanics has been coupled with non-local concept. The basis idea of this non-local continuum model is, that only the strain-softening damage is non-local, while all the other variables (elastic strain, total strain) used as kinematic variables, ought to be local.
As an extension of non-local approach the gradient of inelastic, softening strain is introduced, what acts as a 'stabilizer'. A prominent feature of 'gradient models' and, higher-order continuum models is the presence of an internal scale-length. This internal scale-length makes localization areas to be confined into a specified width and not to provide the singularity. At the same time a material, structural parameter is introduced. Due to this concept one may explain the size effect which is a transition between plasticity (no size effects) and linear-elastic fracture mechanics (the strongest possible size effect). There are some empirical arguments supporting non-local approach (Bažant [1991]):
- fracturing strain caused by damage is the result of the release of stored energy from a microcrack neighbourhood, the size of which is not neglible,
- existence of interactions among microcracks implies nonlocality,

- if a continuum is considered sa the interaction of the local domains as shown in Fig.2.15 the formation of the microcracks will not be determined by the local strain in the crack center.

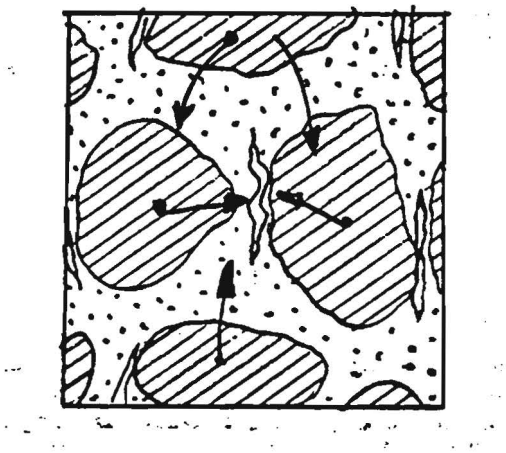

Fig.2.15. Interaction between microcracks and local domains.

The overall deformations of the group of aggregates, which are characterized by the average strain from the corresponding domains (representative volume) of the continuum, will dominate the behaviuor of microcracks. In the non-local type of analysis, the key parameter is the chracteristic length, that defines the volume of the material over which the strains are averaged. It is still not clear wheather this lenght is a material parameter or depends also on the geometry of the structure and stress-strain field.
Some authors report this value to be in the range 40 mm or 2.7 time the maximum aggregate size (Bažant and Ožbolt [1991a], Pijaudier-Cabot and Bažant [1988]).
Micropolar continua - higher order continuum models.
In micropolar continuum formulation, which may be straightforward Cosserat Continuum, the so-called 'couple-stresses' are additional components in the stress tensor. To define properly new strain components associated with the stress components, the additional degree-of-freedem is required.
These extra strain components (micro-curvatures) are coupled with an additional parameter having the dimension of length. So it is the same like in gradient models, where an internal lenght scale has been introduced.
Muhlhaus et al. [1991] have developed a Cosserat model for inelastic material with microstructure and have established relations between the Cosserat elastic constants and chracteristics of material components. For quasi-static loading conditions, the addition of rotational-degree-of-freedom has a good physical substantiation in processes, where frictional slip is the most prominent failure mechanism.
A disadventage of the Cosserat Continuum is, that the rotational-degree-of-freedom is activated under shear loading only. For instance in pure tension, rotational-degrees-of-freedom do not become active, and the couple-stresses vanish. It should

be stressed, that Cosserat Continuum may be very useful for the description of compression tests, where the failure mode often includes the kind of localization zone of a high shear intensity. At micro level in concrete high-shear-strain can be entailed by intensive microcracking.

Continuum damage models.

Continuum damage models - being an extension of a classical continuum mechanics concept - provide the stress-strain relations, which are always associated with a localization criterion or localization limiter. General continuum damage models have three essential parts:

- a set of independent internal variables, which added to the stress-strain tensor may characterize uniquely the stress-strain field of a body at the desired time instant,
- a set of 'state-equations' relating the stresses to the strain and to the internal variables,
- a set of 'flow-rules' specifying the way, in which the internal variables change when loading proceeds.

Recently, continuum damage models have been succesfully applied to concrete by Mazars[1985], Ortiz [1987] or Pijaudier-Cabot and Bažant [1988], the last one has been already categorized into separate group (microplane models). The increasing complexity of this models does not always go together with the comprehensive and realistic description of concrete behaviour, what may be discouraging.

Stochastic models

The next approach involved in the analysis of complex heterogeneous material like concrete is stochastic modelling. Material is henceforth no longer considered to be homogeneous at a certain level but heterogeneous. The constituents of this multiphase medium have a random distribution in space and it is the probabilistic approach, which permits the insight into mechanical behaviour of concrete. Mostly, Weibull's statistical theory serves as a basis in many stochastic models for concrete. Weibull [1939] deduced the probability of fracture in a brittle structure on the basis of the 'weakest link' concept. Having established a link between Weibull's asymptotic function and Griffith's crack instability criterion it is possible to handle the scatter of fracture phenomena in brittle solids (Freudenthal [1968], Jayatilaka [1979]). More recent applications of this theory to concrete-like composites have been given by Mihashi [1938], Carpinteri [1989], Oritz [1987]. Despite of those numerous applications, there sre some questionable aspects of classical Weibull-type-theories raised by Bažant [1991]:

- the growth of macrocracks causes a strong deterministic size effect, which prevails over the statistical size effect due to random strength,
- the features of failure mechanism and structure geometry are not incorporated in 'weakest-link' concept,
- the differences in size effect between two and three-dimensional problem obtained according to Weibull's concept are pronounced too strongly, when compared with experimental data,
- classical Weibull-type theories neglect spatial statistical correlation of random material properties.

Also in this case, the application of non-local approach provides a possible solution to the problems mentioned above (Bažant [1991]). It should be mentioned here, that the distinction between damage mechanics and stochastic models is rather

artificial, since damage mechanics parameters are often defined in terms of probability functions.

Micromechanical modelling.

Micromechanical attempts to simulate the real concrete structure may be also called 'stochastic procedure', due to random generation of the structure parameters. These procedures for creation of realistic concrete simulate the shapes and location of aggregates by a random process for concrete cross-section, in two or three dimansions. Such ' micromechanical models' reflect usually the properties of concrete in terms of the two-phase composite composed of cement mat⁄rix and gravels of different sizes. The fracture proces is studied through the interrelations between aggregates and matrix.

Reliable results were obtained according to LEFM formulation (Zaitsev and Wittmann [1991]), truss modell (Bažant et al. [1990]), lattice model (Schlangen and Van Mier [1991]), or applying sofisticated Finite Element programms (Roelfstra [1989]. Willam et al.[1989], Vonk et al. [1991]).

Notwithstanding the limitations connected with the proper description of the real structure of concrete there is an important factor of the time of calculations and the capacity of a computer, which provides the upper limit for numerical modelling.

Above remarks aim to give only some overall hints about possible ways of the treatment of the softening process in concrete.

Since it has been recognize, that fracturing process in concrete under tension and compression is accompained by strain softening being the feature of cement-matrix composites, it is still not clear wheather it can be concidered as a material property. Especially in the compression tests, the softening phenomenon seems to be different than for tension. This finding calls for more empirical observations to build a model taking into account more factors, than strain localization only.

3. Fracture process in concrete

The properties of a heterogeneous material are linked to its internal composition and physical-mechanical processes occuring inside a material. It is commonly accepted to consider the structure of concrete-like materials on three different levels (Wittmann [1983]):

- at the macroscopic level, concrete is studied as a continuum. Stress-strain characteristics describe the behaviour of structure as well as basic elastic constants. The characteristic length is in the order of 0,1 m or more,
- at the meso-level, we are able to monitor crack formation and the developing of fracture mechanism. The processes at macro-level are directly influenced by meso-level phenomena. The characteristic lenght is in the range 10^{-2}-10^{-3} m,
- at the micro-level tractions among particles and the physical and chemical processes can be studied. Characteristic length is of the order 10^{-4} m or less.

Phenomena observed at a certain level must be interpreted in terms of mechanisms acting at a lower stuctural level. In engineering practice it is sufficient to deal with concrete properties on macro-level, however, for more detailed insight into concrete structure it is recommended to lower the degree of observation at meso-level. That means that concrete is considered as a two-phase material- particles of gravel are embedded in homogeneous cement matrix. Voids, which are always present in the internal structure of concrete may be considered as the very weak inclusions, so the two-phase model holds in this case also.

3.1. Fracture of normal concrete

It is assumed in this report that'normal concrete' is a cement-matrix composite based on natural gravel, having compressive strength in the range 20-60 MPa and average density of 2300-2500 kg/m^3 . The fracture of normal concrete under compression is a well known process. The tests of HSU et al. [1963],which were later confirmed by many investigators, had showed that a significant number of cracks already existed in unloaded concrete due to volume changes in matrix (shrinkage) and bleeding. Under compression load a high stress concentration occurs in the specimen according to interaction between aggregates and voids, what leads to the initiation of crack propagation (Fig.3.1).

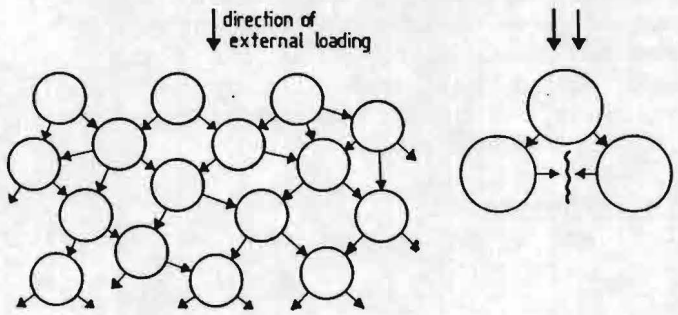

Fig. 3.1. Interaction among aggregates (after Reinhardt [1977]).

For uniaxial compression test , tensile forces are necessary to balance the lateral components of the compressive load. The micro-cracks happen to appear at the interfaces of aggregate-cement matrix which are the weakest links in normal concrete.
With increasing stress bond cracks start to grow above the level of 0,3 of the ultimate stress (σ_u). It is shown schematically in Fig.3.2.

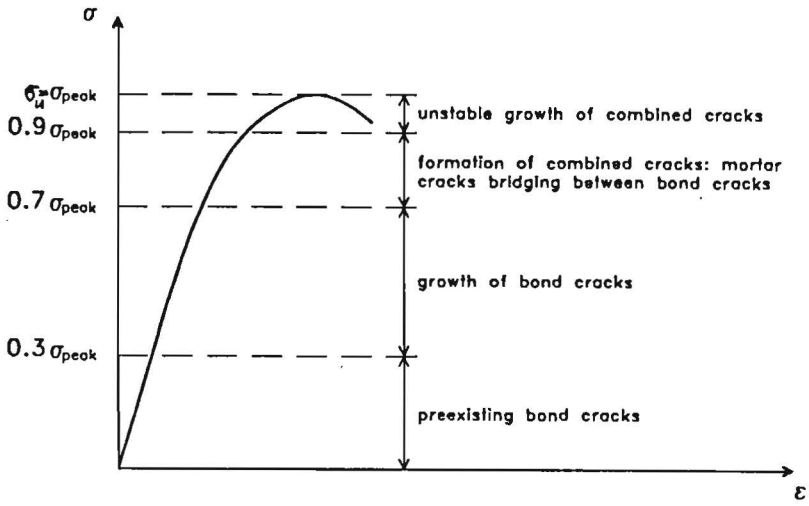

Fig.3.2. Crack formation process under compression for various stress-intensity levels (Hsu et al. [1963]).

A macroscopic stress-strain curve deviates from linearity. Further increasing of axial stress, shows an accumulation of bond-cracks and at 0,7 - 0,9 σ_u, mortar cracks start to propagate together with the crack-bridging effect. Due to the branching effect, the majority of the combined cracks is oriented parallel to the direction of loading and a continuum mechanics model becomes irrelevant at this stage of material detorioration.
The combination of isolated micro-cracks forming main cracks seems to govern the failure process in high-strenght concrete also (Carrasquillo et al. [1981], Chen et al. [1987]).
An important phenomenon observed during fracturing of concrete is 'crack arrest'. It is an effect connected with the heterogeneity of concrete. Cracks grow into areas of lower stress or higher strength and are arrested there until the influx of strain energy is provided by the increasing loading. In normal concrete the aggregates are much stronger than cement matrix, so the cracks are forced to grow around the aggregates. The tortous crack pattern demands more energy than the formation of a straight-line crack. As it has been already mentioned (Fig.3.1) the stiff aggregates can be considered as the fracture initiaters.

3.2. Initial anisotropy of concrete

The anisotropy of concrete is connected with the two aspects of anisotropy:
- initial anisotropy,
- stress or strain induced anisotropy,

the second one being mainly dependant on testing conditions and specimen geometry. For uniaxial compression test the

initial anisotropy is of primary importance. The influence of the direction of loading with regard to the direction of casting on the axial stress- strain curve was demonstrated by Van Mier [1984].

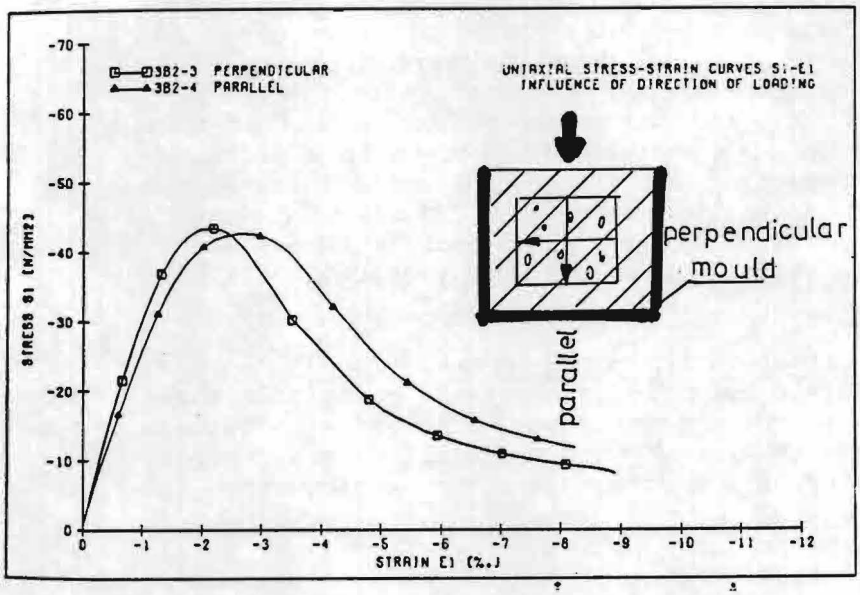

Fig.3.3. Influence of initial anisotropy on the uniaxiakl stress-strain curve in compression (after Van Mier [1984]).

The analysis of Fig.3.3. reveals that in the ascending branch of the stress-strain curves, the initial slope was found to be smaller when loading had been applied parallel to the direction of casting. In the descending branch, both stress-strain curves were similar. As an explanation for the above phenomenon, the creation of voids and weaker matrix material zones under larger aggregates was reported. The formation of structural defects is furnished by shrinkage and hardening processes in concrete. When loading is applied parallel, the initial defects are in favorable direction for being hampered (Fig.3.4) and more energy is required for supporting the fracture process.

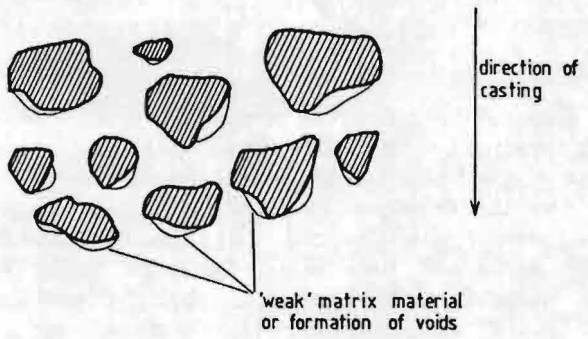

Fig.3.4 Location of voids and weak domains under aggregate particles (after Van Mier [1984]).

An increase of energy requirement of approximately 10% was measured when a specimen was loaded parallel to the direction of casting (Fig.3.3).
Considering the aformentioned anisotropy one should take special precautions to perform compressive tests in the same orientation of loading axis to the direction of casting.
The preparation of the samples for laboratory tests often requires specimens to be cut out from the larger prisms. This procedure largely eliminates the segregation effect which arises during compacting and hardening of concrete (Van Mier [1984]). The position of a particular specimen in a prism during casting and compacting (middle or end) seems to have some minor influence on deformational response and fracture mode.
For a given type of test, it is recommended to choose specimens at random from various locations with respect to the bulk of prism.

3.3. Influence of gravel on fracture process

The isolated fracture domains in concrete are parts of a chain of the energy dissipation process. The stiffness ratio between aggregate and matrix is one of the principal factors controlling the extent of crack-arrest and as consequence the stress-strain curve.
It may be shown schematically as in Fig.3.5.

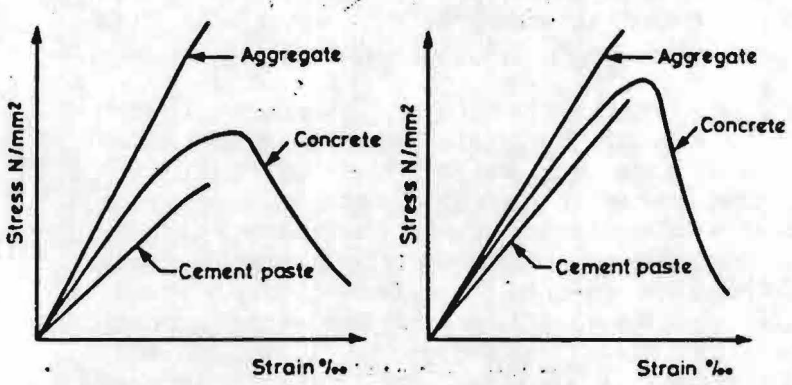

Fig.3.5. Influence of stiffness ratio between aggregate and matrix for stress-strain behaviour of concrete: a) big difference in stiffness, b) minor difference in stiffness.

A kind of paradox may be observed. Despite the fact that both cement paste and gravel are usually considered as brittle, the material being a mixture of them behaves in a different way.
This may be attributed to the difference in rigidity that normally exists between the cement paste and aggregates. When this difference is less the material behaves in a more brittle way, otherwise, like for normal concrete, its behaviour is more ductile. Generally, the fracture energy increases with increasing maximum aggregate size and its volumetric amount.
Fig. 3.6 gives the relation between fracture energy and maximum aggregate size as obtained in a number of investigations. The inconsistencies in experimental resulsts may be atributed to the different types of aggregate used (limestone, granite).

The post-peak softening behaviour of concrete is strongly affected by the tortuous path of the main crack and microcracking entailed by the crack arresting action of the aggregates.

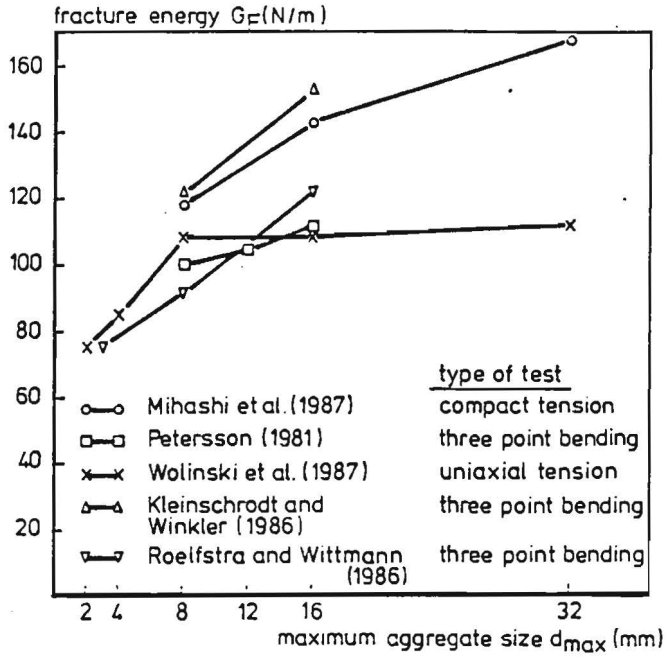

Fig. 3.6 Fracture energies for concrete, with different maximum aggregate size (after Hordijk et al. [1989]).

3.4. Fracture of high-strong concrete

A limited number of standards or national codes provide regulations with respect to maximum concrete strenght and application to high strenght concrete (Swamy [1987], FIP/CEB report [1990]).

As a crude approximation one may consider the compressive strength of about fc=60 MPa as a lower limit for high-strength concrete(HSC). The mechanical properties of concrete are improved by obtaining a denser packing of solids and by improving the paste-aggregate bonds. The first effect is connected to the application of 'Densified System containing homogeneously arranged ultrafine Particles' - DSP. These particles, which are often silicafumes (SF) are two order of magnitude smaller than the cement graines. Their size and spherical geometry allow them to fill effectively the voids between the larger cement grains. The variation in the structure of cement matrix is shown in Fig.3.7.

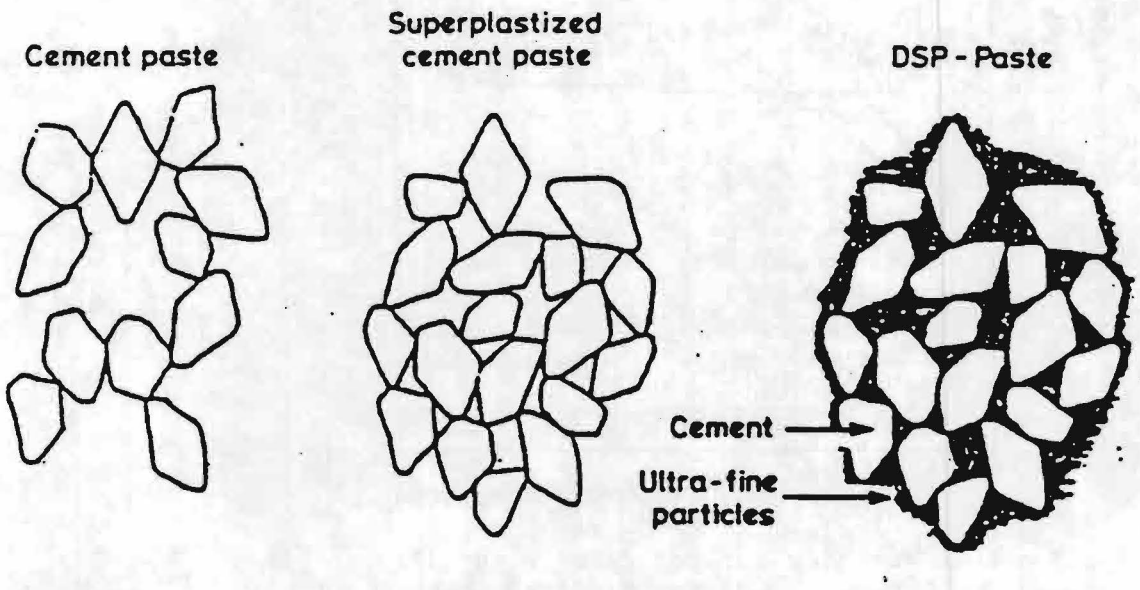

Fig.3.7 Different degrees of the refinement of cement paste structure.

Also the interfacial zone, considered as the weakest link in normal concrete can be substantially strengthent by the addition of SF. This is due to SF's ability to pack densily at the aggregate surface and reduce internal bleeding of concrete.
The HSC is known to be more brittle than normal concrete, what can be seen in uniaxial compressive and tensile tests which indicate that it is very difficult to obtain the post-peak curve (see testing techniques for HSC).
It comes directly from Fig.3.5 that for small differences between the stiffness of aggregates and matrix the fracture energy demand is less what results in more brittle behaviour.
According to more homogeneous distribution of mechanical properties, the microcracks proceed simultaneously through the all phases of composite-matrix, gravel and interface layers.
The microcracked zone which precedes macrocracking is smaller than in normal concrete and has a smaller microcrack density (Carrasquillo et al. [1981]).
The stress-strain characteristics of HSC in compression are reported by many investigators (Carrasquillo et al. [1981]), Chen et al. [1987], Glavind and Stang [1991]). The examples of such curves are shown in Fig.3.8.

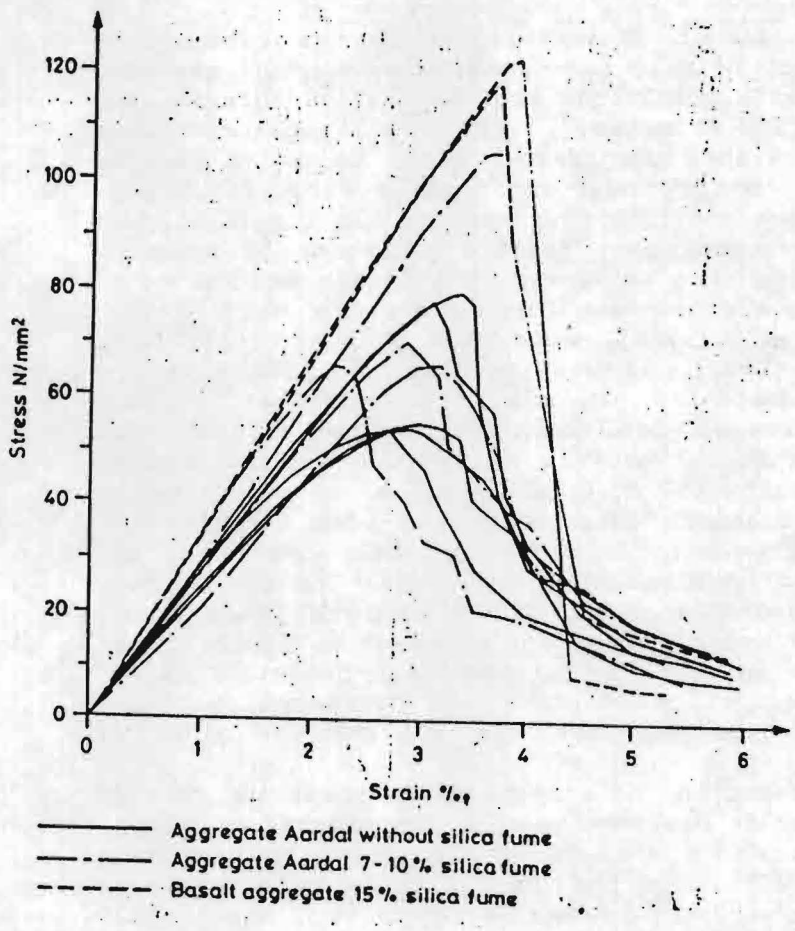

Fig.3.8. Stress-strain behaviour of HSC measured on 150x300 mm cylinders (after Helland et al. in FIP/CEP Report [1990].

The main differences between the normal and the HSC concrete may be summarized as follows:

- a more linear stress-strain curve for HSC. The discontinuity point occurs at a higher stress-strength ratio at about 80% of ultimate strength (discontinuity point indicates the onset of unstable self-propagating crack growth). The proportional limit and the discountinuity point increase as the ratio of modulus of elasticity for aggregate and mortar (Ea/Em) approaches unity,
- a higher strain at maximum stress,

- a steeper slope of the descending part of the curve.

The changes in material response are a consequence of improved aggregate-paste bond. The more linear stress-strain curve reflects the reduced amount of microcracking at lower levels of loading for HSC. Carrasquillo et al. [1981] used an X-ray technique to demonstrate that unstable macrocracks start to develope at the interface between the paste and aggregate at about 90% of the ultimate load for a HSC with the ultimate compressive strength of 76 MPa, what is an empirical confirmation of the anticipated crack pattern development.

3.5. Test techniques for high-strenth concrete.

It is extremely difficult to investigate post-peak behaviour for HSC. Due to very brittle post-peak behaviour the restrictions imposed on tests conditions are very severe (Glavind and Stang [1991], Dahl and Brincker [1989]). Usually there are two ways to arrange a stable compression test: to use a testing mechine with a very stiff frame or to use a close-loop feed-back signal as a test controlling parameter. In the first case the absolute, incremental post failure stiffness of specimen has to be smaller than the stiffness of the machine. The other ways of controlling a close-loop feed-back signal were presented by Stang et al. [1981], Dahl and Brincker [1989] or Glavind and Stang [1991]. It was performed for HSC with the application of a combination of axial deformation and circumferential deformation in feed-back test control system. The complete stress-strain curves were available even for testing machine with a capacity 250 kN.

Some valuable informations concerning post-peak behaviour of HSC may be drawn from standart bending tests (Swartz et al. [1987]) or tests on double-cantilever beams. Despite of performing tests under displacement controlled condition a stable post-peak behaviour was observed for compression zones of beams. This may be an indication that post-peak behaviour of HSC is dependent on geometrical factors and boundary conditions for a particular type of test and specimen (Hordijk et al.[1989]).

Taking under consideration the effect of the stressing rate it is not clear whether it has some meaning for testing of HSC.

The experimental results are ambiguous. Jones and Watstein (FIP/CEB Report [1990]) reported the HSC to be more sensitive to stressing rate than low or normal strength concrete , while recently Dahl and Brincker [1989] reported that the loading rate had no significant influence on neither the peak stresses nor the value of the fracture energy. These discrepancies may be partially contributed to the different test conditions and different specimen sizes.

3.6. Fracture of light-weight concrete.

Structural light-weight concrete (LWC) is often manufactured by using light-weight aggregate like for instance sintered pulverized-fuel ash (Lytag) having a density of 800-1000 kG/m^3. The dry density of this type of concrete can be varied in the range of 1500-2100 kG/m^3. The strength depends on the same parameters like for ordinary concrete. In the following testing program the upper limit for compressive strength for this type of concrete has been assumed at approximately 35 MPa. From the standpoint of fracture process and post-peak behaviour there are apparent similarities between HSC and LWC.

Both materials are more brittle than normal concrete due to a more homogeneous internal structure. Assuming that the important parameters influencing the fracture of concrete are different mechanical properties of matrix and gravel, one may obtain a h gher homogeneity of material by increasing the strenght of matrix with respect to the strength of gravel (HSC) or by decreasing the strength of gravel with respect to matrix strength (LWC). Crucial to this is also the proper transfer of load across aggregate-matrix interface which for LWC is much better then for usual concrete. The surface of light, porous particles offers excellent bond to cement paste, since the presence of absorbed water in the particle pores enables the continued hydration at the aggregate-matrix boundaries what highly improves continuity.
It results for LWC in similar behaviour under compression like for HSC. The actual stress-strain relation for most LWC differs from that for normal dense aggregate concrete in the two important aspects. First, the ascending part of stress-strain curve is less steep and more straight than for dense concrete (decrease of E-modulus of about 30-40%).
Secondly, for LWC the descending branch of stress-strain curve drops more rapidly after reaching maximum stress as it is shown in Fig.3.9.

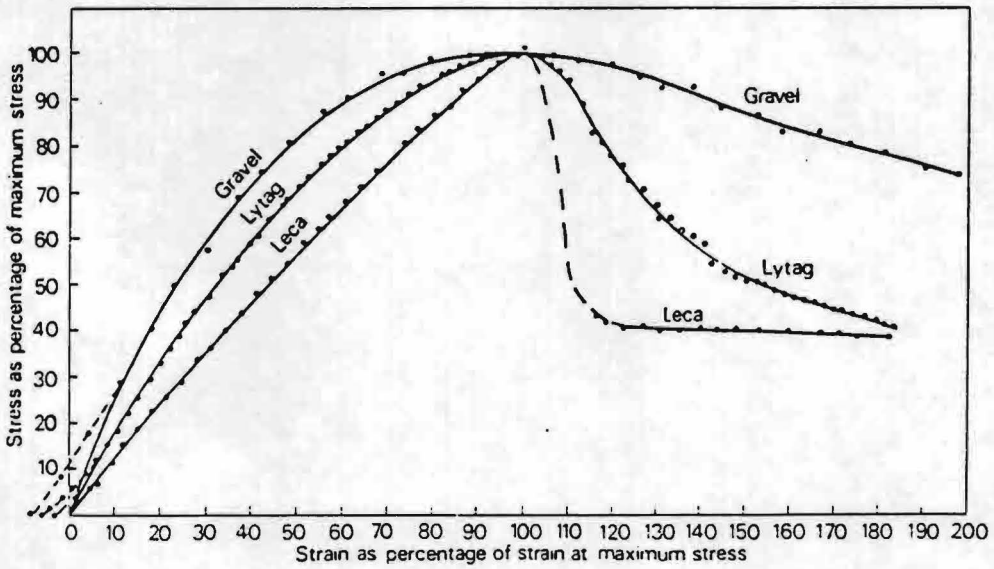

Fig. 3.9 Comparative stress-strain relation for dense and lightweight concretes (after Short and Kinniburg [1978]).

The results of compression tests indicate also that the maximum strain reached by LWC is in the range 2,0 - 2,5 x 10^{-3} , what is slightly lower than for normal concrete (about 3,0 x 10^{-3}).
Considering the fracture energy of LWC, in some experiments (Hordijk et al. [1989]) it was found to be 30% lower than for normalweight concrete of the same strength.Another important finding in terms of fracture mechanics analysis is that since

both materials - LWC and HSC - are more prone to brittle fracture the relevant dimensions of a structural member need not be as large, compared with normal concrete, in oreder to have fulfilled the requirements for the application of linear-elastic fracture mechanics (Ashrabov [1988]).

4. Influence of boundary conditions

When performing a complete uniaxial compression test for concrete, particular attention should be paid to the boundary conditions for specimen under investigation. Above problem has been treated in details by Schickert [1980], Kotsovos [1983], Van Mier [1984], Vonk [1989].
The conclusions coming from investigations reported above are not convergent, however.
Regarding the loading system, there are the two extreme situations to be distinguished: a uniform stress distribution along the specimen boundary, or a uniform boundary displacement. Both situations are presented in Fig.4.1.

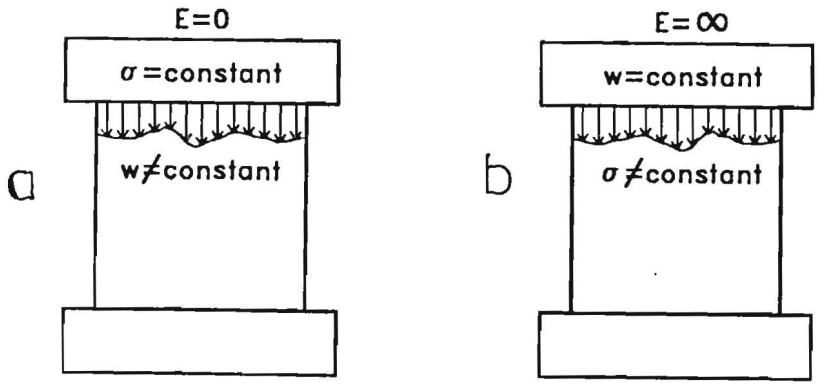

Fig.4.1 Effects of the application of different loading systems:a. loading platens flexible, b. loading platens rigid.

Under uniform boundary stress (flexible loading platens) the local irregularities of concrete-like material provide the nonuniform distribution of displacements along boundaries.
Since the loading system is of zero stiffness, no shear forces will be acting at the specimen-loading platen interface, and there are no constrains and shear deformation of the specimen.
Another extreme point is when an infinitely stiff system is applied what results in a uniform boundary displacement and a non-uniform stress state. For different lateral deformations of loading platen and specimen, shearing forces of variable intensity will be induced in between them. As the result a multiaxial state of stresses wil appear at the specimen ends.
These stresses result in a different mode of failure for particular loading systems. According to triaxial compressive stress at the ends of specimen, microcracks initiate along the boundaries of the conical blocks and hour-glass mode of failure commences. The common practise to reduce the influence of lateral restraints is increasing specimen height. The mode of failure changes when lateral restraints are reduced. Several experimental techniques have been developed for this purpose. They may be briefly categorized as:

- systems with intermediate layers reducing the friction between specimen and loading platens. It can be augmented by

polishing loading platens surfaces (Mills and Zimmermann [1970], Erdei [1980]),

- system with sophistically constructed loading platens like for instance: steel brushes (Holsdorf [1965], Kupfer [1973], Van Mier [1984], or flexible loading platens (Schickert [1980]). This last method is applicable up to the peak-stress only, since after the threshold of peak-stress the test becomes unstable.

Kotsovos [1983], investigated the influence of boundary constraints on the fracture process of uniaxially compressed cylinders (250 x100 mm^2) made of ordinary and low-strength concrete. The system had been equiped with hinged loading platens what made the behaviour of specimens more brittle. Some of the results are given in Fig.4.2.

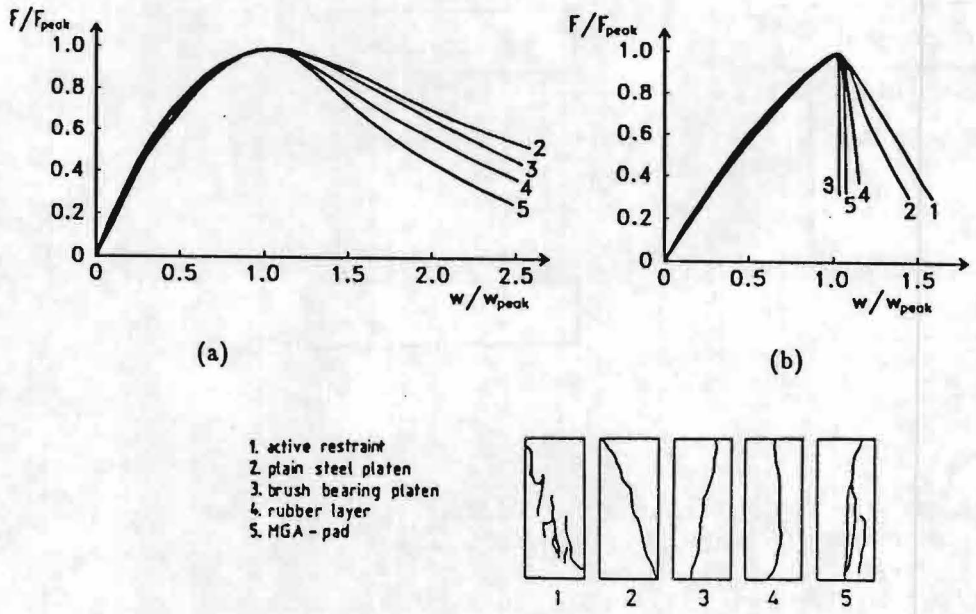

Fig.4.2. Influence of boundary conditions on the befaviour of concrete under uniaxial compression: b) normal-strength concrete, a) low-strength concrete, c) modes of failure (after Kotsovos [1983]).

Decreasing the friction at the specimen -loading platen interface the shape of the softening curve became more steep. The fracture modes were influenced by boundary constraints also. The less the friction present at the interface zone was, the lower the inclination of the macroscopic fracture plane was and a more distributed type of failure was found. As the final conclusion, softening of concrete under compression was contributed to crack growth entailed by a nonuniform stress-state and was claimed to be a structural and not a material property. One may postulate a contradictory point of view observing the post-peak behaviour of low strength concrete (Fig.4.2a) were for different boundary restraints, still pronounced softening can be found.

The results of similar type investigations were also reported for HSC (Dahl and Brincker [1989]), however the dimensions of specimens had been small-cylinders:34 mm, 45 mm, 57 mm in diameter and height. They are presented in Fig.4.3.

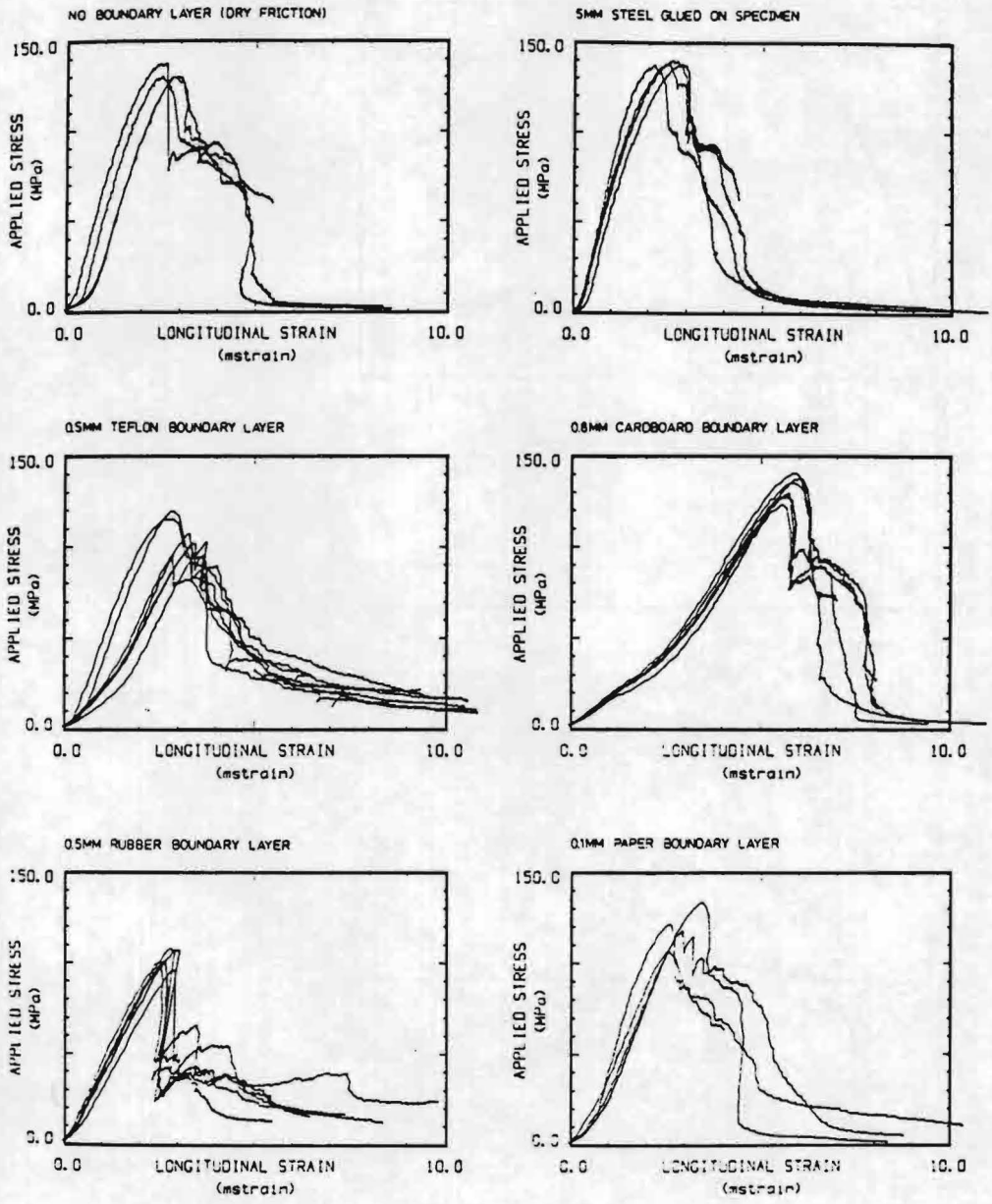

Fig.4.3 Stress-strain relations in HSC for different kinds of boundary layers (Dahl and Brincker [1989]).

It had been suggested that for rubber and teflon boundary layers the crack pattern is more homogeneous and more diffused. The post-peak behaviour is more ductile and apparent load-carying capacity is maintained until the end of tests. Vonk [1989] measured the complete stress-deformation curves for the different loading platens. The results are presented in Fig.4.4. The curves represent average values of two tests with identical loading platens.

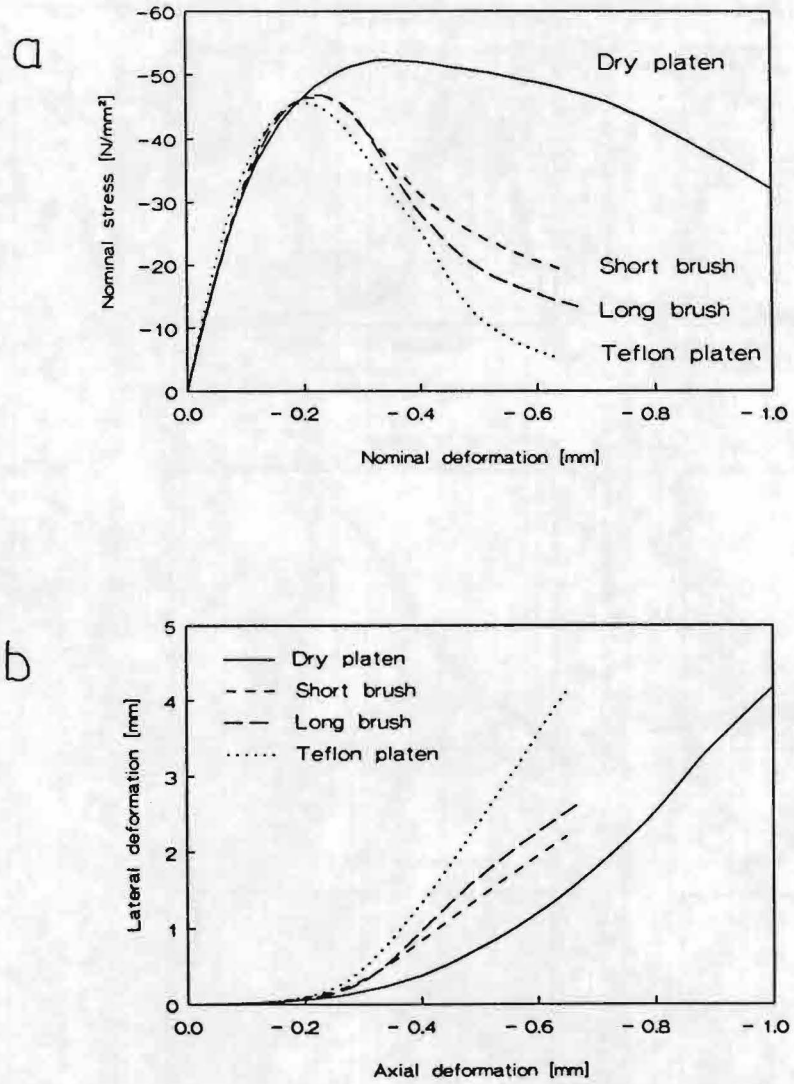

Fig.4.4. Axial stress-deformation curves for tests with different loading platens - a), axial versus lateral deformations - b) (after Vonk [1992]).

An interesting aspect of that investigation was the quantitative analysis of the shear stresses introduced - due to friction - in the concrete specimen by the loading system. The results are briefly outlined in Fig.4.5.

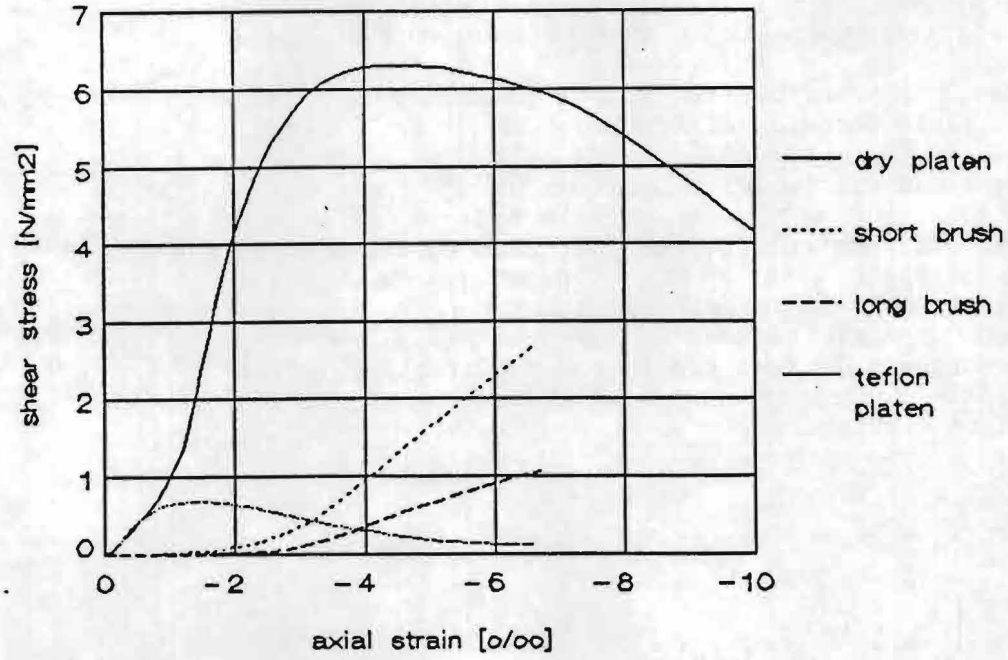

Fig.4.5. Shear stresses exerted on concrete specimen by the different types of loading platens (Vonk [1989]).

For dry platens resulting in high boundary restraints peak stress is higher, post-peak behaviour is more ductile and the lateral deformations are smaller in comparison with the other types of boundary conditions. Compressive failure occurs under nonuniform triaxial stress-state conditions as a typical structural phenomenon.
The tests with brushes and teflon platens exhibit a lower peak-stresses, a more brittle post-peak behaviour, and a larger lateral deformations in comparison with the dry platens tests. The behaviour of steel brushes and teflon platens is similar except the final fragment of the post-peak softening curve. It is important to notice that softening of the specimen loaded with brushes is hampered by increasing deformations of steel rods forming the brushes. For the same loading range shear stresses exerted by the teflon platens decrease due to self-lubricating properties of teflon, so the post-peak behaviour is less disturbed in this case. The teflon platens act more favourable when the softening proceeds and for that reason they have been applied in the research program reported in the following chapters.

4.1. Stiffness of the loading apparatus

Considering the experimental set-up for strain-softening testing of concrete under compression, the stiffness of loading apparatus is of primary importance. For this kind of tests one of the loading platens can be either hinged or fixed, while the second remains fixed. The tests with one hinhed loading platen revealed a highly nonuniform deformation. The post-peak softening curve was more brittle than in tests with fixed loading platens, and complex structural response was found.

A more diffuse failure mode observed in tests with fixed platens changed into a localized failure with dominating shear macrocracks (Vonk [1989]). It is clear that application of fixed loading platens is more preferable for strain-softening tests, but still the stiffness of loading apparatus should be accounted for.
The longitudial stiffness of the testing machine can be expressed by the simple formula (Hillerborg [1989]):

$$\delta = \delta_o - F/k \qquad (4.1)$$

where δ - is the deformation transfered to the specimen, δ_o - is the stroke of the machine, F - is a force, and k - is the longitudial stiffness of the machine. This equation corresponds to the straigth lines with a constant slope but with different location what is visualized in Fig.4.6.
The upper crossing point between a line and F-δ curve for a material shows the stable test condition. The stability criterion-excluding the tangent position of the curve to the sloping line- can be written as:

$$k > -\frac{dF}{d\delta} \qquad (4.2)$$

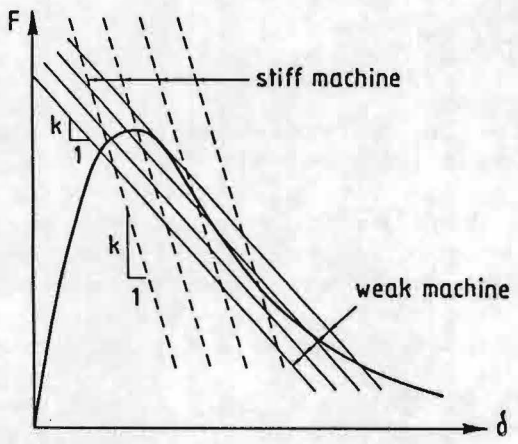

Fig.4.6 Stability condition for a load-deformation test (Hillerborg [1989]).

It is a common experimental practise to controll test condition by closed-loop fast compensating loading system what prevents this kind of instability.
Another kind of instability pertinent to the strain-softening tests is rotational instability entailed by the effect of nonuniform loading. Due to structural irregularities and nonuniform distribution of stresses in the specimen some factors connected with the performance of tests emerge as being important (Van Mier and Schlangen [1989], Vonk [1992]).They are:
- the effect of initially imperfect contact between the loading platens and the specimen caused by the eccentricity of load and nonparalellism of the platens of contact,
- nonflatness of specimen and loading platens surfaces,
- different curing conditions contributing instress and deformation gradient within the specimen.

While the influence of the last two factors can be diminished by controlled curing conditions and by application of the

special treatment to the surfaces sticking to one another (grinding the specimens and polishing the platens), the first one requires more attention.
A simple analytical model including rotational stiffness of the loading device has been proposed by Vonk [1992]. The parametric study using micromechanical computer simulation (UDEC program) has been performed also. The main characteristics of the model are given in Fig.4.7.

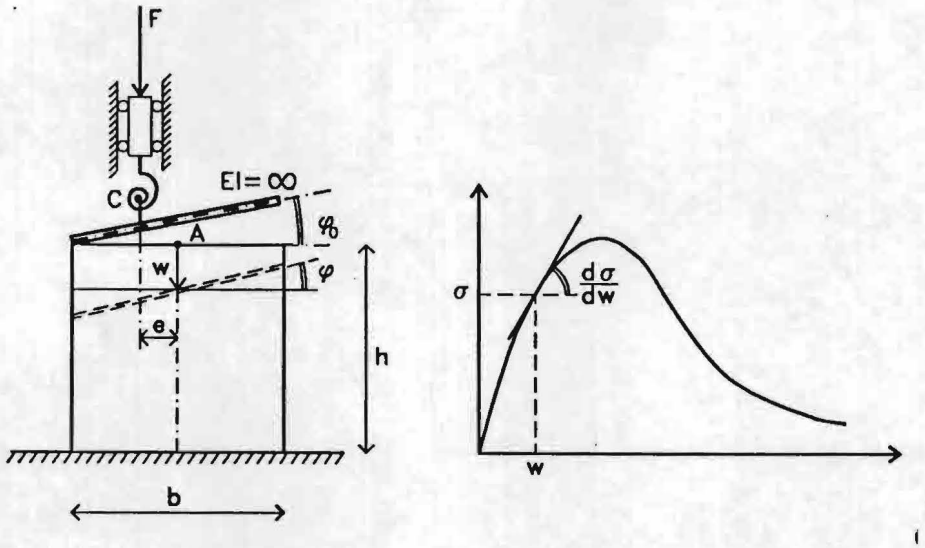

Fig.4.7. Model of a uniaxiual compression test (Vonk [1992]).

The specimen is loaded by rigid loading platens under deformation control conditions. The imperfections of loading are expressed in terms of eccentricity 'e' and initial angle of the contact plane 'ϕ_o'. The resistance of the loading machine to a rotation of loading platen is related to rotational stiffness C. The angle 'ϕ' is the angle of both loading platen and specimen surface,to the initial position of the specimen surface, and 'w' is the average deformation of the specimen. From the equilibrium equation:

$$\phi = (-db\sigma e + C\phi_o)\,[C + (db^3/12)(\frac{d\sigma}{dw})]^{-1} \qquad (4.3)$$

one gets stability criterion:

$$C > -(db^3/12)\,(\frac{d\sigma}{dw})_{critical} = C_{critical} \qquad (4.4)$$

Above equation puts a limitation on the inclination of a descending branch in softening tests. Since the stability criterion depends on $d\sigma/dw$,, the brittle types of concrete (HSC and LWC) are more prone to instability phenomenon. The higher specimens which behave in a more brittle way are endangered by this kind of instability also.
Another important factor is connected with the dimensions of specimen cross-section (bxd). The critical stiffness for the loading apparatus increases 16 times when the dimensions of the cross-section double. The research program reported in the following chapters aimes at the investigation of brittle types of concrete (HSC and LWC) so according to the above remarks,

there is a probability that instability phenomenon will occur. This is the reason for keeping the cross-sectional dimensions unchanged in size-effect invetsigations and differentiating only the height of the specimens.
The rotational stiffness of the loading apparatus applied in forgoing tests has been found approximately 1,35 x 10^9 Nmm/rad (Vonk [1992]).

5. Subject of research

5.1. Aim of tests

The aim of research program is to investigate the softening of concrete under uniaxial compression with special attention paid to structural factors and size effect e.i.:

- variations in compressive strength,
- differences in gravel size,
- variations in specimen's height.

To be able to proceed with comparisons between previously mentioned experimental results, the same three types of prismatic specimens have been used in compression tests.

5.2. Testing program

Four concrete-mixes are planned to be used for specimens of three sizes. Details are provided in Table 5.1.

Table 5.1. Number and dimensions of specimes.

concrete mix / type of specimen		high strength concrete C1	medium strength concrete with max. grain 16 mm C2	medium strength concrete with max. grain 2 mm C3	light weight concrete C4
(S)	100x100x50	4	4	4	4
(M)	100x100x100	4	4	4	4
(L)	100x100x200	4	4	4	4
		12	12	12	12

The total number of specimens equals 48. All tests are supposed to be performed under displacement controlled conditions in stiff testing machine originally designed for three-dimensional tests.

Deformations and strains are monitored through the LVDTs transducers and electric resistant strain gauges. Only one type of loading platens is applied: greased rigid steel platens with a teflon foil. The loading is assumed to increase monotonically at the rate of 1 μm/s. In this report all tests are denoted by following code:

- concrete mix (C1, C2, C3, C4),
- type and number of specimen (large -L, medium - M, small-S, each serie consisting of four specimens 1-4).

For instance: C1L 4 means 'fourth specimen of large type (100x100x200 mm^3) made of concrete-mix C1 (high-strength concrete)'.

6. Testing procedure

6.1 Preparation of specimens

Four concrete - mixes have been used for preparation of specimens with the three sizes. The details are provided in Tab.6.1, 6.2. C1 concrete is a high-strength concrete prepared with the admixture of silicafume, C2 and C3 concretes vary with respect to maximum gravel size (2 and 16 mm), and C4 is a light - weight concrete based on lytag gravel. Five prisms 600x150x150 mm and six cubes 150x150x150 were casted from each concrete mix. They were compacted on vibrating table. Later, the moulds were covered with wet burlap and plastic foil to prevent it from drying. After 48 hours they were demoulded and stored in water. After 40-50 days (details are given in the following section) blocks were taken out of the water and roughly sawn. The outer layers were removed and specimens were sawn out at random to avoid systematic error connected with the position in the mould. It is schematically shown in Fig.6.1. The direction of casting was marked on the specimens in order to keep the same loading direction with respect to the direction of casting. Then, the specimen were ground to their required size with special attention paid to the flatness and parallelism of the loading surfaces. For all tests reported herein, the deviations in surface flatness were always found to be less than ± 12 μm. After grinding, the specimens were immersed in water again and stored until the last few hours before testing.

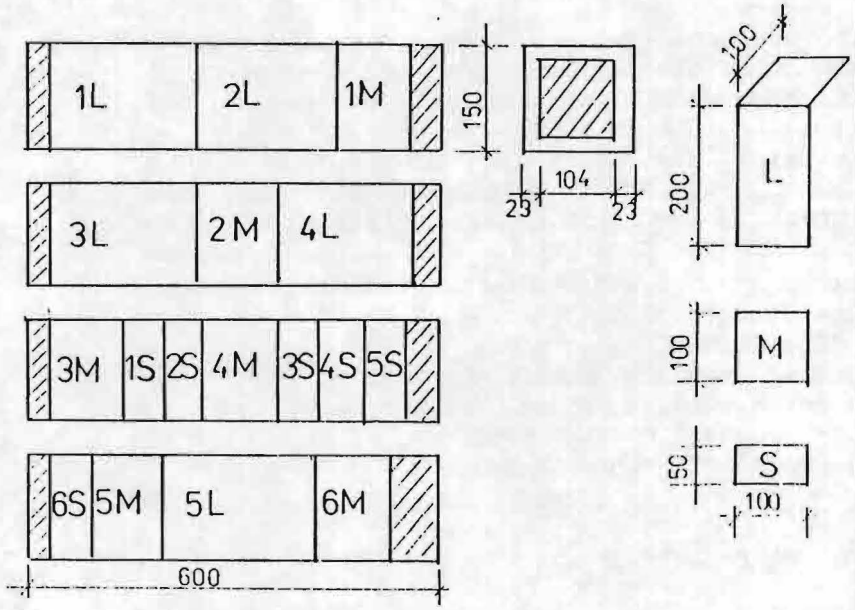

Fig.6.1. Location of specimens in concrete prisms.

Table 6.1. Characteristics of concretes.

Concrete	Mix proportions water:cement:sand: gravel	Type of gravel	d_{max} [mm]	Density [kg\m^3]	Cube compressive strength f_c [MPa]	Age [days]
1	2	3	4	5	6	7
C1	1:2.68:3.87:6.73 (sand 0-2mm, gravel 2-8mm, superplast 11 l\m^3, silicafume 45 kg\m^3)	river stone	8	2345	72.48	42
C2	1:1.97:4.74:7.11 (sand 0-2mm, gravel 2-16mm)	river stone	16	2341	35.28	48
C3	1:2.88:3.07:1.90 (sand 0-1mm, gravel 1-2mm, superplast 3.75 l\m^3)	river stone	2	2088	22.92	50
C4	1:1.38:3.60:2.70 (sand 0-2mm, gravel lytag 8 mm)	lytag	8	1957	34.30	55

6.2 Experimental technique

For all compression tests the triaxial apparatus built by Van Mier at Eindhoven University of Technology was used.
Tests were performed under displacement control conditions at constant loading rate 1 μm\s. Only one type of loading platens was used - teflon platens. The surface of the steel loading platens were first polished, what resulted in surface roughness of about 0.05 μm. Later, a thin layer of grease (Molykote BR2plus) was put between teflon foil and steel platen. According to data reported by Vonk, it was found profitable to use a very thin sheet of teflon foil - 0.05 mm. In all tests two Linear Voltage Displacement Transducers- LVDT type HBM W10-K, range 10 mm were used for displacement control.They were placed in a diagonal position opposite to each other, at a fixed distance of the center of the loading platens. A special, external signal generator was used for controlling loading parameters. Data were recorded at constant time intervals by HBM scanner and stored in the computer. The experimental set - up is shown in Fig.6.2.

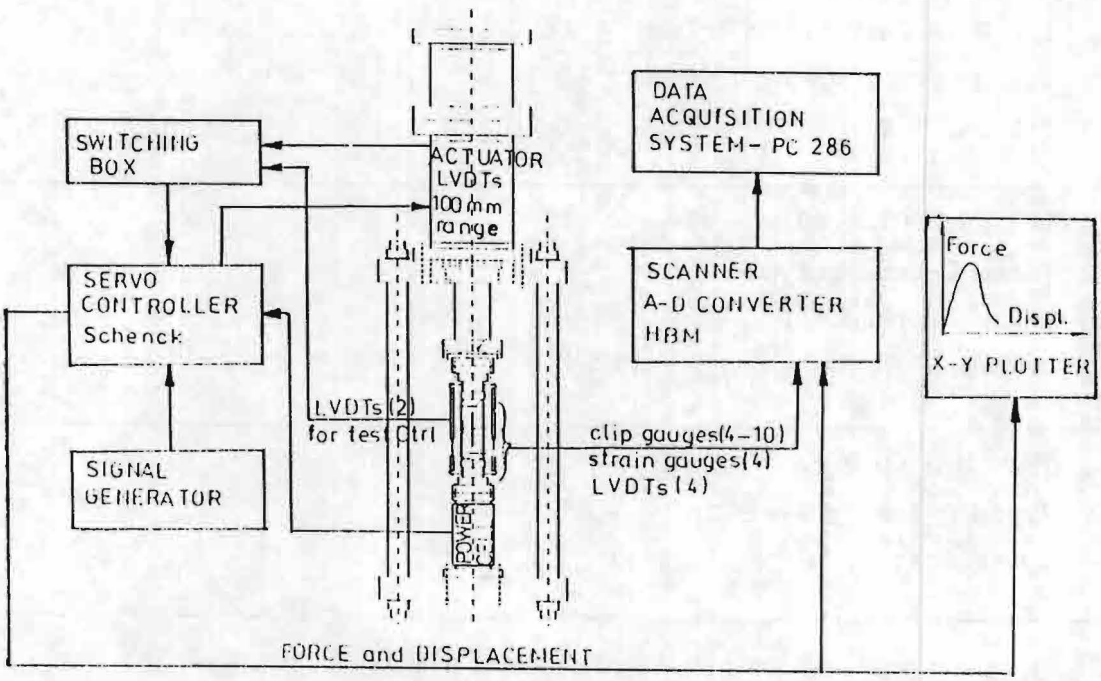

Fig.6.2. Experimental set - up for compression tests.

The forces were measured by means of load cell with a range 2000 kN. Axial deformations were measured by means of strain gauges and LVDTs. The strain gauges were glued to the four sides of the specimens, what is presented schematically in Fig.6.3.

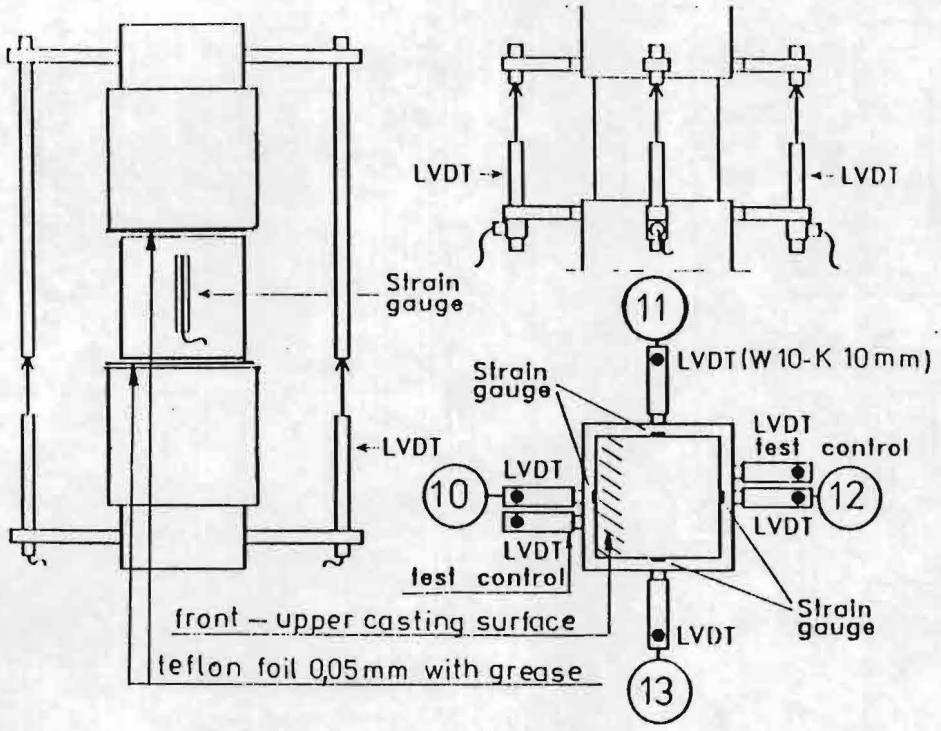

Fig.6.3. Location of strain gauges and LVDTs.

The length of strain gauges was 30, 60 and 120 mm (TML, PL - 30/60/120 - 11, maximum strain 2%) and corresponded to the specimen heights 50, 100 and 200 mm. For monitoring a rotation of the loading system, four LVDTs were attached to the loading platens at each side of the specimen (HBM, W10-K, 10 mm range).
The lateral deformations were measured by means of clip gauges.The clip gauges (maximum 10 sensors) were placed on the sides of specimen near the upper (top) and lower (bottom) edge, and in the middle (for 200 mm specimens). The bending of the steel strip in the middle of the clip gauge, upon which two strain gauges were fixed in a half Wheatstone bridge configuration, was a measure of the displacement of the two fixing point of the gauge. The fixing points, in the form of small circular plates, were glued according to the pattern presented in Fig.6.4. The clip gauges were used over a range of 12 mm. Calibration curves for clip gauges showed a linear relation in the range of 8 mm. All numbers from Fig.6.4, concerning particular strain and clip gauges are in accordance with the number of channels from HBM scanner, and are used consequently henceforth. To assure a good contact, the adjustable hinge was loosened when a loading platen was placed against the concrete specimen. During the tests the spherical hinge was fixed.

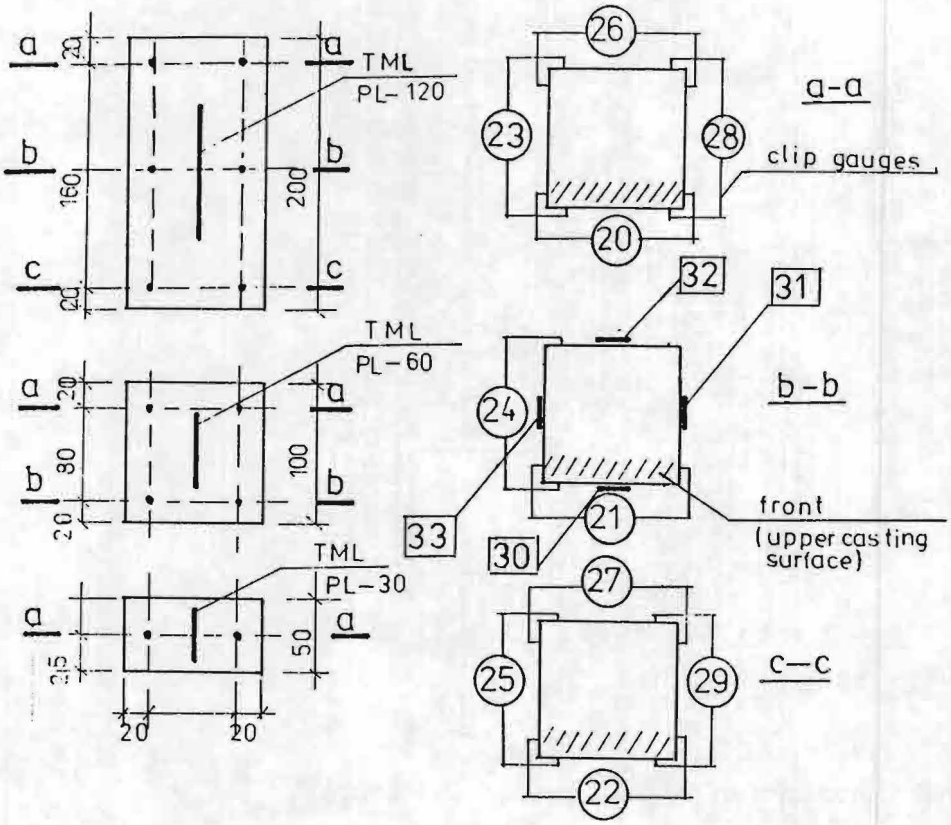

Fig.6.4. Location of the LVDTs, strain and clip gauges.

When placing a concrete cube in loading apparatus, the direction of casting was always perpendicular to the loading axis. The plane connected to the upper surface of the mould was also in the same position in every test.

6.3 Correction of the measurements

Since The LVDTs measurements include the deformations of a part of the loading platens they have to be corrected to obtain the real deformations of concrete block. Separate tests were carried out to determine the deformations of the loading platens with the teflon foil in between. Fig.6.5 present deformations of a teflon platen up to the level of 500 kN. Deformations of teflon platens were linearly approximated and subtracted from the LVDTs readings, together with elastic deformations of steel platens. The initial settings have been eliminated in Fig.6.5. They are due to nonflatness of the specimen surfaces and nonparallelism of loading platen and specimen surfaces. A zero correction was carried out to the stress - displacement (LVDTs) and stress - strain

(strain gauges) curves by translation along the horizontal axis. The zero strain was calculated from the maximum tangent modulus and the point of corresponding stress.

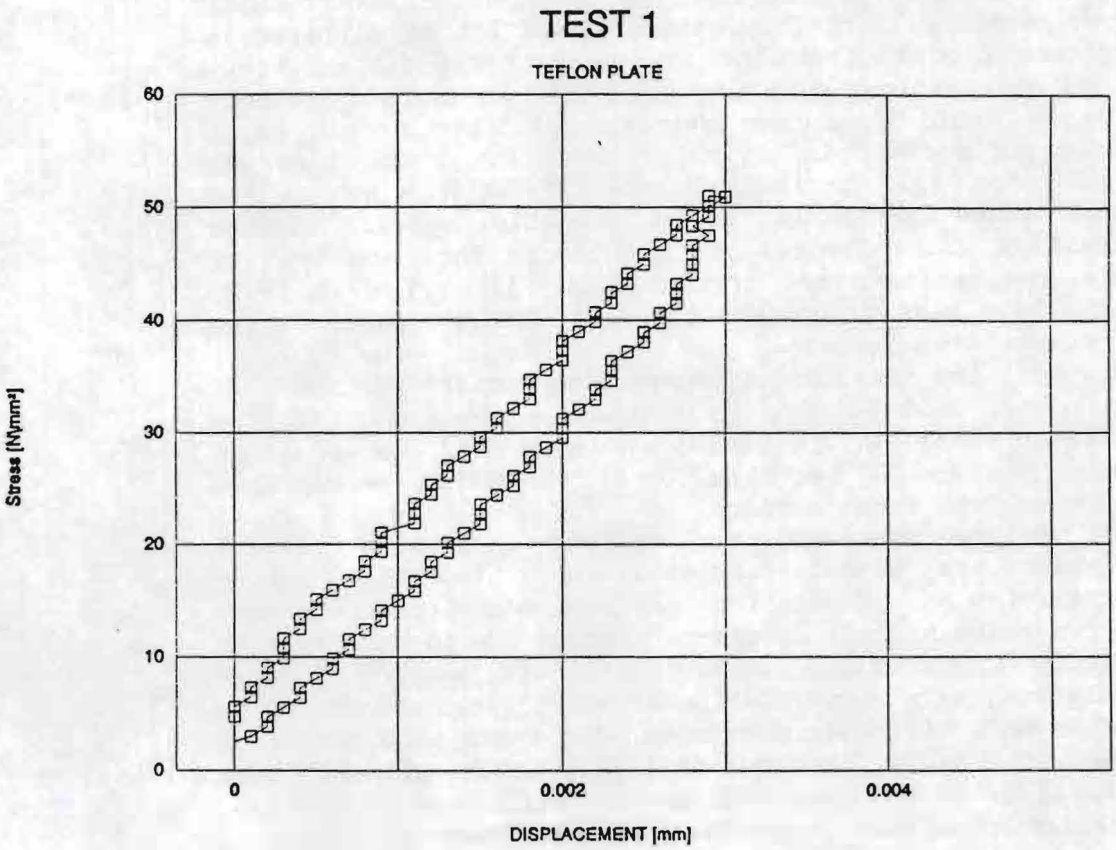

Fig.6.5. Deformations of a teflon platen up to 500 kN.

7. FAILURE MODES

One may urge that the mode of failure is the result of a particular test configuration. Notwithstanding the fact that properties and compositions of concretes are very different, the modes of failure are more or less similar for a particular specimen geometry. Certainly, there are a lot of differences in fracture process from the micromechanics point of view. Since all observations were performed with an unaided eye only macrocracks could have been detected. Another factor which should be put forward is drying process. The drying time was not equal for all specimens (from 1.5 to 4.0 hours) and in some cases shrinkage could possibly entail surface microcracking. Some typical crack patterns for each type of concrete and specimen are presented in Fig. 7.1, 7.2, 7.3, 7.4. They have been drawn from the final failure modes at the end of compression tests.

In every test the position of the casting surface was the same (front), and loading axis was perpendicular to the direction of casting. It certainly influenced the fracture process since in 30 tests (62.5 %) the first macrocracks started from 'the front surface'.

For HSC S-type specimens are spalled into many conical parts which are almost completely separated. For M-type specimens a few macrocracks form and a kind of 'core response' is observed. The highest specimens rupture due to uncontrolled propagation of a single shear macrocrack passing through the whole specimen. Some additional macrocracks developed in the bottom part of L-type specimens. The tests were performed with the upper hinge fixed but still all tests with HSC were strongly affected by the rotation of the loaded boundaries. A localized snap-back behaviour can be observed which is balanced by remaining undamaged structure of the specimen. Fig.7.4 gives an example of typical deformations of lateral surfaces for M-type specimen. At every post-peak loading step there is a part of specimen which exhibits snap-back behaviour and yet the global stability is maintained.

The stress-deformation curves are obviously influenced by the rotational stiffness of the specimen and loading apparatus. It is a similar phenomenon like for concrete loaded in tension (Hordijk et al.[1989]). Even the smallest heterogeneity of the material can trigger considerable redistributions of stress and strain in concrete. However it is believed that softening of concrete under compression is more ductile than softening in tension due to friction in the shear cracks.

For C2 concrete (maximum aggregate size 16 mm) the conical fragments in S-type specimens are bigger than for HSC. The corners spall and some conical pieces remain in the core region. The height of these pieces equals the size of the specimen. There are cone-shaped cement matrix elements on the top of larger aggregate particles. M-type cubes are fractured rather uniformly. The cohesive forces between segments separated by macrocracks are still present at the end of test. The crack arrest phenomenon plays an important role in crack formation process. Cracks pass around aggregates and are often hampered by tough gravels.

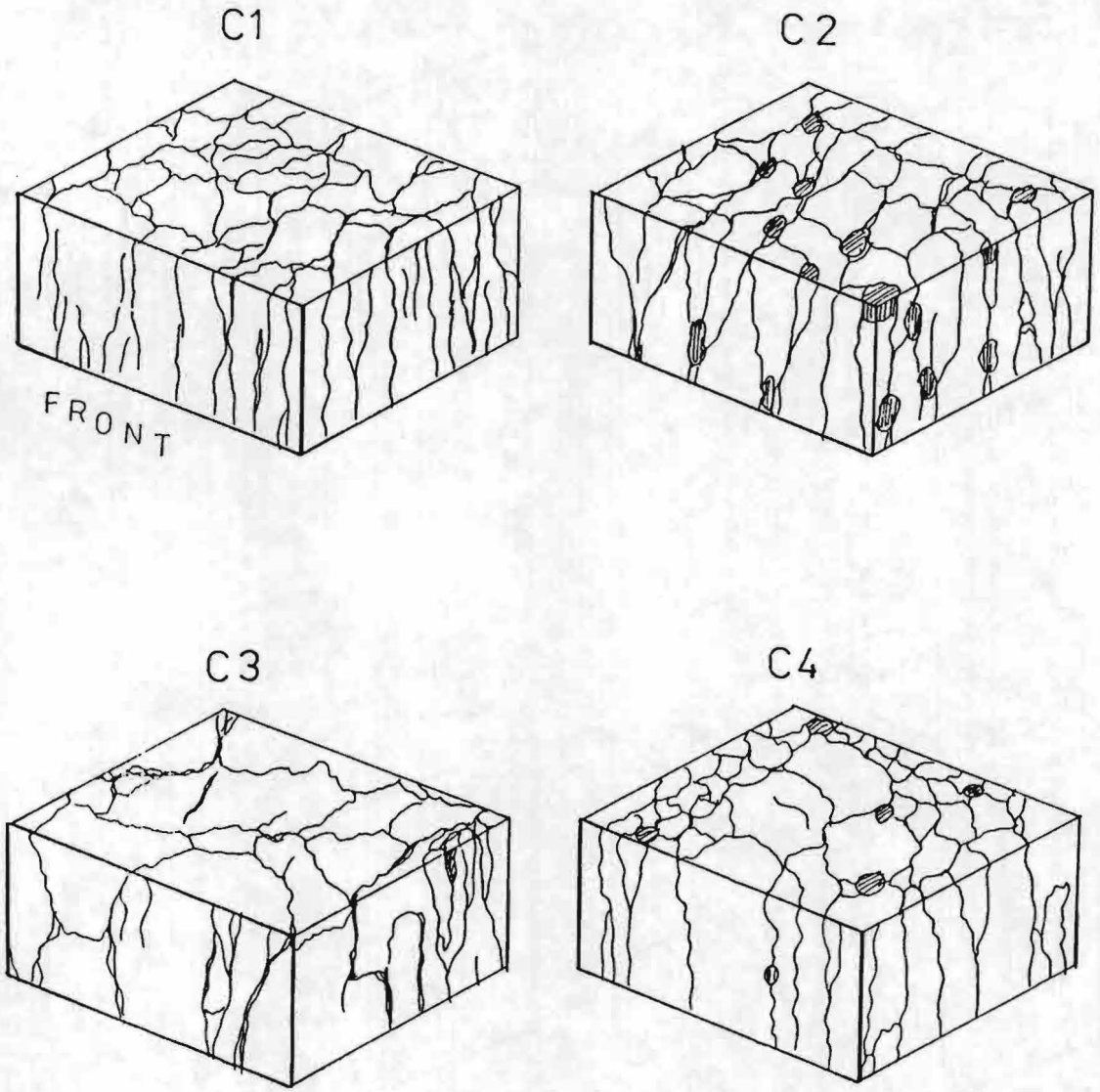

Fig.7.1. Typical crack patterns for S-type specimens.

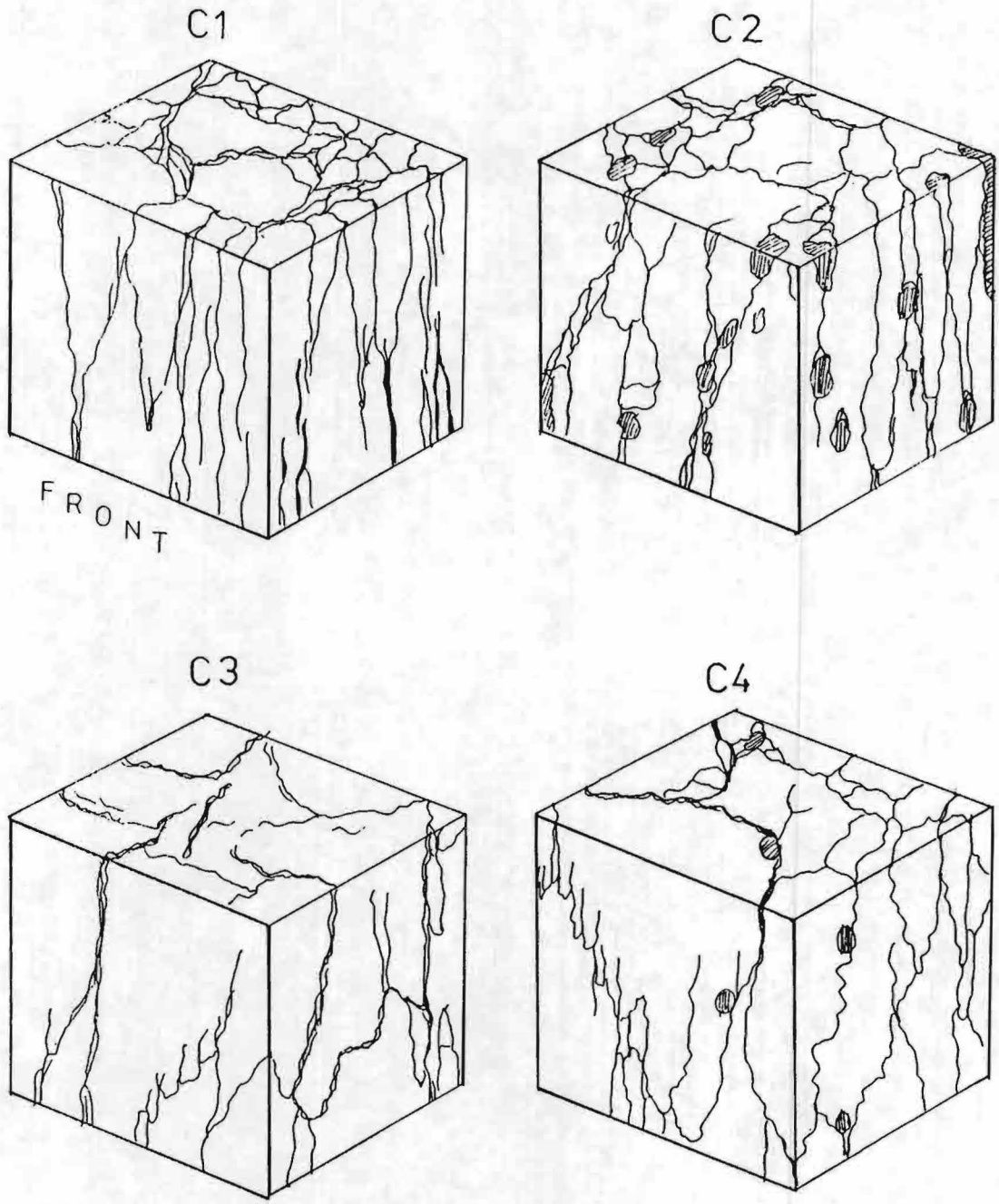

Fig.7.2. Typical crack patterns for M-type specimens.

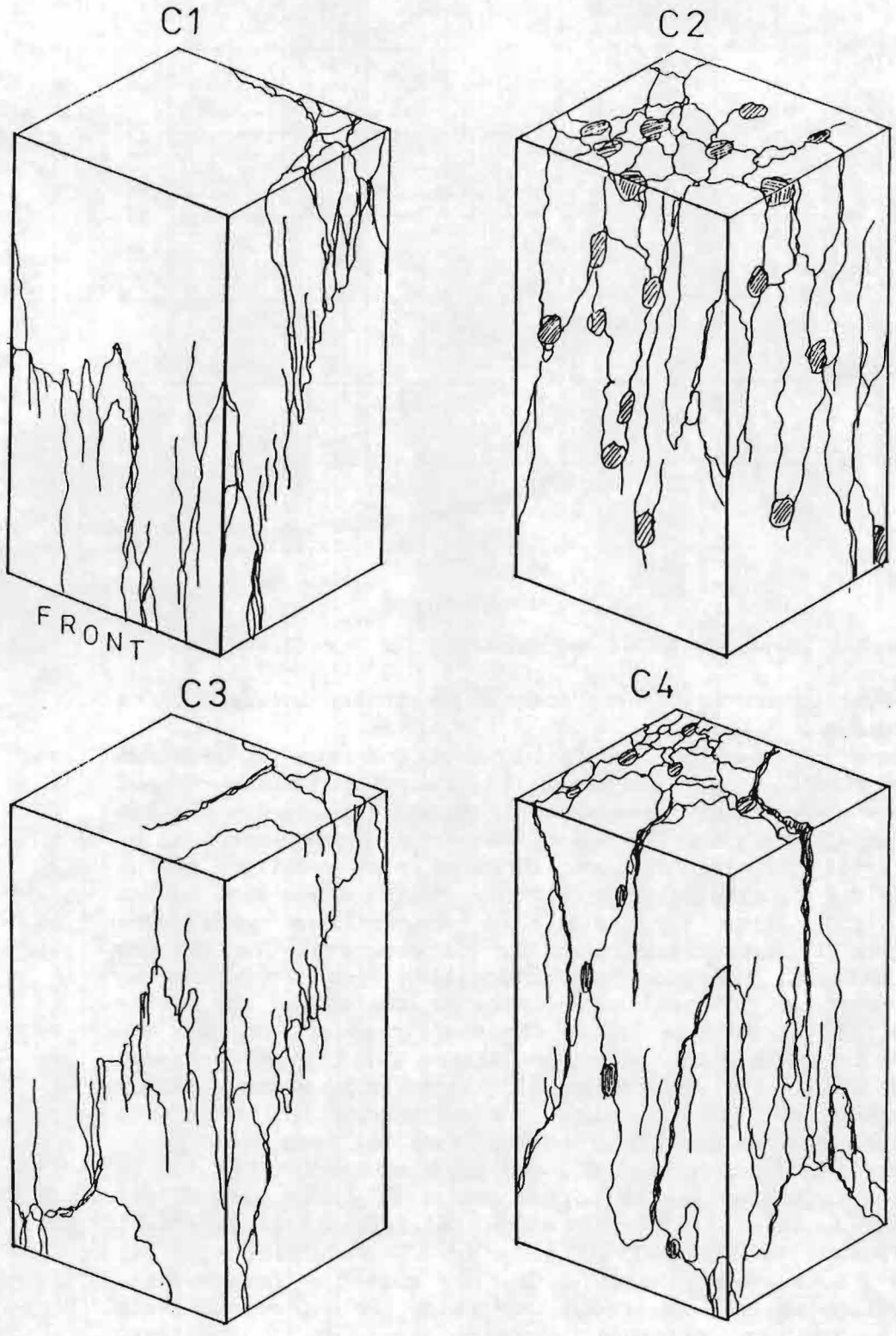

Fig.7.3. Typical crack patterns for L-type specimens.

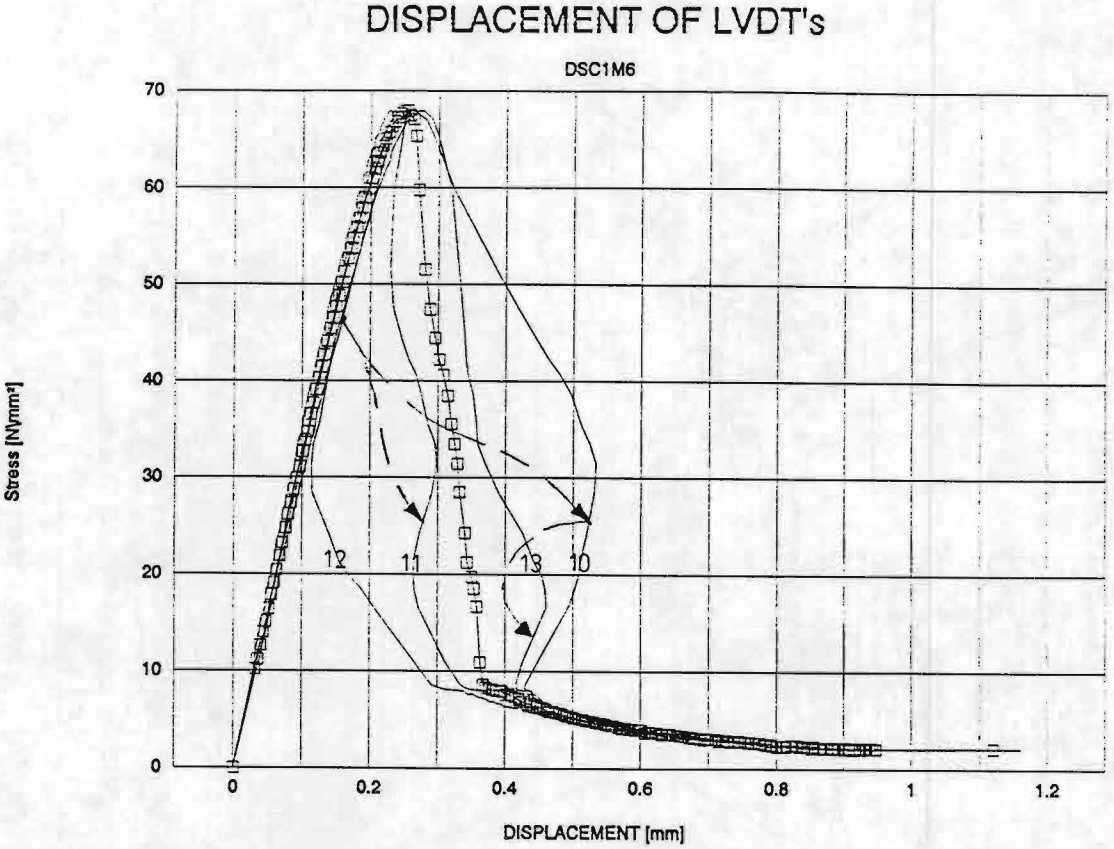

Fig.7.4. Separate LVDTs measurements for specimen C1M6.

For L-type prisms fracture process concentrates in upper parts of specimen.
Specimens of S series manufactured of concrete C3 (maximum gravel size 2.0 mm) disintegrated according to cone-shaped fracture mode either. Dimensions of conical pieces are similar like for C2 concrete. Planes of macrocracks are separated by many small debris. Failure surfaces show smaller grains crumble due to sliding with friction. M-type cubes were broken in several large fragments. The deformations were more localized in macrocracks than for C2 concrete. The feature which discerns this concrete composition from the others is the presence of internal macrocracks on the top and the bottom planes. They propagate inside the boundaries of specimen and do not coincide with the edges. Again, for L-type specimens the fracture is a rather localized phenomenon. After inspection of the fracture modes no particular cracks concentration on the top or bottom level has been noticed.
Concrete C4 (lytag gravel 8.0 mm) absorbed much water due to hygroscopic properties of porous grains of lytag. Cement gel penetrated into the grains and reinforced matrix-gravel interfaces. The internal structure of the resultant material became more homogeneous. Cracks passed through the aggregates, as well as around the grains. Both processes were visible in the fracture planes. For cube specimens macrocracks split the volume into a few large cones. Fractured elements stuck together at the end of test - the horizontal

part of descending branch is long due to the presence of cohesive forces. The large L-type prisms were fractured more intensively at the upper part.

It seems that despite meaningful differences in composition and mechanical properties of particular concretes, failure mode is mainly affected by the specimens size. Certainly, there exist differences in fracture process at the micro-level, but the overall macrocracks pattern is the result of interaction between testing conditions (stiffness of loading apparatus, kinematic conditions at the specimen-loading platens interface) and specimen size.

It is known that microcracking process and slow crack growth begin in the pre-peak region (Hsu et al. [1963]). The observations of the initiation of macrocracks formation at the outer layers of specimens started at the descending branch at stress level $(0.7\text{-}0.85)\sigma_u$. Unfortunately, the important phenomena connected with the microcracks formation could not be monitored. During this phase the differences in internal structure of concrete play dominant part in fracture process. In the subsequent post-peak range deformations more and more localize in macrocracks which evolved from the field of microcracks. In the final stages of post-peak testing, open for direct visual observations, fragmentation is far in progress and crack patterns are size dependent.

The inward direction of failure process (from outside to the inside) has been reported by some researchers (Van Mier [1984]). Considering the fact that macrocracks at the lateral surfaces form well beyond post-peak stress, the opposite hypothesis may hold true. For several specimens (especially for C3 concrete with maximum gravel 2.0 mm) numerous internal macrocracks, without boundary connections, have been noticed at the horizontal surfaces of specimens.

In specimens of all sizes vertical splitting cracks and inclined shear cracks have been found. Only for large specimens of C1 concrete failure took place due to propagation of a single crack (inclined shear crack). Several inclined cracks have been always observed after fragmentation of the specimens. The number of separated fragments depends on specimen size. The larger the specimen is the bigger the pieces are after fragmentation. For smaller prisms many small debris rest after fracture.

8. SIZE EFFECT IN COMPRESSIVE STRENGTH

In Fig.8.1, 8.2, 8.3, 8.4 all values for peak stresses for each concrete composition are presented.

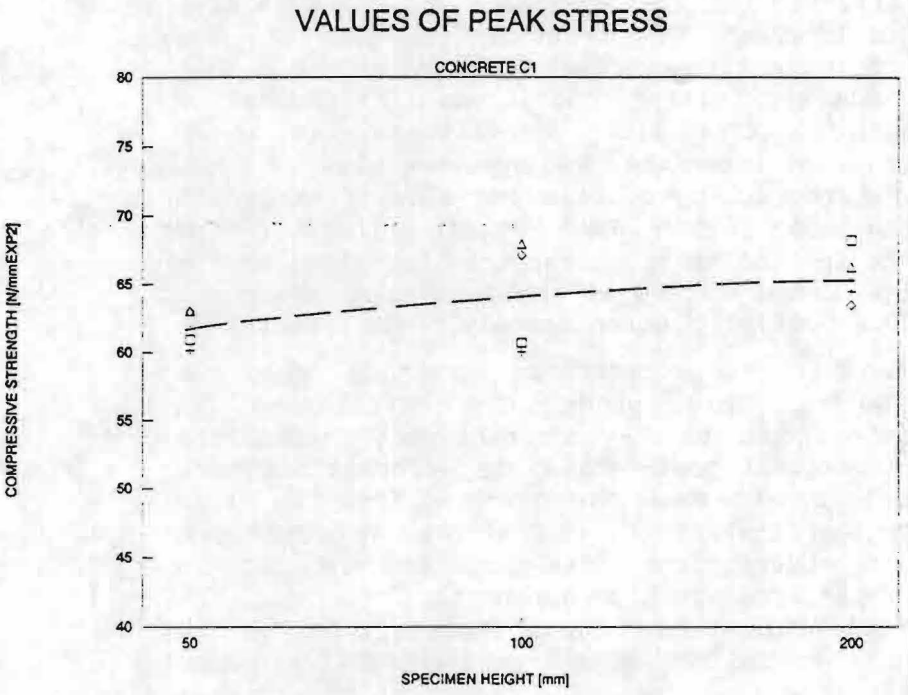

Fig.8.1. Values of peak stress for concrete C1.

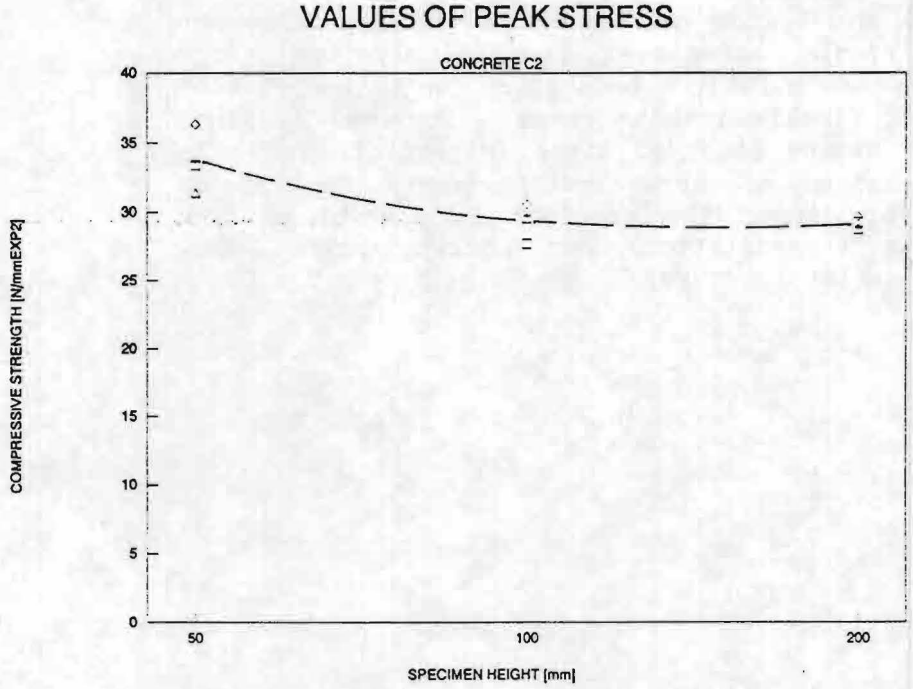

Fig.8.2. Values of peak-stress for concrete C2.

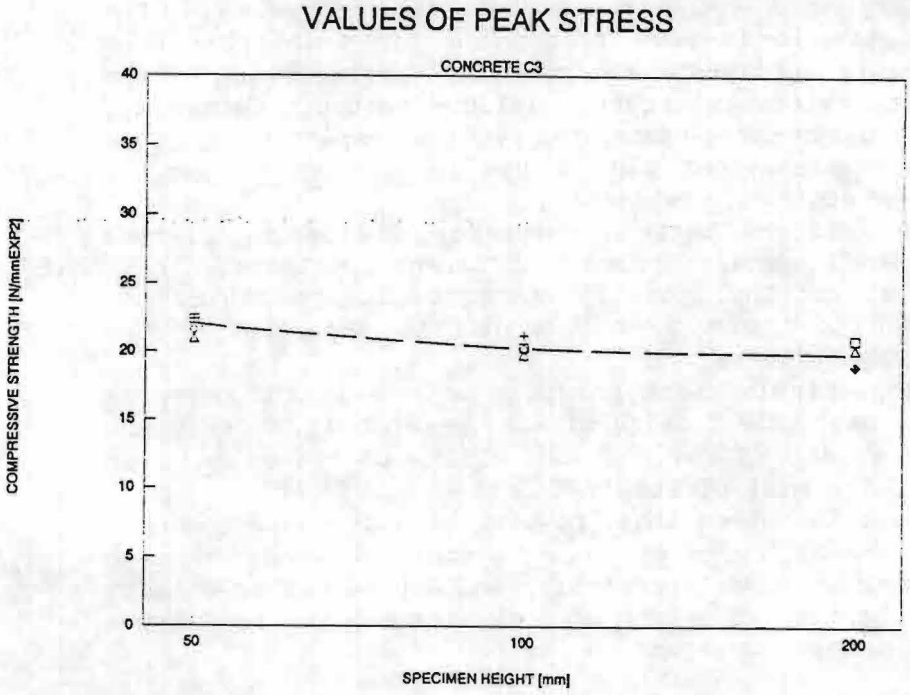

Fig.8.3. Values of peak-stress for concrete C3.

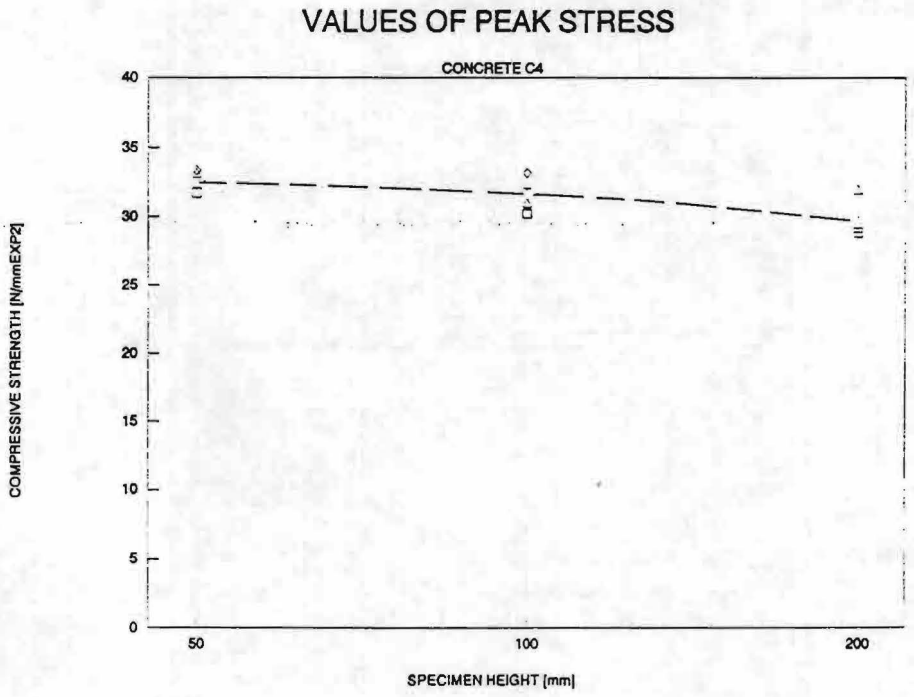

Fig.8.4. Values of peak-stress for concrete C4.

Despite the fact that no rigorous statistical analysis has been performed, one may notice the influence of the height of specimen and type of concrete to be statistically significant. For concretes C2, C3, C4 it is the same tendency for peak stresses. They tend to decrease with the increase of the specimen height. It is more pronounced for transition from S-type to M-type specimens. For cube (M) specimens and L-type specimens peak-stresses reach similar values. Generally, presented findings are close to results reported by Vonk [1992]. Some explanations can be put forward as a possible causes for the observed phenomena :

- friction conditions between specimen and loading platens influence small specimens more than larger specimens,
- direction of casting, position in prism before sawing and drying conditions are by all means the important factor changing peak stresses,
- assuming that stable crack growth commences in the pre-peak region we may expect size-effect predicted by fracture mechanics (Bazant [1976]) - peak stress decreases with an increase of the size of specimen.

It is important to notice that, however the types of concrete are very different (type of gravel, grain dimensions), the changes in peak stresses are similar and depend rather on test conditions. The average values of peak stresses for four types of concretes are put together in Fig.8.5.

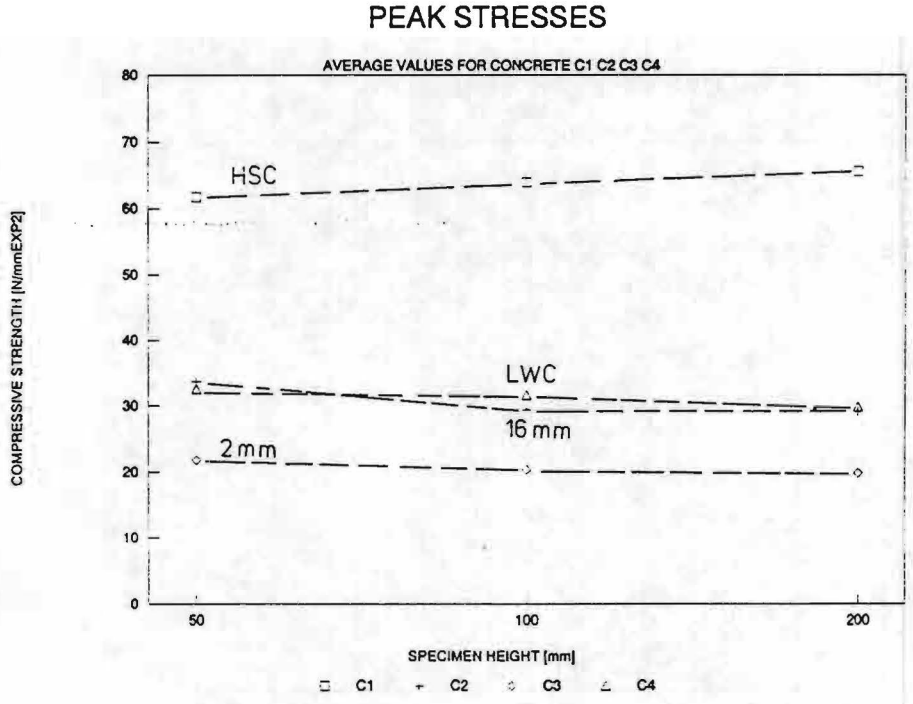

Fig.8.5 Average values of peak stresses for various concretes.

The opposite tendency is observed for HSC (C1). What is rather unexpected - with the increase in specimen size the peak stress increases also. A possible explanation for this observation provides the analysis of the failure mode for HSC. Three out of four L-type specimens failed in an uncontrolled way due to propagation of an inclined macrocrack passing through the specimen height, just after post-peak stress had been reached. For M and S specimens a localized snap-back behaviour was observed almost in every test, despite the global stability had been maintained in the whole range of descending branch. It is in good agreement with Van Mier suggestion (Van Mier [1984]) claiming the localized deformations to be the main reason for failure of concrete in uniaxial compression. Post-peak stress-displacement curves for different specimen dimensions are almost identical what can be seen in Fig.10.4 and Fig.10.6. For HSC the microcracking process is less intensive than for normal concrete (Carrasquillo et al. [1981]). High strength concrete behaves elastically up to a higher stress-strain ratio and can be analyzed, in this range, in terms of bulk behaviour of continuous material. According to experimental data (FIP/CEB Bulletin d'information No.197 [1991]) the observed failure modes of HSC under compression indicate that failure occurs when a certain ultimate tensile strain is attained in the direction perpendicular to the loading axis. The potential energy provided by the loading system is stored as a strain energy of the continuum and dissipated mainly in a friction and microcracking process until uncontrolled crack propagation takes place. For particular loading set-up (stiffness of loading apparatus and boundary restraints) the strain energy demand for macrocrack creation is higher for larger specimens due to bulk behaviour in the pre-peak region. It may the reason that peak stresses increase for L and M-type specimens while compared with the smallest ones.

For all types of concrete the strain at the peak stress measured at the lateral surfaces was always behind the strain value measured via overall displacement between the loading platens. The difference between both measured strains was less pronounced for higher specimens. It is presented in Fig.8.6 for concrete C4.

This differences can be the result of the load-application system and kinematic conditions at the specimen-loading platens interface (Van Mier [1984]). Partially, it can be also attributed to the failure mode connected with the size of specimen and to the shrinkage effects.

The discrepancies in surface and overall strains increase after peak stress level is reached. Remarkable unloading of the outer surface layers of the specimens is observed. Loading capacity of the fractured element is provided mainly by the intact specimen core. For different sizes of specimens location and orientation of macrocracks change. For smaller specimens fragmentation is very intensive and outer layers with strain gauges are unloaded even in the ascending branch of the stress-strain curve. For higher specimen (L) a few large fragments rest after fragmentation which can still transfer stresses, so the differences in strains become less.

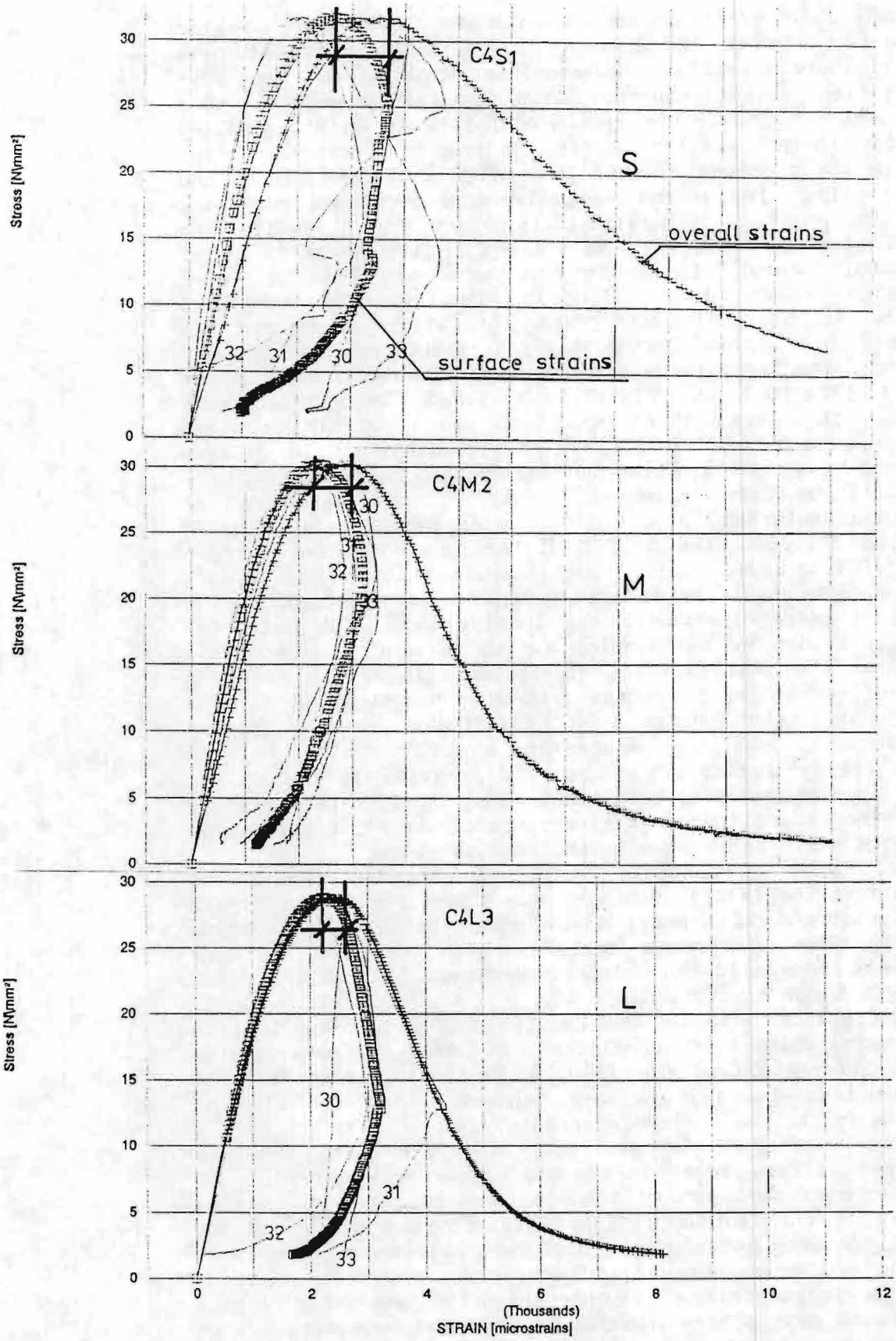

Fig.8.6. Differences between surface strains and overall strains for S, M and L-type specimens of concrete C4.

9. Influence of gravel size on the post-peak behaviour

As it was already mentioned, it is believed that for elements in tension the fracture energy increases with increasing maximum aggregate size and its volumetric amount. The crack formation in concrete under compression is connected with tensile lateral strains so we can expect the same factor to be responsible for changes in in fracture energy of concrete under compression. More information can be deduced from the analysis of stress-strain curves and deformability of different kinds of concrete.

Concrete C3 (maximum gravel 2.0 mm) exhibits less steep post-peak stress-strain curve in comparison with concrete C2 and C4. Stress-strain curves in the post-peak region are given in Fig.9.1 for different types of concrete. They are presented as the envelope curves - characterized by the minimal and maximal values for a particular type of specimen . It is a result of plastic properties of the cement matrix. Small gravel inclusions make the concrete-like material homogeneous. Its behaviour is fairly brittle under tension and deformable under compression. The post-peak stress-displacement curves are placed relatively collinear for concrete C3 (Fig.11.2) what is characteristic for the localization of deformations. It is rather unexpected in the presence of long horizontal post-peak curve. There are also some characteristic features in the crack formation process. Macrocracks form the bands of smeared microcracking and have no sharp edges. Groups of microcracks contribute into areas of strain localization what can be the explanation for this plastic-brittle behaviour.

The reproducibility of stress-strain curves gets worse with the increasing of maximum gravel size. Scatter of the results is the biggest for concrete C2 (maximum gravel 16 mm). For concrete C4 stress-displacement curves are essentially the same as for concrete C2 what reflects similar failure process. Since the surfaces of lytag gravel were impregnated and reinforced by cement gel cracks often propagate through the interface of the cement matrix and gravel like it is in concrete C2 with tough natural aggregates. Influence of type and dimensions of aggregates is not as explicit as one would expect.

The strains at peak-stress for each type of concrete and specimen are shown in Fig.9.2. They are equal to 2.3 o/oo for C1 concrete and independent of specimen size. In relation to the localized failure of C1L and C1M-type specimens and energy dissipation according to bulk behaviour, it can be the reason for higher peak-stress in tests with larger specimens. The strain at peak-stress for concretes C2, C3, C4 drops with increasing specimen size. The deformability of concrete C4 is the largest among them. Discrepancies among strains measured for different specimen sizes emerge from the disturbances entailed by boundary conditions (Van Mier [1984]).

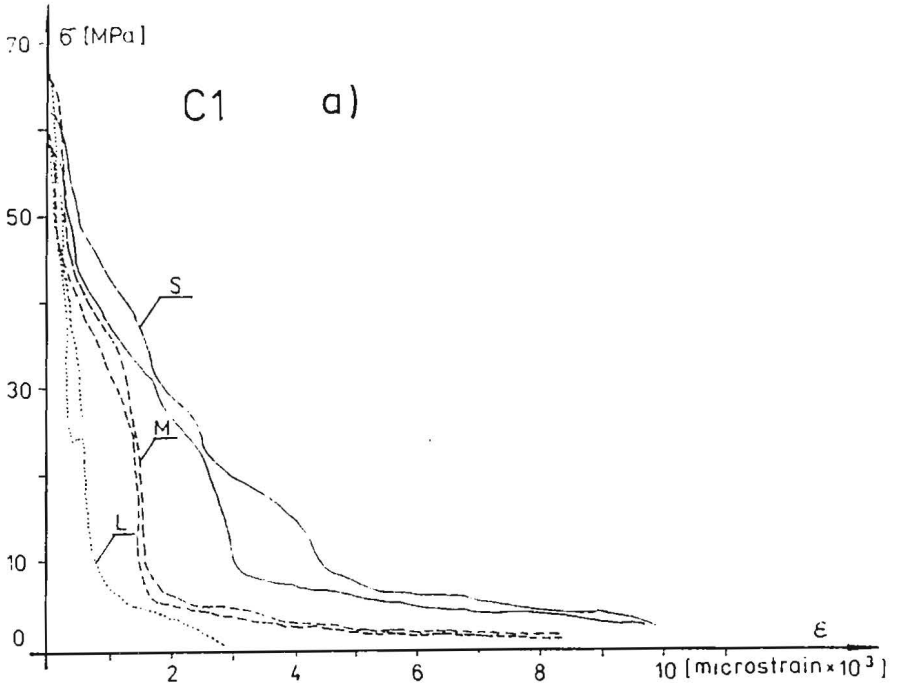
σ [MPa]
C1 a)
70
50
30
10
0
S
M
L
ε
2
4
6
8
10 [microstrain × 10³]

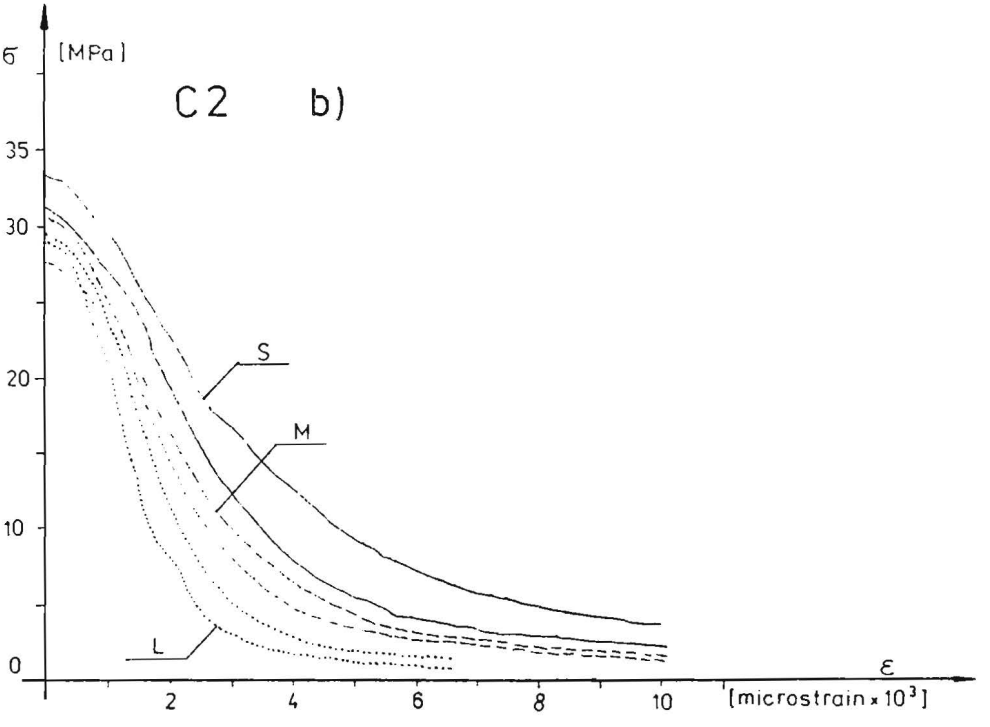
σ [MPa]
C2 b)
35
30
20
10
0
S
M
L
ε
2
4
6
8
10
[microstrain × 10³]

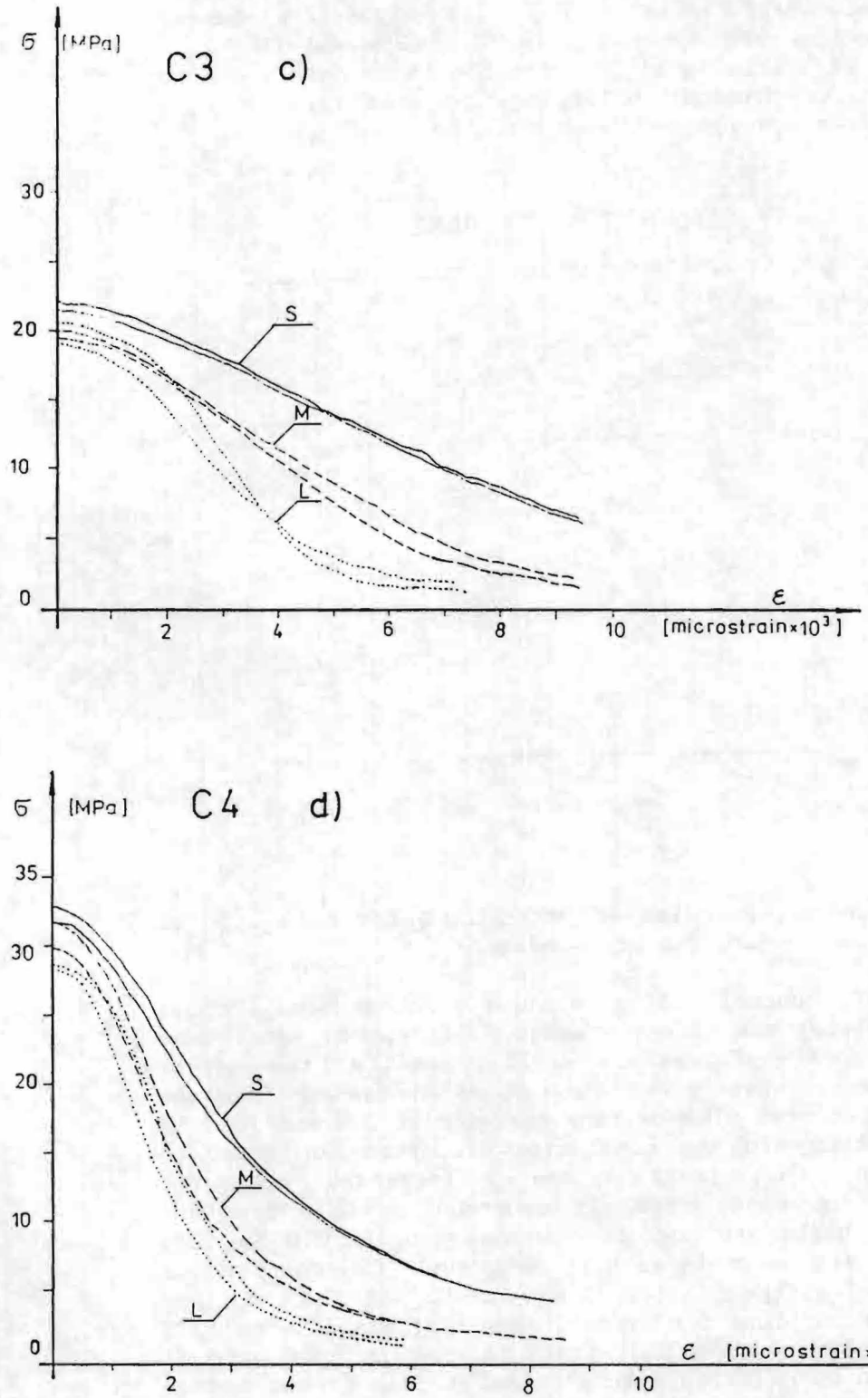

Fig.9.1. Post-peak stress-strain curves for concrete C1 (a), C2 (b), C3 (c) and C4 (d).

The comparison of fracture energies for each concrete composition provides useful informations about component of fracture energy connected with the size and type of gravel. Details about the procedure for fracture energy evaluation are given elsewhere (chapter 11). The highest elementary fracture energies are for concrete C1 (HSC) and C4 (lytag gravel) (Fig.11.8 and Fig.11.9). For HSC it is mainly due to high compressive strength enlarging the area under stress-strain and stress-displacement curves.

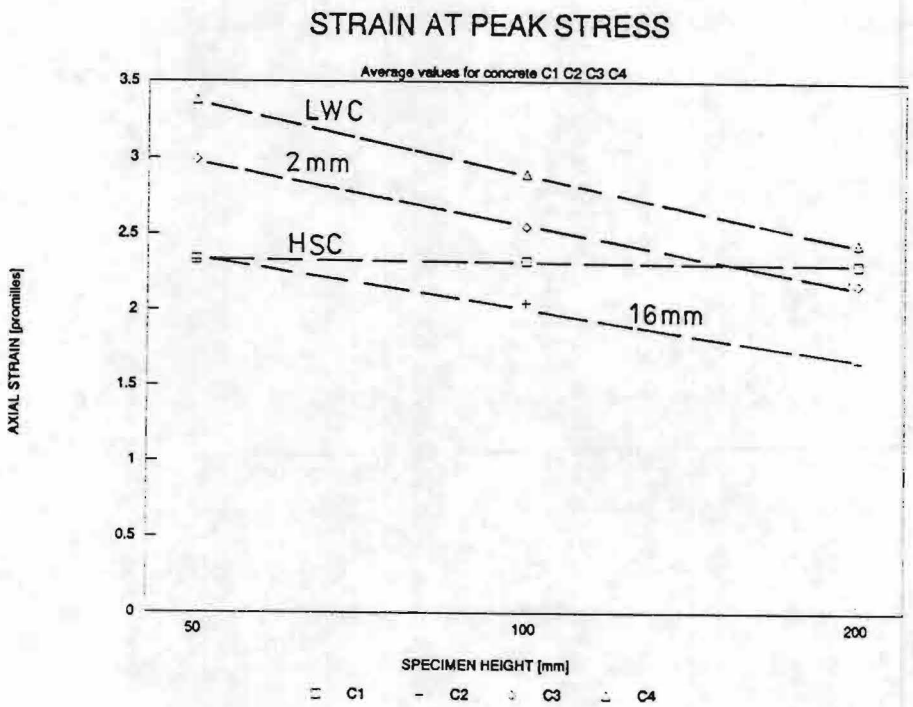

Fig.9.2. The average strains at peak-stress for each type of concrete and specimen .

Composition of concrete C4 is relatively homogeneous. Porous particles of lytag are strongly embedded in cement matrix and significant cohesive forces are still present at the end of post-peak curve, what gives rise to increased fracture energy. For concretes with maximum gravel size 2.0 and 16.0 mm it is in contrary to the conclusions reported for concrete under tension, that fracture energy increases with the increasing of aggregate size. In compression tests fracture energies were higher for concrete with aggregate 2.0 mm (C3) than for ordinary concrete with 16 mm gravel (C2) despite the lower compressive strength (22.93 MPa for C3 and 35.28 MPa for C2). Weight proportions for overall amount of gravel were 1275 kg/m^3 (C3) and 1920 kg/m^3 (C2). Fracture energies per unit of volume are in correlation with strains at peak-stress and go up with the increasing of strains and decreasing specimen size. The only exception is HSC having equal strains for every type of specimen. The reason for this is somewhat different mechanism of energy dissipation in concrete under compression.

10. Lateral deformations

The mode of lateral deformations differs substantially in relation to the height-width coefficient of the specimen. For smaller specimens (h/w = 0.5 and 1.0) lateral deformations are rather uniformly distributed. It is presented in Fig.10.1 that for concretes C2 C3 C4 deformations measured by separate clip gauges are almost equal.

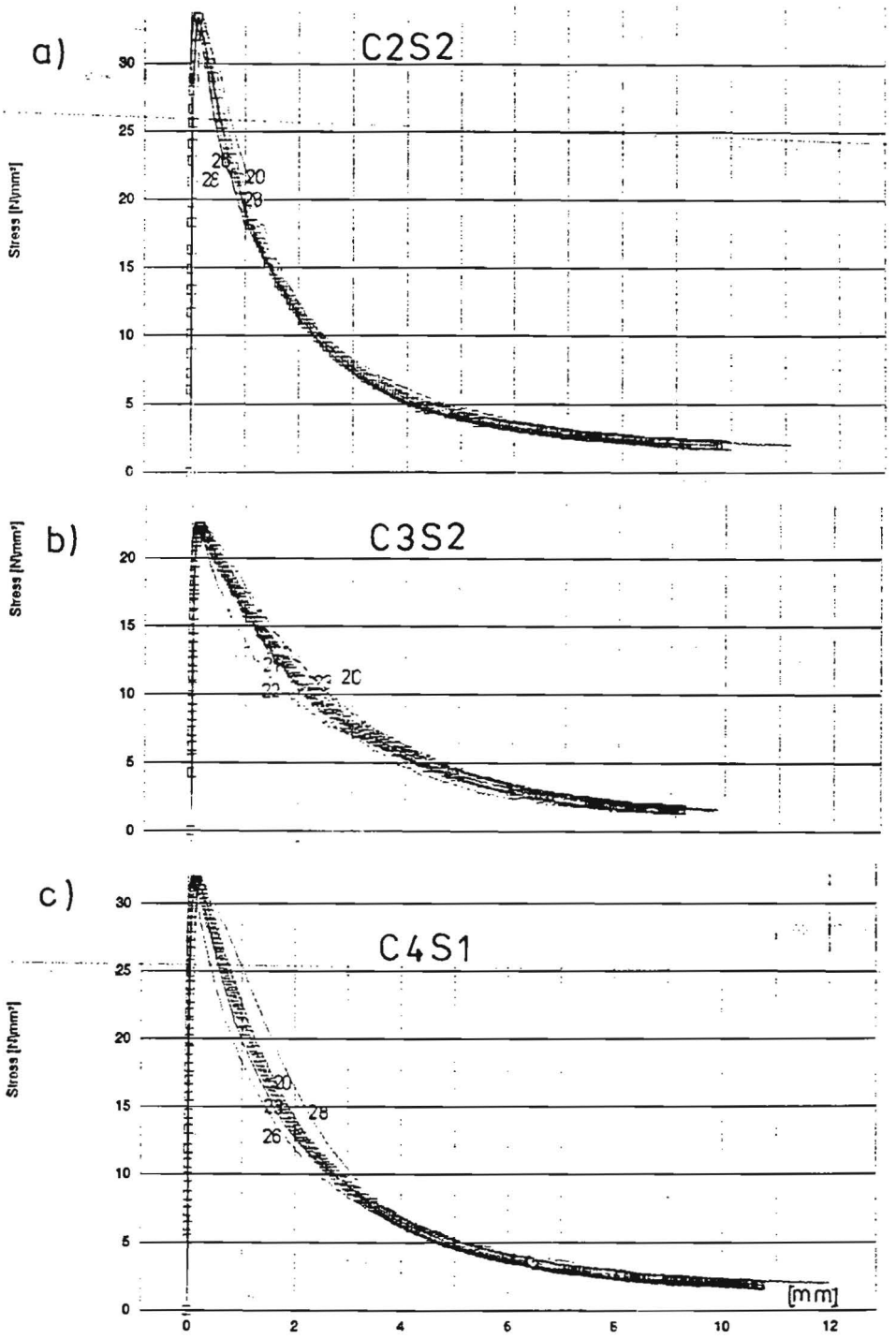

Fig.10.1. Separate and average lateral deformations for S-type specimens for concrete C2-(a), C3-(b), C4-(c).

The average lateral deformations for specimens from Fig.10.1 are put together in Fig.10.2.

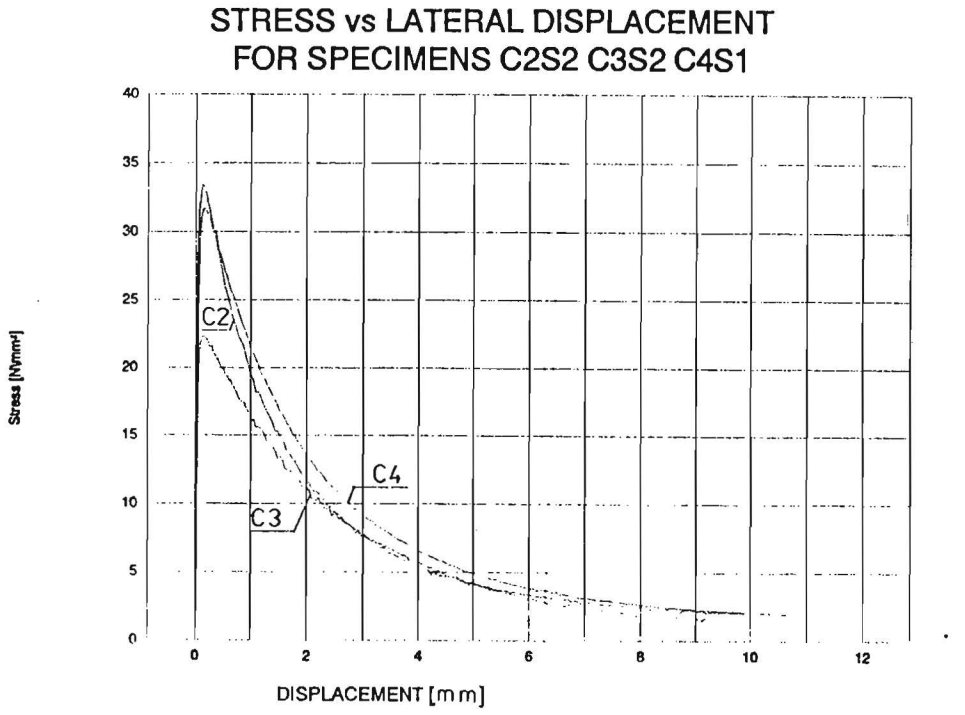

Fig.10.2. Average lateral deformations for S-type specimens from Fig.10.1.

The curves are similar and seem to be independent of concrete composition. Boundary conditions at the top and bottom surface of specimen are responsible for such uniformity.
Lateral deformations do not change a lot for M-type specimens, however the scatter of the individual read-outs is bigger. Figure 10.3 (a), (b), (c) presents the examples of lateral deformations for concretes C2, C3, C4. Concretes are represented by 'Top' and 'Bottom' lateral deformations measured by separate clip-gauges followed by the curve of average deformations marked with symbols. The third figure for each concrete presents the difference between 'Top' and 'Bottom' deformations.
The onset of strain localization is connected with the volumetric expansion. For concretes C2 and C3 there are no favorable directions of the growing of lateral deformations while for concrete C4 cracks concentrate more in the vertical plane, parallel to the loading axis.

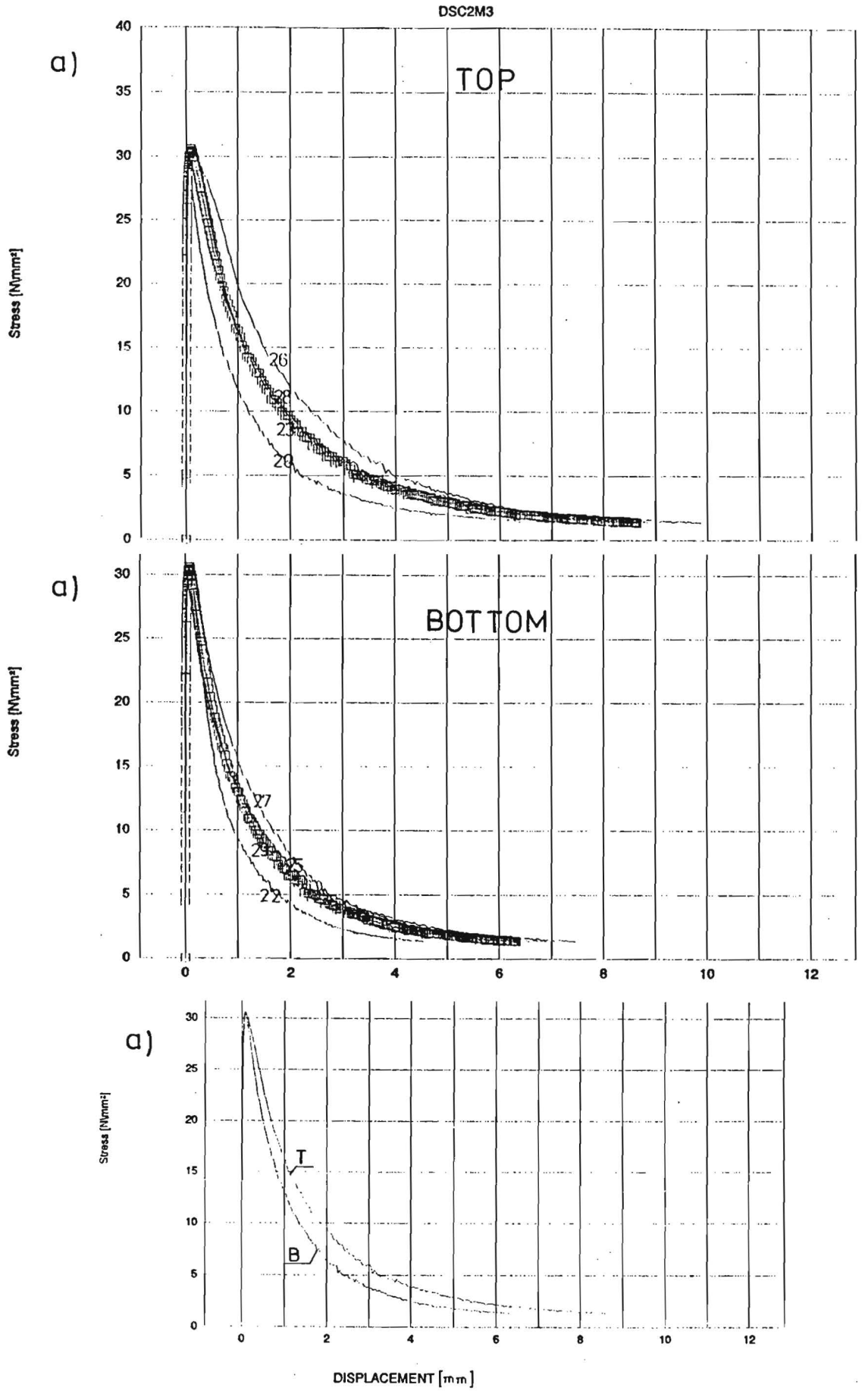
DSC2M3
a)
TOP
Stress [N/mm²]
26
23
20
a)
BOTTOM
Stress [N/mm²]
27
25
22
a)
Stress [N/mm²]
T
B
DISPLACEMENT [mm]

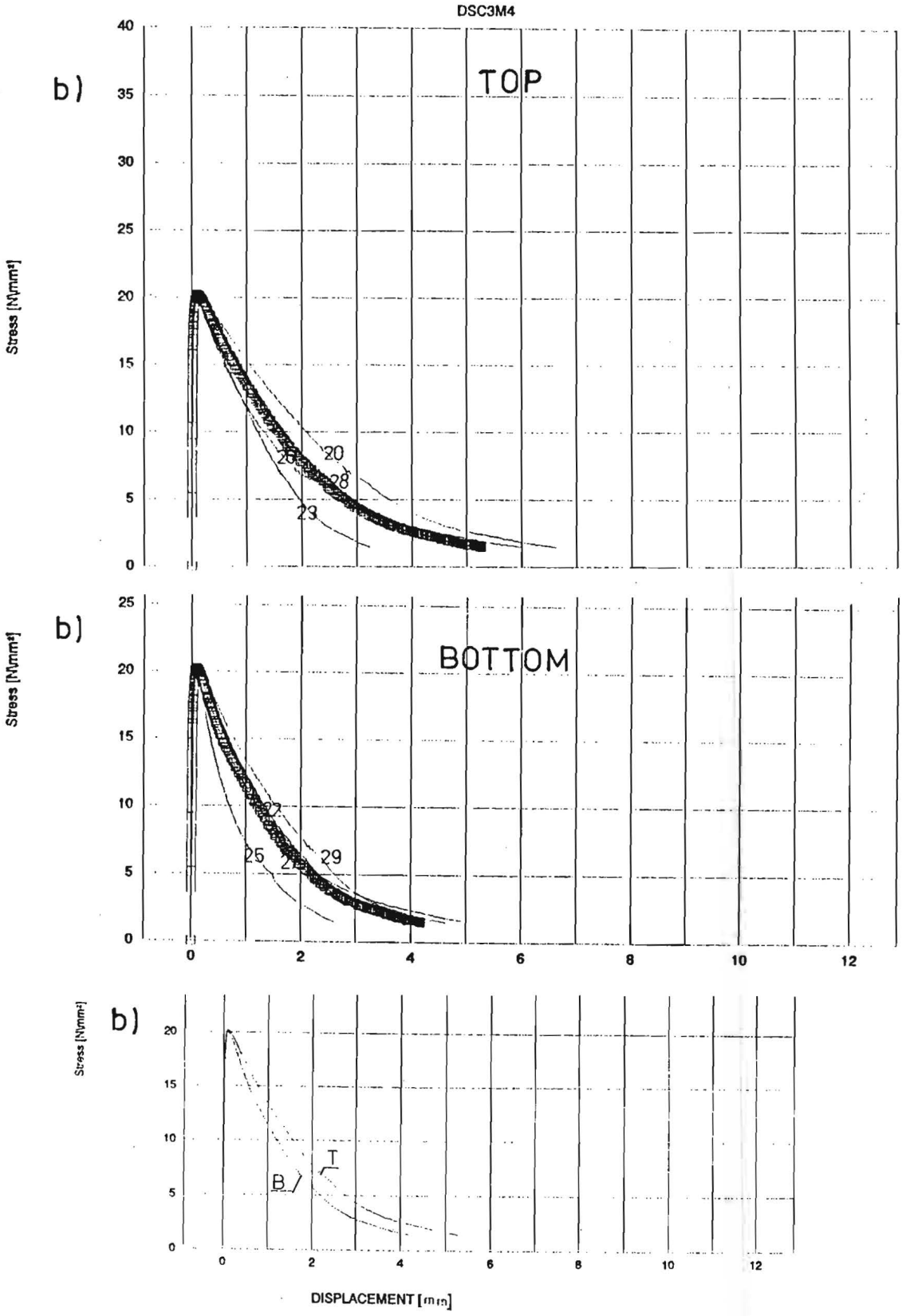
DSC3M4
b)
TOP
Stress [N/mm²]
40
35
30
25
20
15
10
5
0
20
28
23
b)
BOTTOM
Stress [N/mm²]
25
20
15
10
5
0
27
25
29
0
2
4
6
8
10
12
b)
Stress [N/mm²]
20
15
10
5
0
B
T
0
2
4
6
8
10
12
DISPLACEMENT [min]

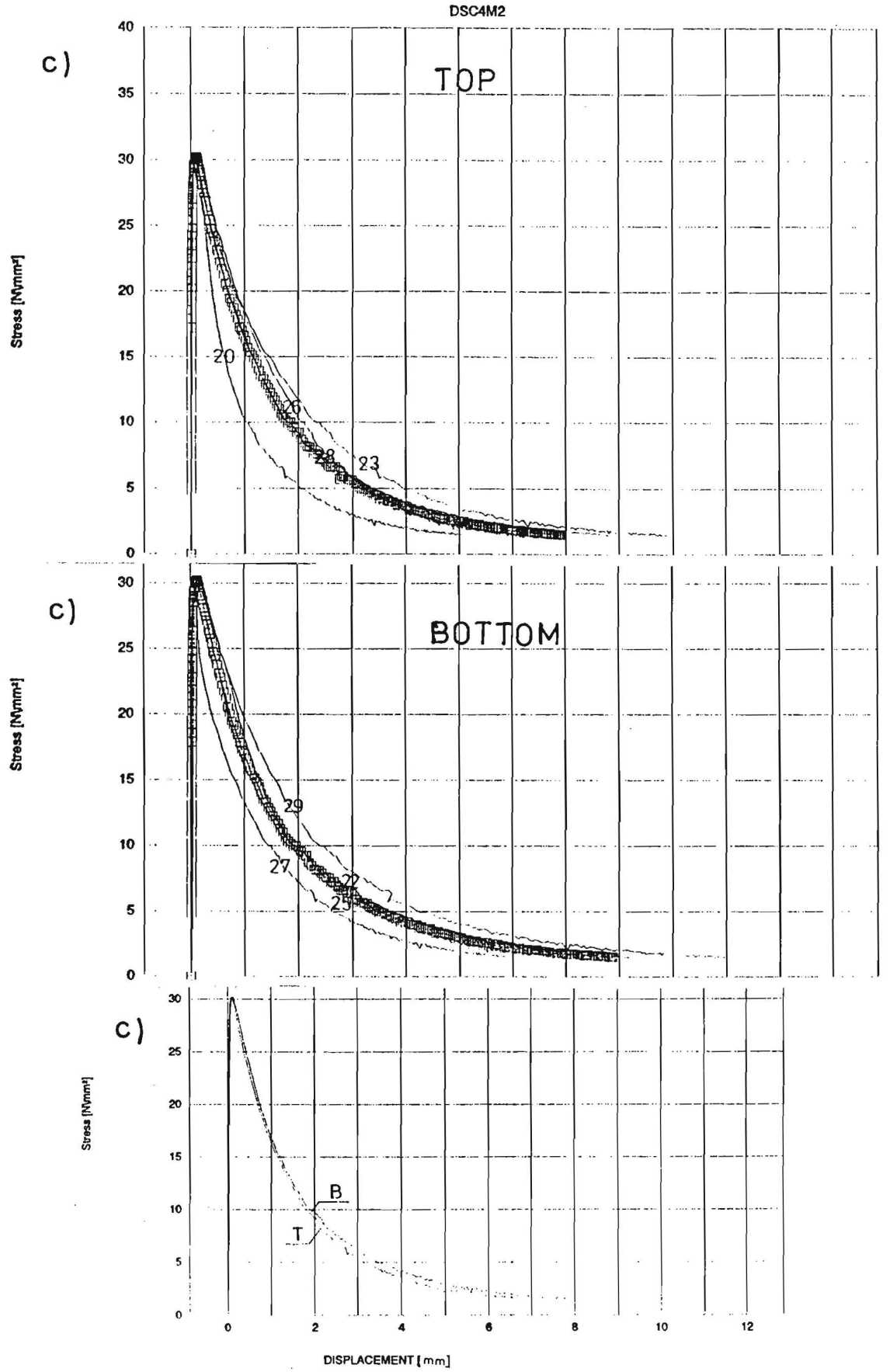

Fig.10.3. Examples of lateral deformations for M-type specimens of concretes C2-(a), C3-(b), C4-(c).

Deformations of specimens made of C1 concrete differ from these for the rest of concrete compositions. M-type cubes deform quite uniformly with respect to the upper-bottom plane, and at the same time clip gauges indications are completely different when compared on particular lateral surfaces. Variations in clip gauges indications were also found for S-type specimens. Figure 10.4 presents an example of lateral deformations for S-type specimen of C1 concrete.

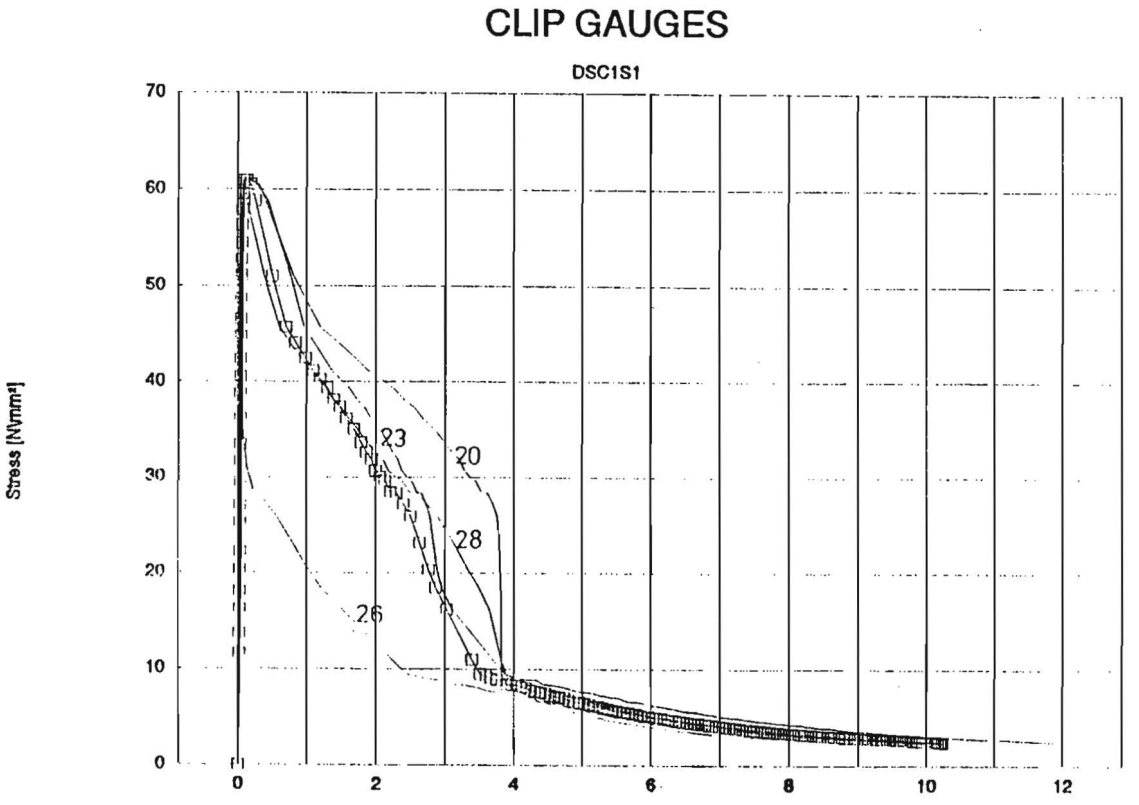

Fig. 10.4. High strength concrete - lateral deformations of S-type specimen.

The failure occurs in the form of vertical cracks passing along the specimen height. Deformations vary substantially on each lateral surface. For M-type specimen it is shown in Fig.10.5. It may be the result of the interaction between loading apparatus and specimen. The rotational stiffness of the testing machine is probably close to the limiting stiffness for stable compression test.

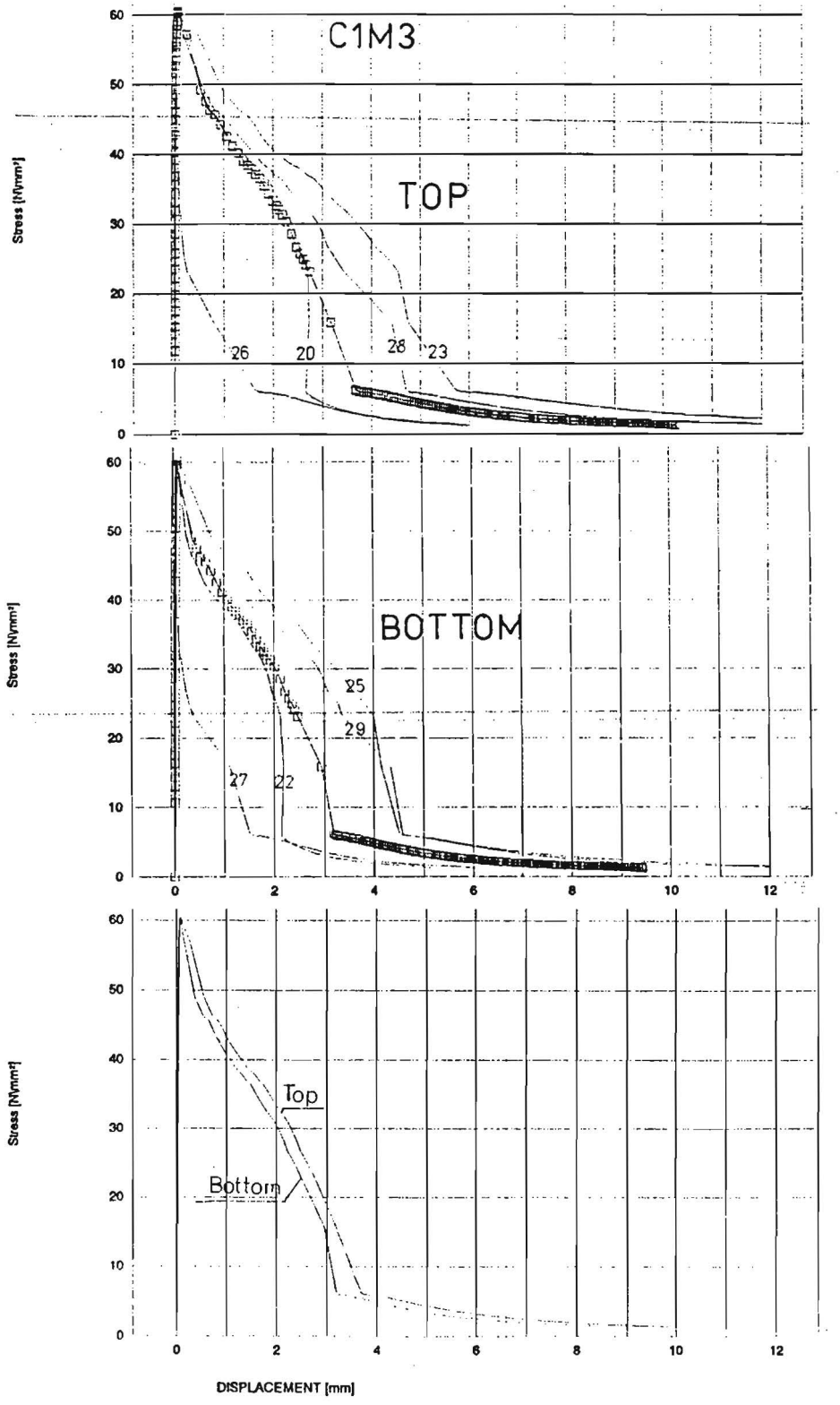

Fig.10.5. lateral deformations for M-type specimen of high strength concrete (C1).

The measurements of the lateral deformations of high prisms (L-type) revealed the localization of deformations with respect to the top-bottom plane with the exception of HSC where again vertical cracks prevailed. Axial stress-lateral displacement curves for L-type specimens of different concretes are given in Fig.10.6. They are average values measured in the top (T), middle (M), and bottom (B) plane.

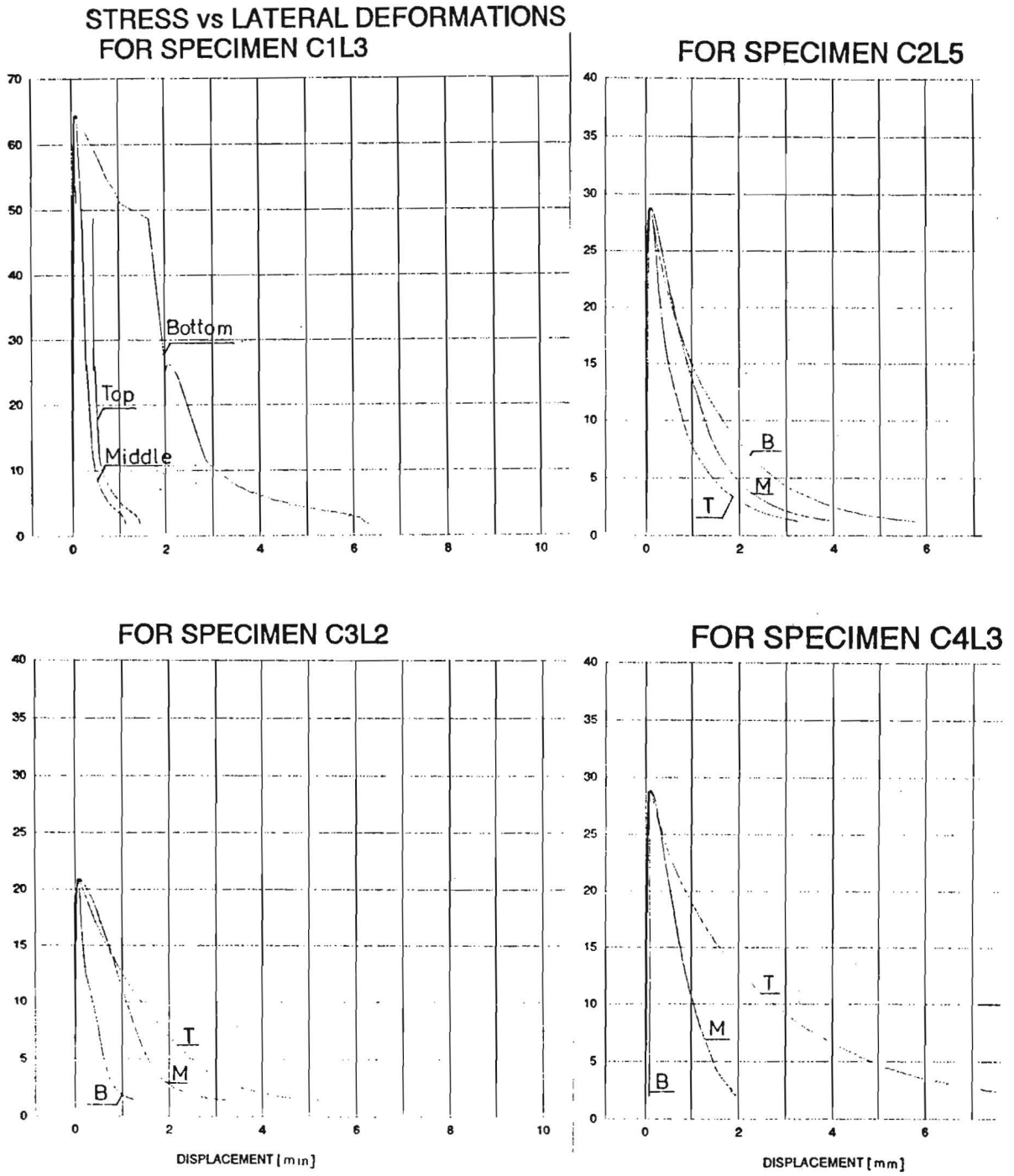

Fig.10.6. Examples of lateral deformations for L-type specimens of concrete C1, C2, C3, C4.

11. Softening process

In section 2 a brief discussion of experimental results obtained from post-peak softening tests has been given. Van Mier [1984] found an apparent resemblance in the post-peak stress-deformation curves for different specimen height, while Vonk [1992] showed that the post-peak curves were not equal as the result of non-local process in the post-peak range. They used different loading platens (brushes and polished steel platens with teflon layer). Also for the presentation of the post-peak results they applied somewhat different procedures. Van Mier compared post-peak stress-displacement curves determined by subtracting the deformation at peak-stress. Vonk evaluated the same curves by subtracting inelastic pre-peak displacement. The absolute values of post-peak deformations are different, however the relative distances between post-peak curves for various specimen sizes do not change significantly when evaluated consequently according to a chosen procedure. We may evaluate the post-peak softening brunch by subtracting the overall pre-peak deformations, just by shifting vertical axis of a diagram (curve called 'post-peak deformations' in Fig.11.1), or by subtracting the inelastic pre-peak deformations according to unloading procedure (curve called 'unloading post-peak deformations'). Fig.11.1 presents divergencies in location of the post-peak curves for M-type specimens of concrete C2, C3, C4.

a)

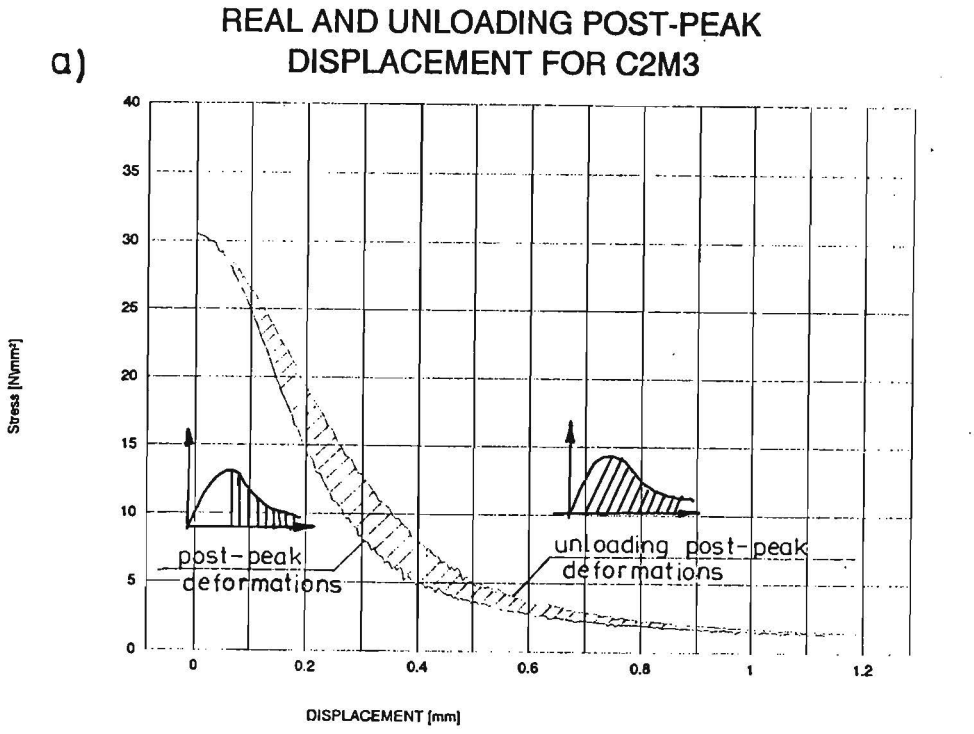

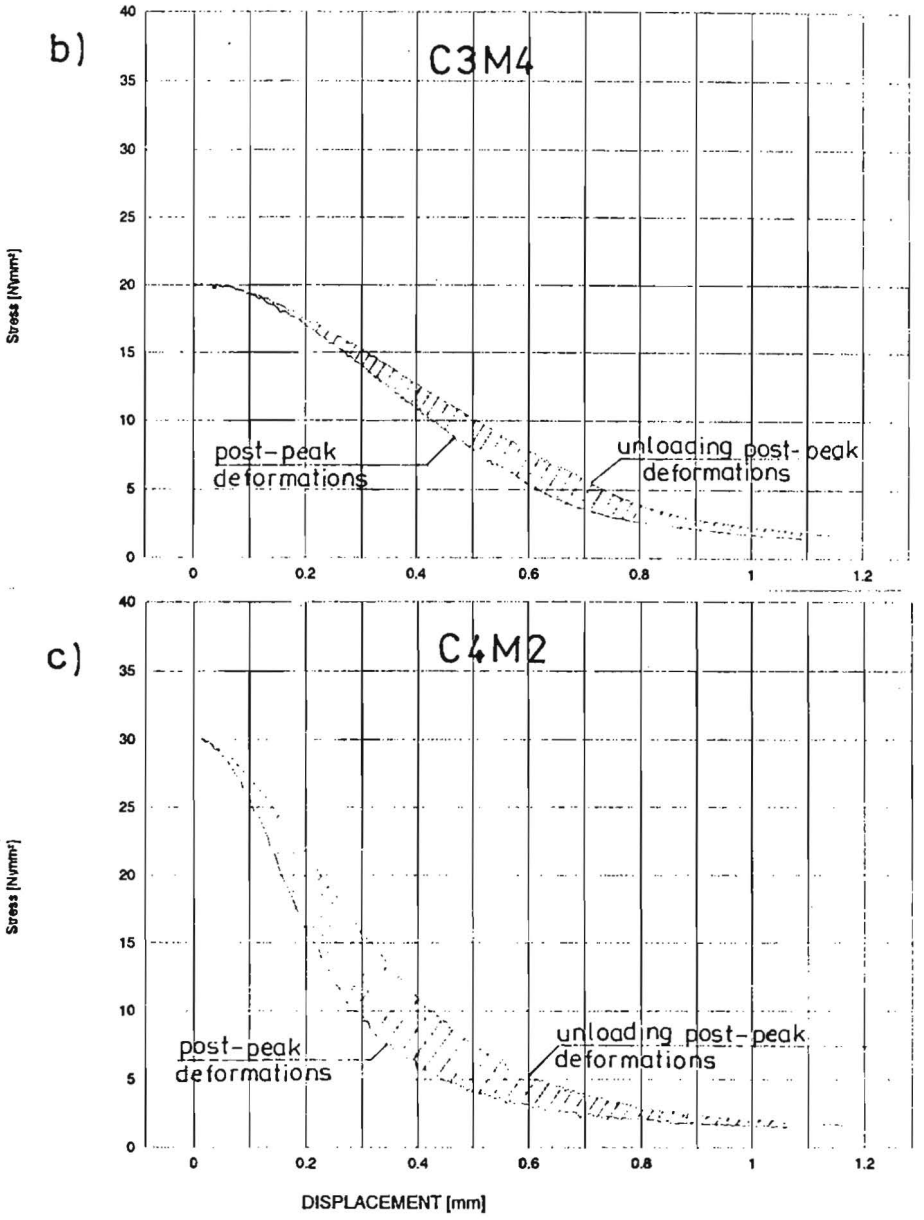

Fig.11.1. Post-peak stress-deformation curves evaluated according to different procedures for M-type specimens of concrete C2-(a), C3-(b), C4-(c).

The larger is the shaded area, the higher is the energy dissipation due to inelastic pre-peak deformations and slow crack growth. For different types of concrete the divergencies seem to be systematic, and consequently, the quantitative differences should be similar for various specimen dimensions, if we apply the same procedure for post-peak softening curves analysis. All diagrams presented below have been prepared by subtracting just the deformations at peak stress ('post-peak deformations').
Figure 11.2 provides the post-peak stress-strain and stress-deformation curves for representative specimens of each type of concrete - C1, C2, C3, C4. Vertical stress axis has been made dimensionless for more convenient presentation of the results.

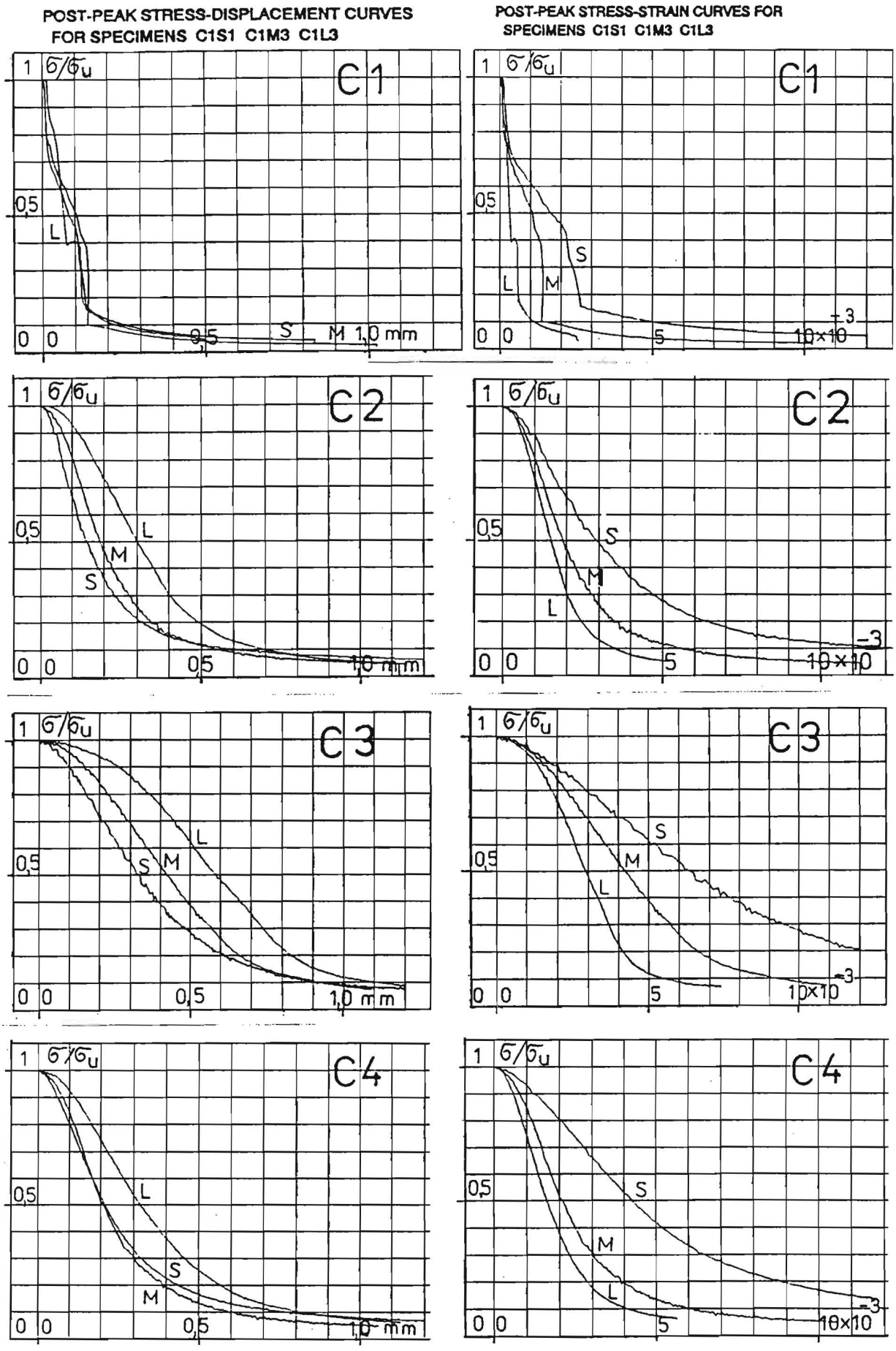

Fig.11.2. Post-peak stress-displacement and stress-strain curves for representative specimens of concretes C1,C2,C3,C4.

The sets of the complete stress-strain curves for all specimens of the particular type of concrete are visualized in Fig.11.3.

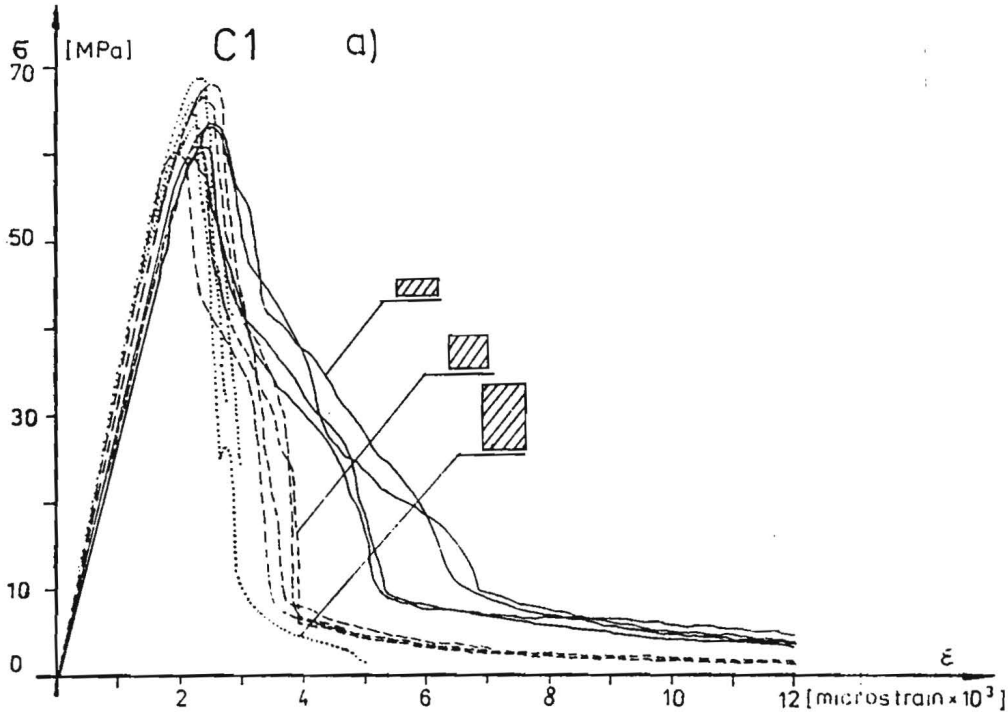

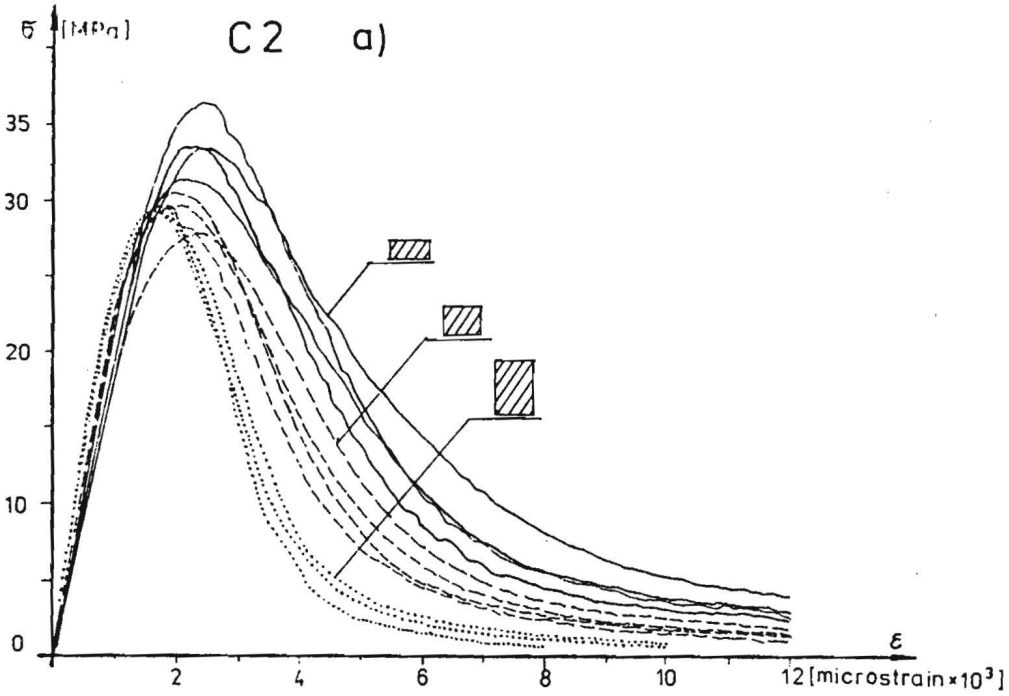

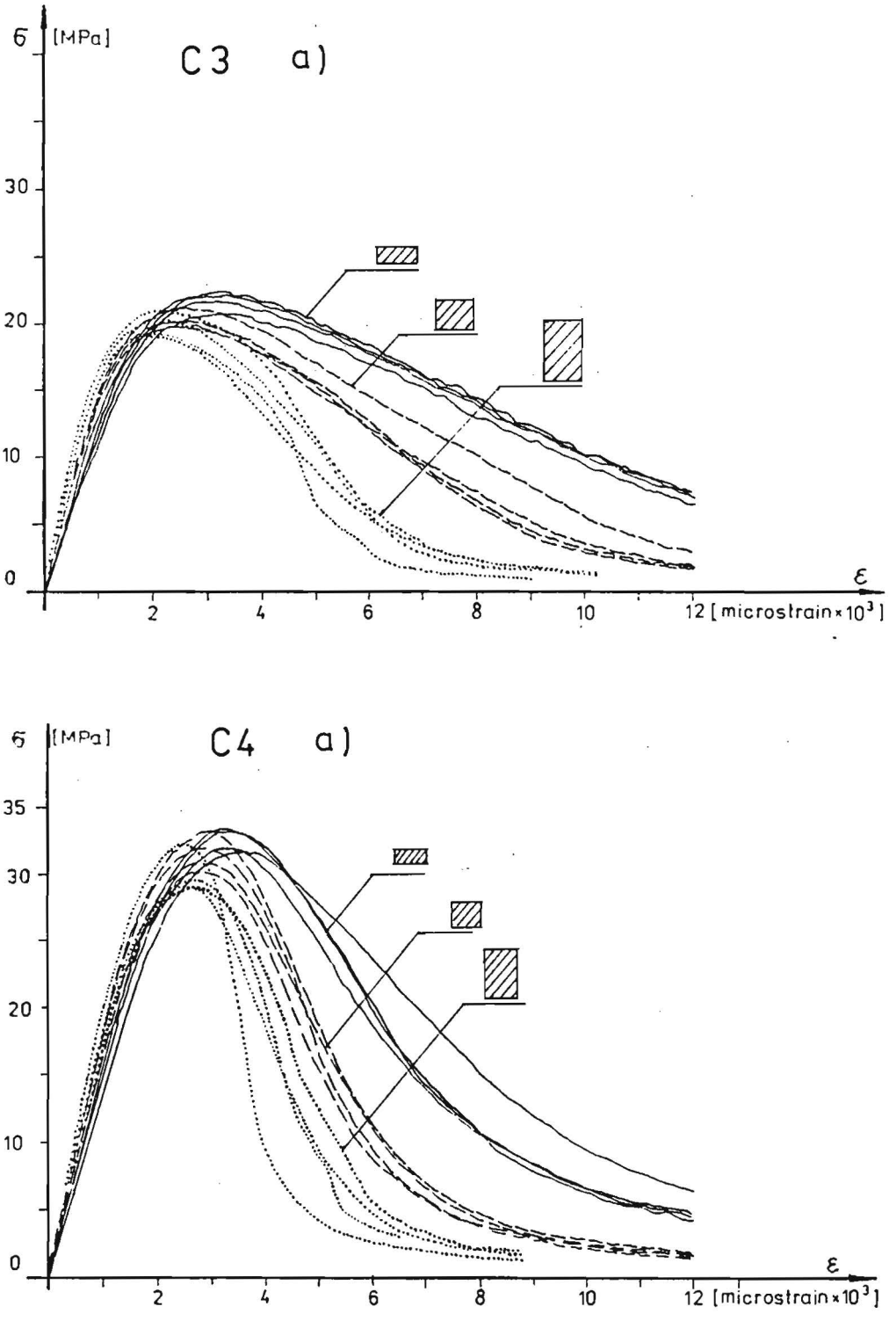

Fig.11.3. Complete stress-strain curves for all specimens of concrete: C1 - (a), C2 - (b), C3 - (c), C4 - (d).

It can be seen from Fig.11.2 that only for HSC (C1) the strain localization is evident. Stress-displacement curves for S, M and L-type specimens practically coincide. The localization of deformations is also confirmed by the mode of failure. Some inconsequences emerge when the process of the localization of deformations is considered in terms of fracture energy per unit of cross-sectional area for S,M and L specimens of C1 concrete (Fig.11.6). Certainly, they are not equal and bulk behaviour is still of importance. The partition of energy components into local fracture energy and continuum fracture energy (Fig.2.13) reveals a big share of local energy in the overall energetic balance for C1 concrete.
There are also good reasons to mention that softening process in HSC is influenced by the interaction of the loading apparatus and the specimen. Especially for L-type specimens of HSC the incremental post failure stiffness of specimen was probably bigger than the stiffness of the testing machine.
Certainly, it is recommended to perform more tests on HSC specimens under various loading conditions. A possible way is the application of a combination of axial and circumferential deformation in feed-back test control system.
For the rest of concrete compositions post-peak stress-displacement curves do not coincide. Similarity of diagrams for S and M specimens for concrete C2 and C4 (Fig.11.2) is related to the similarity of the stress-strain diagrams connected with deformability and process of cracks formation. The global characteristic of all post-peak stress-displacement curves for concretes C2, C3, C4 is approximate by equal to the results presented by Vonk [1992]. It holds for these concretes that post-peak resistance increases as the height of the specimen decreases (stress-strain curves). The influence of a diffuse process occurring in the volume of the specimen becomes more clear and can be observed in concretes with various internal structure and mechanical properties. The similarity of S and M curves for concrete C4 (Fig.11.2) is not systematic what can be seen comparing stress-displacement curves for Concrete C4.
In all tests pronounced differences between the strain gauge measurements and the LVDTs measurements were found. It has already been presented in Fig.8.6. The process is connected with the global behaviour of specimen and particularly with the lateral deformations and crack formation. Unloading of large pieces of concrete under increasing deformation results in the concentration of deformations in the macrocracks and redistribution of load carrying capacity among virtually undamaged larger concrete blocks.
In the majority of tests indications of particular LVDTs differ apparently. It is systematic and does not depend on specimen type and concrete composition. The only exception is high strength concrete, where snap-back behaviour occurred locally. Figure 11.4 presents results of the separate LVDTs measurements for M-type specimens of different concretes.

DISPLACEMENT OF LVDT's

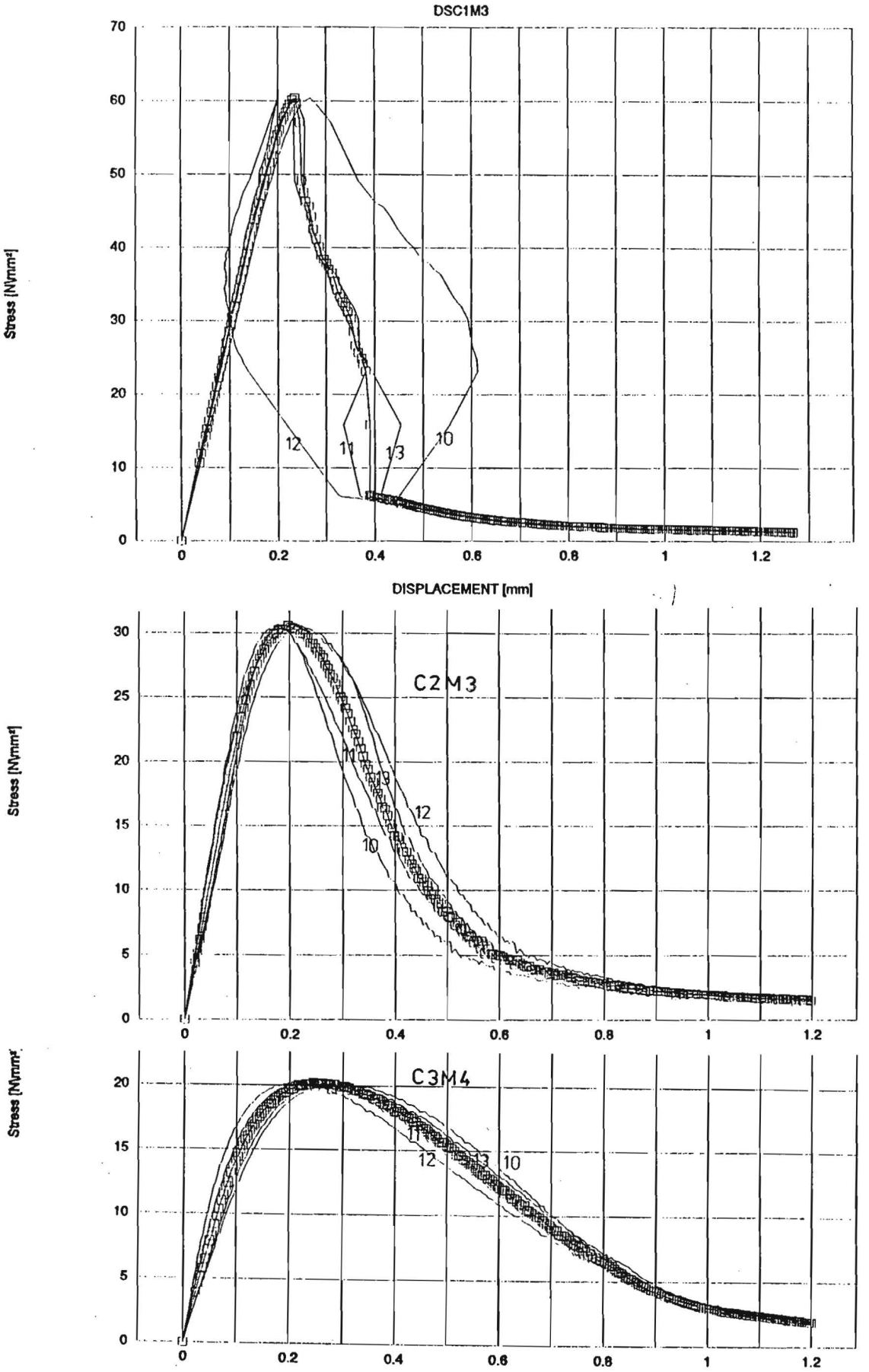

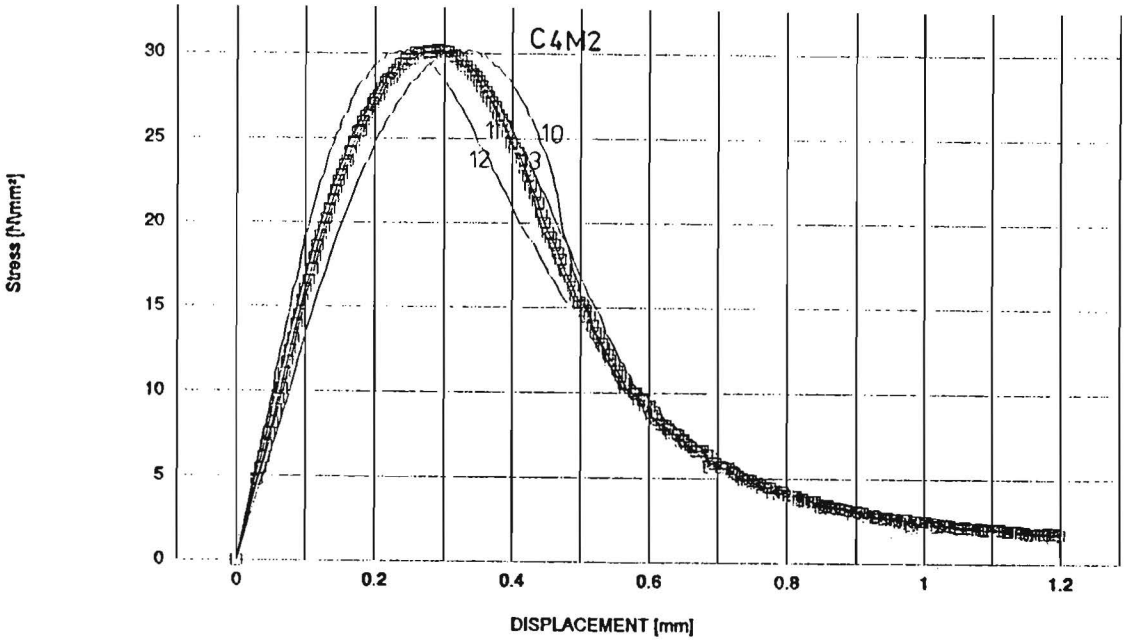

Fig.11.4. Displacement of the separate LVDTs for M-type specimens of different concretes.

Strain localization in HSC goes together with the rotation of the loaded boundaries. It is not so clear for the rest of the other concrete mixes, however, obviously nonsymmetric failure of the specimen influences the response of the loading apparatus. Loading platen surfaces rotate due to nonuniform deformation of concrete block. After peak-stress the rotation increases due to strain localization process. At the end of a test the scatter in LVDTs measurements disappears since fractured specimens behave uniformly and small residual stresses are still present.
The strain localization due to various levels of heterogeneity of concrete can be observed via rotation of the loading platens. For concretes C2 and C3 from Fig.11.4 one may conclude that the rotation of the loading platens entailed by local deformations of concrete is smaller for more homogeneous concrete C3 with smaller aggregates.

11.1. Fracture energies of concrete under compression

Following section provides experimental data concerning local fracture energies per area of the specimen's cross-section (100x100 mm^2). They were estimated by integrating post-peak stress-displacement curves to a softening stress -3.0 MPa with a subtraction of the inelastic component as it is shown in Fig.11.5. For perfect localization of deformations the fracture energy do not depend on the height of the specimen (cross-section is the same for every test).

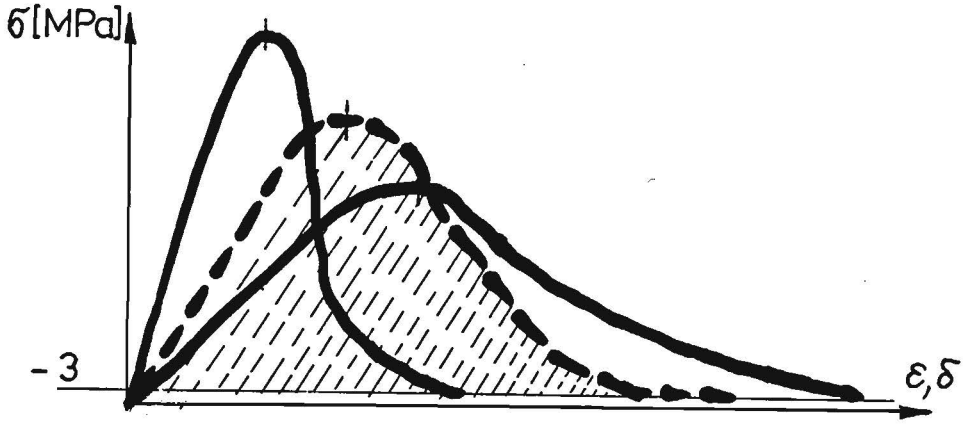

Fig.11.5. Determination of local fracture energy.

Figure 11.6 presents the average values of local fracture energies per area of cross-section for different types of concrete.

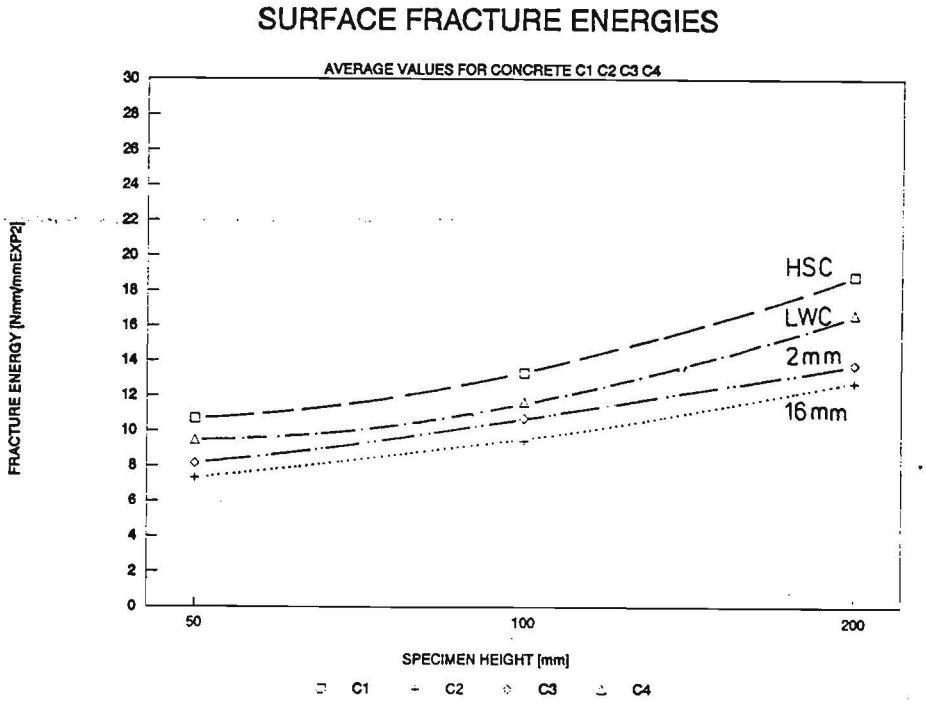

Fig.11.6. Average values of local post-peak fracture energies per area for different types of concrete.

The influence of the specimen geometry on the stress-strain relation can be analyzed by the energetic approach also. Fig.11.7 presents the dependence of the fracture energy per volume on specimen geometry for different concrete mixes. The fracture energies have been calculated by integrating the stress-strain curves to a softening stress -3.0 MPa as it .is shown in Fig.11.5.

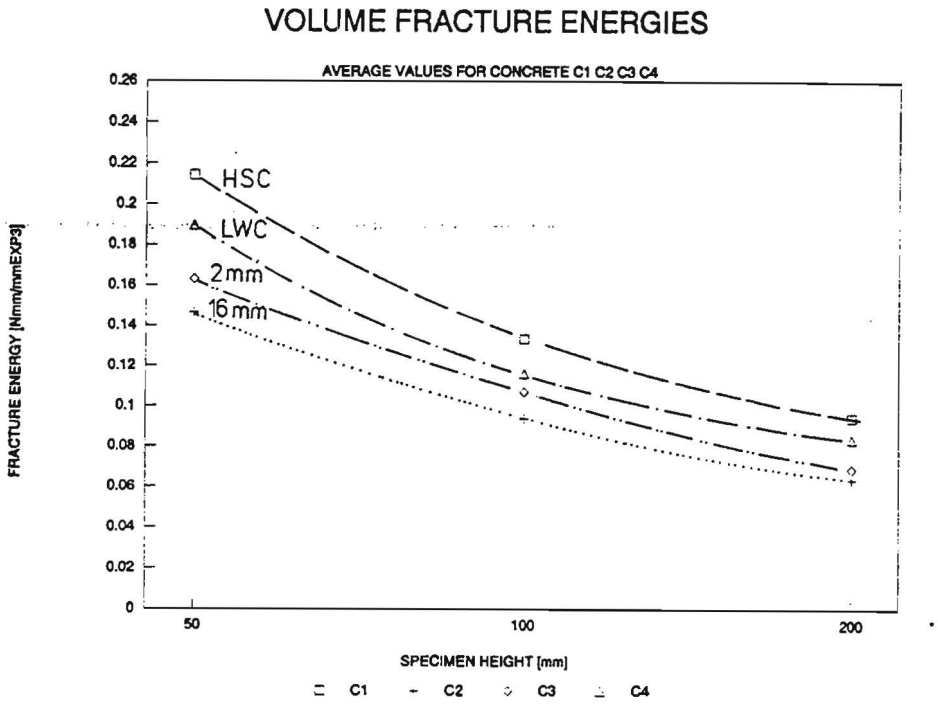

Fig.11.7. Average values of fracture energies per volume for different types of concrete.

Local fracture energies per area depend on the height of the specimens what comes directly from Fig.11.6. That means the localization of cracking is not perfect and is size dependent.
For an ideal continuum with microdefects scattered homogeneously inside the entire volume of the specimen, the fracture energy per volume would be independent of specimen size. It is not the case for the investigated concretes where macro-defects are localized and for bigger specimens fracture energies per volume tend to decrease - they are distributed over larger volume (Fig.11.7).
Energetic considerations given above confirm the hypothesis that fracture of concrete under compression is a combination of a local and a diffuse volumetric process and is size dependant for various compositions of concrete.

12. Conclusions

The influence of concrete composition and mechanical properties on the softening of concrete specimens loaded in uniaxial compression has been investigated. Attention has been focused on the contribution of compressive strength, specimen size and dimensions of gravel to the post-peak strain softening behaviour of concrete. There are some crucial points in testing of HSC which should be taken into account when dealing with the analysis of the experimental results. One may expect that softening process in HSC is influenced by the interaction of the loading apparatus and a specimen. The insufficient rotational stiffness of the testing machine resulted in uncontrolled failure of HSC specimen (especially L-type). Under displacement control feed-back signal the stability of test could not be maintained in the post-peak region. Another disturbing factor is the friction between specimen and loading platens. It tends to increase with increasing concrete compressive strength. Several conclusions coming from the experimental program can be summarized as follows:

1. Differences in composition and mechanical properties of high-strength concrete, light-weight concrete (lytag gravel), normal concrete (maximum gravel 16 mm), and small gravel concrete (2 mm) do not affect significantly the failure mode for particular specimen size. Differences in the fracture process can be observed at micro-level, but the macrocracks pattern is mainly the result of interaction between testing conditions (stiffness of the loading apparatus, kinematic conditions at the specimen-loading platen interface) and the specimen size.

2. The influence of the height of specimen and type of concrete on peak-stress can be observed, though no rigorous statistical analysis has been performed. For concretes C2, C3, C4 it is the same tendency for peak stress which tends to decrease with the increasing of specimen size. It is more pronounced for transition from S-type (50 mm) to M-type (100 mm) specimen. Similar phenomenon has been reported by Vonk [1992]. HSC shows the opposite tendency. What is rather surprising, with the increase in specimen height the peak stress increases also. It can be attributed to the specific loading conditions (displacement control), stiffness of the loading apparatus, boundary conditions (friction), and partially to the volumetric effects connected with microcracking process in HSC.

3. for all types of concrete the strain at the peak stress measured at the lateral surfaces was always behind the strain value measured via overall displacement between the loading platens. The difference between both measured strains was less pronounced for higher specimens. As a possible reason for this finding the interaction between load - application system and specimen has been reported (Van Mier

[1984]). Again, there is a difference in high-strength concrete behaviour since the strains at peak stress are equal and do not depend on specimen size. Reported divergency in compressive strength of HSC and size independence of strains call for further experimental investigation.

4. The comparison of fracture energies for particular concrete compositions provided informations about the component of fracture energy connected with the size and type of gravel. The highest elementary fracture energies are for HSC and LWC. For HSC it is mainly due to a high compressive strength enlarging the area under stress-strain and stress-displacement curves. Composition of LWC is relatively homogeneous. Porous particles of lytag are strongly embedded in cement matrix and significant cohesive forces are still present at the end of post-peak curves. In compression tests fracture energies are higher for concrete with aggregate 2 mm (C3), than for normal concrete with 16 mm gravel (C2) despite lower compressive strength of concrete C3. The fracture process in concrete under compression seems to be somewhat different from that for tensioned concrete. The mechanism of energy dissipation in compressive tests related to plastic, irrecoverable effects in cement matrix and deformable gravel (lytag) participates strongly in the overall energetic balance. The crack pattern in concrete under compression is much more diffused and distributed than in tension.

5. The analysis of stress-strain and stress-displacement curves has shown that only for HSC the localization of deformations is evident. Stress-displacement post-peak curves for S, M, and L-type specimens of HSC practically coincide. When a localized deformation is smeared over different specimen heights (50,100,200 mm) the divergencies in the softening slope in terms of stress-strain dependence are observable. The localization of deformations in L-type specimens proceeds mainly in a separate shear macrocrack formed through an array of small parallel splitting cracks. For S, and M-type specimens the combination of many splitting and slightly inclined shear macrocracks is observed. For the rest of concrete compositions (C2,C3,C4) post-peak stress-displacement curves do not confirm the strain localization process like they do for HSC. It holds for these concretes that post-peak resistance in terms of stiffness degradation (stress-strain curves) increases as the height of the specimen decreases. The influence of a diffuse process occurring within the volume of specimen can be observed in these compositions of concrete.

6. Analysis of fracture energies confirms the hypothesis that fracture of normal and light-weight concrete under compression is a combination of a local and a diffuse volumetric process, and is size dependent for various compositions of concrete. The only exception is HSC. Taking into account some doubts concerning stiffness of the loading apparatus and load machine - test specimen interaction, the continuation of tests on HSC is recommended.

REFERENCES

[1] Ashrabov,A.A. [1988]
'Modelling of properties and fracture processes of light-weight and reinforced concrete.'
Tashkient, Academy of Science. Uzbeck Republic of Soviet Union, 1988 (in Russian).

[2] Bažant, Z.P. [1976]
'Instability, Ductility and Size Effect in Strain-Softening Concrete.'
J. of Engng. Mech.Div.,ASCE, vol.102, No. EM.2, April 1976, 331-334.

[3] Bažant, Z.P., Tabbara, M.R., Kazemi, M.T., Pijaudier-Cabot,G. [1990]
'Random particle model for fracture af aggregate or fiber composites.'
Journal of Engng. Mech., vol. 116, No. 8, August 1990, 1686-1705.

[4] Bažant, Z.P. [1991]
'Why continuum damage is nonlocal: micromechanics arguments.'
Journal of Engng. Mech., vol. 117, No. 5, May 1991, 1070-1087.

[5] Bažant , Z.P. and Ožbolt,J. [1991a]
'Compression failure of quasibrittle material: nonlocal microplane model.'
Journal of Engng. Mech., vol. 118, No. 3, March 1992, 540-555.

[6] Bažant, Z.P. and Yunping Xi [1991b]
'Statistical size effect in quasi-brittle structures:
I. Is Weibull Theory Applicable?'
Journal of Engng. Mech., vol. 117, No. 11, 1991, 2609-2621.

[7] Bazant, Z.P. and Yunping Xi [1991c]
'Statistical size effect in quasi-brittle structures:
II.Nonlocal Theory.'
Journal of Engng. Mech., vol. 117, No. 11, 1990, 2623-2639.

[8] De Borst, R. and Muhlhaus, H.B. [1991]
'Continuum models for Discontinous Media.'
Fracture Process in Rock and Ceramic, 1991 RILEM, vol 2,601-618

[9] Carpinteri, A. [1989]
'Decrease of apparent tensile and bending strength with specimen size: two different explanations based on fracture mechanics.'
Int. Journal of Solids and Struct., vol. 25, No. 4, 1989, 407-429.

[10] Carrasquillo, O.,Slate, F.O., Nilson, A.H. [1981]
'Micro-cracking and behaviour of high-strength concrete subjected to short term loading.'

ACI-Journal, 78-15, May-June , 179-186.

[11] Chen, R.C. and Carrasquillo, R.L. and Fowler, D.W. [1987]
'High-Strength Concrete - Mechanical Properties and Structural Behaviour.'
High-Strength Concrete, Special Publication of ACI, ed.H.G. Russel, SP-87-14.

[12] Dahl, H., Brincker,R. [1989]
'Fracture Energy of High-Strength Concrete in Compression.'
Int. Conf. on Fracture of Concrete and Rock: Recent Developments ,ed. S.P.Shah,S.E. Swartz, B.Barr, Elsevier Applied Science, Cardiff, UK, September 1989, 523-536.

[13] Elices, M. and Planes, J. [1989]
'Fracture Mechanics of Material Models. Concrete Structures. From theory to applications.' Edited by L. Elfgren, Chapman and Hall, RILEM, Technical Committee 90FMA.

[14] Erdei, C.K. [1980]
'Finite element analysis and tests with a new load-transmitting medium to measure compressive strength of brittle materials.'
Materials and Structures, RILEM, 13, 83-90.

[15] Fanella, D.A. and Krajcinovic, D. [1988]
'Size effect in concrete.'
Journal of Engng. Mech., vol. 114, No. 11, April 1988, 704-715.

[16] Freudentahl, A.M. [1968]
'Statistical approach to brittle fracture.'
Fracture - an Advanced Treatise, ed. H. Liebowitz, vol.2, Academic Press, 591-619.

[17] Glavind, M. and Stang, H. [1991]
'Evaluation of the complete stress-strain curve for high-strength concrete.'
In "Fracture Process in Concrete, Rock and Ceramics", RILEM Proceedings 13, eds. J.G.M. Van Mier, J.G. Rots and A. Bakker, E. and F.N. Spon, London , 749-760.

[18] High-strength Concrete-State of the Art Report [1991]
FIB/CEB, Bulletin d'information No. 197, SR 90/1.

[19] Hillerborg, A. [1989]
'Stability problems in fracture mechanics testing.'
Int. Conf. Fracture of Concrete and Rock: Recent Developments, ed. S.P.Shah, S.E. Swartz, B.Barr, Elsevier Applied Science, Cardiff, UK, September 1989, 369-378.

[20] Hilsdorf, H. [1965]
'Die Bestimmung der Zweiachsiger Festigkeit das Betons.'
Deutsche Ausschuss fur Stahlbeton, 173, Berlin.

[21] Hordijk, D.A., Van Mier, J.G.M., Reinhardt, H.W. [1989]
'Material Properties.'
Fracture Mechanics of Concrete Structure. From theory to applications. Edited by L. Elforen, Chapman and Hall, RILEM, Technical Committee 90 FMA.

[22] Hsu, T.T.C., Slate, F.O., Sturman, G.M. and Winter, G. [1963]
'Microcracking of plain concrete and the shape of the stress-strain curve.'
ACI Journal, 60(14), 209-224.

[23] Hurlbut, B.J. [1985]
'Experimental and Computational Investigation of Strain-softening in Concrete.'
University of Colorado, Bulder, Department of Civil Engineering, Structural Research Series 8508, 1985.

[24] Jayatilaka, A.S. [1979]
'Fracture of engineering brittle materials', Applied Science Publishers, London.

[25] Kotsovos, M.D. [1983]
'Effect of testing techniques on the post-ultimate behaviour of concrete in compression."
Materials and Structures, RILEM, 16, 1983, 3-12.

[26] Kupfer, H.B. and Gerstle, K.H. [1973]
'Behaviour of concrete under biaxial stresses.'
Journal of Engng. Mech. Div., ASCE, 99 (EM4), 852-866.

[27] Mazars, J. [1985]
'A model for a unilateral elastic damageable material and its application to concrete.'
In: Fracture Toughness and Fracture Energy of Concrete, ed. F.H.Wittmann, Elsevier.

[28] Mihashi, H. [1983]
'A statistic theory for fracture of concrete.'
In: Fracture Mechanics of Concrete, ed. F.H. Wittmann, Elsevier Science Publishers.

[29] Mills, L.L. and Zimmermann, R.M. [1970}
'Compressive strength of plain concrete under multiaxial loading conditions.'
ACI Lournal, 67, 802-807.

[30] Muhlhaus, H.B., De Borst, R., Aifantis, E.C. [1991]
'Constitutive models for numerical analysis for inelastic materials with microstructure.'
Proc.Seventh Conf. Int. Assoc. Comp. Methods and Advances in Geomechanics, eds.G.Beer and J.R.Booker, Balkema, Rotterdam and Boston.

[31] Oritz, M. [1987]
'An analysis study of the localized failure modes of concrete.'
Mechanics of Materials, No. 6, 159-174.

[32] Pijaudier-Cabot, G., Bažant, Z.P. [1988]
'Local and nonlocal models for strain-softening and their comparison based on dynamic analysis.'
Cracking and Damage, Strain Localization and Size Effect.
J. Mazars, Z.P. Bazant. Research Workshop, Cachan-France, 6-9 Sept. 1988, 379-390.

[33] Reinhardt , H.W. [1977]
'Anspruche des Konstrukteurs an den Beton, hinsichtlich Festigkeit und Verformung.'
Beton 5/1377. 135-139.

[34] Roelfstra, P.E. [1989]
'Simulation of strain localization processes with numerical concrete.'
In "Cracking and Damage" eds. J. Mazars and Z.P. Bazant, Elsevier Applied Science , London 79-90.

[35] Schickert, G. [1980]
'Schwellenwerte beim Betondruckversuch.'
Deutsche Ausschuss fur Stahlbeton, Heft 312, Berlin 1980.

[36] Shah, S.P. Godoz, V., Ansari, F. [1981]
'An Experimental Technique for Obtaining Complete Stress-Strain Curves for High Strength Concrete.'
ASTM Cement, Concrete and Aggregates, vol.3, No. 1.

[37] Short, A. and Kinniburg, W. [1978]
"Lightweight Concrete", third Edition, Applied Science Publihers, London , 1978.

[38] Swamy, R.N. [1987]
'High-Strength Concrete - Mechanical Properties and Structural Behaviour.'
High-Strength Concrete, Special Publication of ACI, ed. H.G. Russel, SP-87-8.

[39] Swartz, S.E. and Nikaeen, A. and Narayan Babu, H.D. and Peryiakaruppan, N. and Refai, T.M.E. [1987]
'Structural Bending Properties of Higher Strength Concrete.'
'High Strength Concrete - Mechanical Properties and Structural Behaviour.'
High-Strength Concrete, Special Publication of ACI, ed. H.G. Russel, SP-87-9.

[40] Van Mier, J.G.M. [1984]
'Strain-softening of concrete under multiaxial loading conditions.'
PhD Thesis, Eindhoven University of Technology, The Netherlands.

[41] Nan Mier , J.G.M. [1986]
'Fracture of concrete under complex stress'
Heron 31(3), 1986.

[42] Van Mier , J.G.M. [1987]
'Fracture propagation in concrete under complex stress.'
SEM/RILEM International Conference on Fracture of Concrete and Rock, Houston, Texas, June 1987, 587-610.

[43] Van Mier, J.G.M. and Schlangen, E. [1989]
'On the stability of softening systems.'
Int. Conf. Fracture of Concrete and Rock: Recent Developments , ed. S.P.Shah, S.E. Swartz, B.Barr, Elsevier Applied Science, Cardiff, UK, September 1989, 387-396.

[44] Van Mier , J.G.M., Noorn-Mohammed, M.B., Timmers, G. [1991]
'An Experimental Study of Shear Fracture and Aggregate Interlock in Cement-based Composites.'
Heron, 36(4).

[45] Vonk, R.A. [1989]
'Influence of boundary conditions on softening of concrete loaded in compression.'
Technical Report TUE/BKO-89.14, October 1989, Technical University of Eindhoven.

[46] Vonk, R.A., Rutten, H.S. Van Mier, J.G.M., Fijneman, H.J. [1991]
'Micromechanical simulation of concrete softening.'
Fracture Process in Concrete, Rock and Cramic.
J.G.M. Van Mier, J.G. Rots and A. Bakker, RILEM/ESES, 1991, vol. 2, 601-619.

[47] Vonk, R.A. [1992]
'Softening of Concrete Loaded in Compression.'
PhD thesis, Eindhoven University of Technology, The Netherlands.

[48] Weibull, W. [1939]
'A stasistical theory of the strength of material.'
Royal Swedish Academy of Engineering, Sci. Proc. 151, 1-45.

[49] Willam, K. Stankowski, T., Runesson, K., Sture, D. [1989]
'Simulation issues of distributed and localized failure computations.'
In "Cracking and Damage"' eds. J. Mazars and Z.P. Bazant, Elsevier Applied Science, Londom 363-378.

[50] Wittmann, F.M. [1983]
'Fracture Machanics of Concrete.'
Developments in Civil Engineering 7, Elsevier Science Publishers B.V., Amsterdam.

[51] Zaitsev, Y. and Wittmann, F.M. [1981]
'Simulation of crack propagation and failure of concrete.'
Materials and Structures, RILEM, 14(83), 357-365.